FIBER ELECTROPHORETIC DEPOSITION PROCESSING OF CONTINUOUSLY REINFORCED Fe-40Al / Al_2O_3 INTERMETALLIC MATRIX COMPOSITES

By

Christopher J. Suydam

A THESIS

Submitted to
Michigan State University
in partial fulfillment of the requirements
for the degree of

MASTER OF SCIENCE

Department of Materials Science and Mechanics

1993

Melissa Crimp, Advisor

ABSTRACT

FIBER ELECTROPHORETIC DEPOSITION PROCESSING OF CONTINUOUSLY REINFORCED Fe-40Al / Al_2O_3 INTERMETALLIC MATRIX COMPOSITES

By

Christopher J. Suydam

A technique for producing a continuously reinforced intermetallic matrix composite (IMC) was developed by applying theoretical and experimental examination of the system components in order to determine the optimum processing conditions and parameters. The mechanics of this process involves the adhesion and infiltration of Fe-40Al powder onto Al_2O_3 multistrand fiber bundles without the use of a binder. By evaluating and determining the optimum processing conditions, maximum adhesion between the matrix powder and the fiber reinforcement (and minimum adhesion) between similar system components is achieved. Optimum processing conditions were generated by applying a previously developed theoretical model which describes the multi-component system governed by traditional colloidal theory. By evaluating such parameters as particle size, surface potential, and the component stability ratio, W, verification of uniform adhesion of the particles to the fibers was obtained. A prototype filament winding system was also developed for implementation into the processing scheme.

To my wife, Tasha, and my entire family for all of their love and support.

ACKNOWLEDGEMENTS

First of all I would like to thank my family and all of my friends for their moral support throughout the course of my graduate studies. I would also like to thank my advisor, Dr. M.J. Crimp, for funding me and for all of her support during this research project. In addition, I would like to thank Dr. M.A. Crimp for his support and help with the microscopy and photographic techniques. I would especially like to thank S.C. Tonn and J. Ambriz for all of there help and encouragement. Special thanks go out to B.A. Wilson for all of his guidance in colloidal chemistry and extensive computer knowledge. Finally, I would like to extend thanks to Dr. E.D. Case for all of his intellectual help, within and outside of this research project.

TABLE OF CONTENTS

TABLE OF CONTENTS (CONTINUED)

LIST OF TABLES

LIST OF TABLES (CONTINUED)

LIST OF FIGURES

LIST OF FIGURES (CONTINUED)

LIST OF FIGURES (CONTINUED)

LIST OF FIGURES (CONTINUED)

INTRODUCTION

Due to the increasing technological demands by the aeronautical/aerospace industry there has become a need to produce materials meeting the strict requirements of today's high performance systems, such as reduced weight savings and increased stength and toughness properties. The recurrent theme in the majority of expectations is that the materials need to accommodate significant weight to volume reduction requirements while retaining other desirable properties such as strength and toughness, over a wide range of temperatures.

Intermetallic alloys, and specifically the B2 aluminides, have received considerable attention as possible candidates to accommodate the industrial demand for high performance materials. In addition to their relatively low densities, intermetallic alloys have excellent environmental and oxidation resistance. Unfortunately, there are limitations to the use of intermetallics. Intermetallic alloys suffer from poor ductility and toughness at low temperature ranges and lack high strengths at elevated temperature ranges. It has become apparent that intermetallic alloys have very limited uses as monolithic materials in high performance applications. However, it may be possible to correct the undesirable properties of intermetallic alloys by incorporating them into multi-component systems. By employing the intermetallic alloy as a matrix material for a composite system, varying types of reinforcements can be applied which

enhance the properties of the matrix. This provides a composite material which defines the now common classification of intermetallic matrix composites or IMCs.

The major objective in designing and producing IMCs is to provide a near-fully dense composite containing a high volume fraction of fiber while taking advantage of the desirable properties of the intermetallic matrix. Since the advent of composite materials processing, there has become a need to not only produce materials that meet these general design requirements, but also to establish a means of processing that is effective, simplistic, and economical[1,2,3].

REVIEW OF LITERATURE

History of Processing

Since the introduction of composite materials and composite materials manufacturing, there has been a constant need to produce a material which is cost effective without degrading the original design parameters. Therefore, it is necessary to establish a means to produce a composite having optimum material properties. One of the most evident problems encountered in the processing of IMCs is the inability to produce a material which is fully or near-fully dense with a uniform fiber (or reinforcement) distribution.

There exists a variety of processes which have been used to produce IMCs. Although, many of these processes have been successful in providing near-fully dense composite systems, there are limitations. Several successful IMC processes exist which are generally referred to as powder metallurgy processing techniques. Some of these techniques include: reactive processing [4], powder injection molding [4,5], hot extrusion [4,6], XD™ synthesis [4,6,7,8], and mechanical alloying [7].

Reactive processing utilizes the reaction between the elemental powders. One variation of reaction processing is known as reactive sintering, RS. This process consists of mixing elemental powders and producing a reaction by heating the mixture to the lowest liquidus temperature of the components [4]. Once the reaction has been

accomplished, the product is then separated via grinding, mixed with the desired reinforcement, and then sintered to form the composite. Several intermetallic alloys and their composites have been successfully formed in this manner, including NiAl, Ni_3Al, Ti_3Al, Nb_3Al and TiAl. Modifications of the reactive sintering process include the use of uniaxial pressure during sintering (reactive hot pressing, RHP) and isostatic pressure during sintering (reactive hot isostatic pressing, RHIP).

A similar technique to that of reactive processing was developed by Martin Marietta. This process, known as XD™ synthesis[4,6,7,8], employs the use of an exothermic reaction created between the elemental components of the powder mixture. This reaction provides enough heat to form a liquid phase which help reduce sintering times and ultimately increases the densification of the powder compact. Once reacted, the product is pulverized, mixed and consolidated via hot pressing or HIPing.

Another powder processing technique is mechanical alloying [7]. This typically consists of high energy milling of a dry, ductile matrix with ceramic particles. The mixture is then compacted and consolidated via traditional techniques. Although this type of technique has found limited application in the production of IMCs, there has been some success. Strothers and Vedula successfully produced an $FeAl/Y_2O_3$ composite system via mechanical alloying. This technique is explained in detail in references discussed elsewhere [7,9,10].

Of the previously described techniques, there is one technique which has not only achieved near-fully dense composite systems, but has been able to control the alignment of the reinforcement within the matrix. This technique is known as powder injection molding [4,6,11]. This process utilizes a heated polymeric binder which is mixed with a powder matrix and chopped, discontinuous reinforcement. This mixture

is then extruded through a die. Alman and Stoloff were successful in forming as-CIPed green bodies of Ni+Al/15v/o FP Al_2O_3 with 35v/o binder using this technique [11]. As can be seen in Figure 1, this technique has the possibility of providing alignment of the fiber reinforcement. In order for this process to be successful, a fine powder and a proper binder must be selected. Proper binder selection is crucial in that it must be completely removed during the post-sintering / consolidation steps thereby not becoming a source of contamination [4,6].

Each powder metallurgy technique previously described has been successful in providing near fully dense IMCs. One limitation of all the powder metallurgy techniques is that the processes are limited to applications requiring short, discontinuous reinforcement. There exist a variety of processes, though, that have extended their range to include continuous reinforcement. These include: the powder cloth technique [4,6], the foil-fiber-foil technique [6], various melt processing techniques [6,7], and filament coating techniques [7]. The powder cloth method has achieved considerable success at the NASA Lewis Research Center in producing continuously reinforced IMCs. This technique is utilized to produce alternating lamellae of matrix and reinforcing material. The matrix lamellae is formed by combining a powder matrix with an organic binder and wetting agent and then rolling to form a thin sheet. The reinforcing lamellae are formed by winding the continuous reinforcing fiber around a mandrel or drum and then coating the drum with a polymeric binder. Lamellae are then stacked in the desired arrangement, and consolidated [6]. This process is illustrated in Figure 2. The major problem encountered is the entrapment of the binder within lamellae which provides for a source of contamination. The foil-fiber-foil uses the same design and consolidation

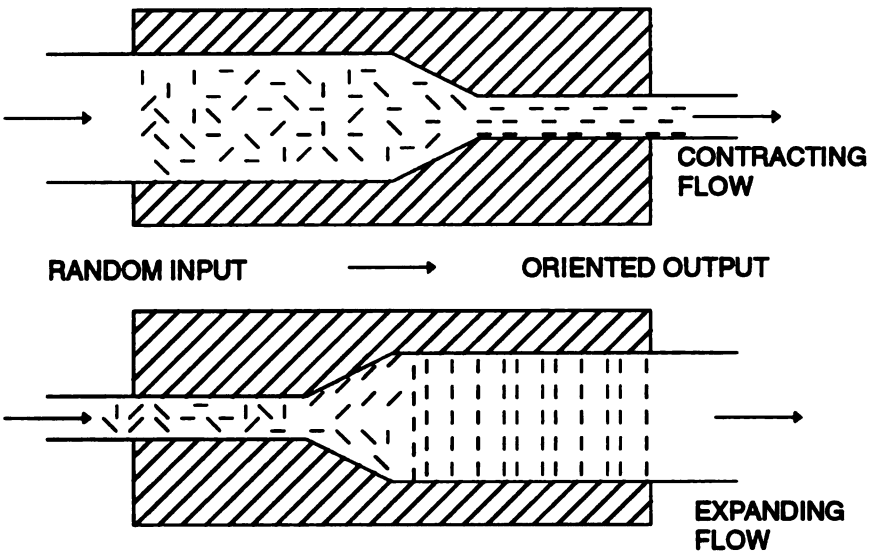

Figure 1. Illustration of possible fiber aligment configurations using binder-assisted molding with either an expanding or contracting flow through the die.

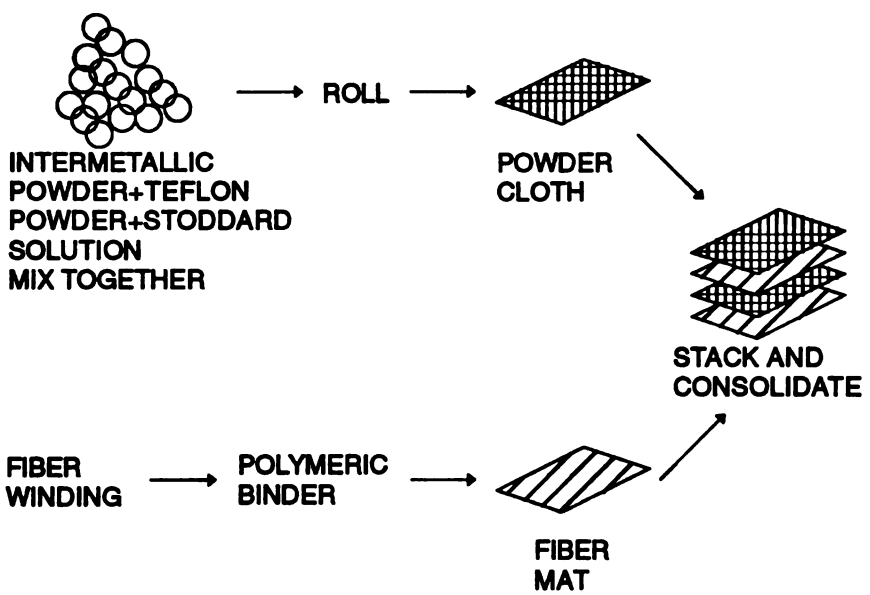

Figure 2. Illustration of the steps involved with the powder cloth processing technique.

principles except that the matrix lamellae are in the form of a rolled sheet instead of a rolled powder slurry. Therefore, no binder-contamination is contributed by the formation of the matrix ply but contamination is produced by entrapment of binder between the plys.

Another successful IMC processing technique for producing continuously reinforced composites is pressure casting. This technique consists of melting the matrix material under vacuum and then forcing the molten material through a continuous fiber preform. This process is schematically illustrated in Figure 3. Nourbakhsh, et al have achieved success in forming IMCs of TiAl, Fe,Al, Ni,Al reinforced with up to 60v/o of Al_2O_3 [6,7,9]. The inability to provide adequate wetting at the matrix/fiber interface for many materials and the resulting poor bond structure poses a problem as applied to IMC systems. Other processes which have been applied to continuously reinforced composites include thermal/arc spray [4,7], CVD [7], plasma spray [4,7] and sol-gel processes [7]. The groundwork for all of these processes involves the deposition of matrix material onto a mandrel containing continuously wound fiber using varying methods for deposition. For the thermal, arc and plasma spray techniques, the matrix is deposited in a molten form in order to provide an impregnated tape which can be cut/stacked and consolidated. Since the matrix is molten, this type of processing encounters the same problems associated with pressure casting [6,7,9].

All of the processes described above are capable of producing near-fully dense IMCs. The limitations inherent to each of these processes hinders the type and range of applications where an IMC can be implemented. The most apparent problems encountered during current processing techniques include: inability to implement

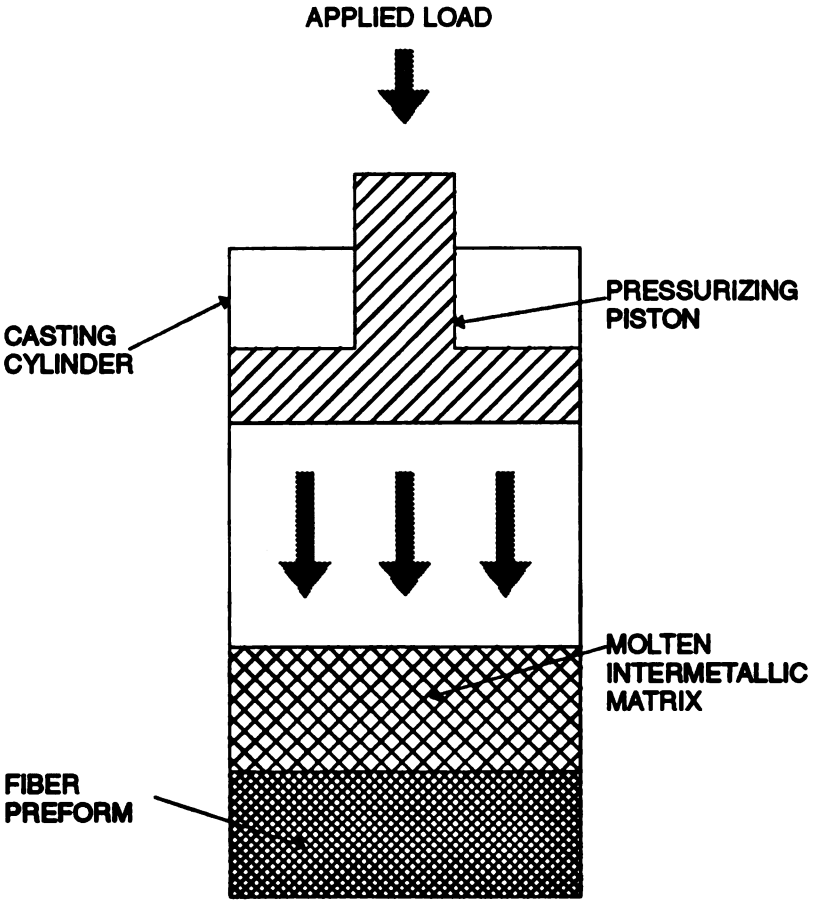

Figure 3. Illustration of the pressure casting technique.

continuous fiber reinforcement, contamination from binders, and wetting problems associated with melt processing. In order to address these problems, an adhesion process, coupled with standard continuous fiber winding techniques, must be designed which does not introduce the complications of polymeric binders and melt processing. One solution would be to implement established colloidal theory to standard processes inherent to powder metallurgy and continuously reinforced composite systems.

Colloid Theory and Principles

The basic fundamentals and principles of colloidal theory describe the behavior and interactions of particles suspended in a fluid medium. The basis for the design of the Fiber Electrophoretic Deposition (FED) process is to primarily take advantage of the existing electrostatic characteristics inherent to particulate suspensions and secondly to control these parameters in order to produce attraction between the powder suspension (intermetallic matrix) and the continuous reinforcement (ceramic fiber). In order to provide a complete explanation of this adhesion phenomena, several colloidal principles inherent to particle suspensions must be examined. Upon immersing some particles into a fluid medium, a charge potential is created via a variety of charge generation mechanisms. These mechanisms include ionization, ion adsorption and ion dissolution [12]. The ionization charge mechanism is dependent on the pH of the particle suspension. Deviation from the suspension's iso-electric point (i.e.p), the pH where the net potential on the particle surface is equal to zero, dictates what the net charge of the particle will be and can be related to the particle's surface charge. A net surface charge may also be acquired by the unequal or preferential adsorption of one ionic species over another, which is known as ion adsorption. Ion dissolution creates

a net surface charge for ionic species by the preferential adsorption of one of the different ionic groups which determines the net surface charge. These individual ionic species, which are responsible for creating a net surface charge, or potential, are also know as potential determining ions, or p.d.i.s. Shaw gives examples pertaining to both the classic AgI system, where both Ag^+ and I^- are the potential determining ions, and the hydrous metal oxide system, where both the H^+ and OH^- ions are the p.d.i.s [12].

Unique to the adsorption of ions onto a particle surface is the creation of an electrical double layer. The electric double layer is modelled as two layers; the diffuse layer of ions and a layer of rigidly held ions immediately adjacent to the particle surface. The diffuse layer of ions has been described in a quantitative manner by Gouy and Chapman [12,13,14]. The layer containing rigidly held ions has also been described quantitatively by Stern [12,13,14]. These two descriptions will be discussed in detail to provide a basis for understanding and interpreting the charge potential phenomena associated with spherical particles immersed in an aqueous solution.

The Guoy and Chapman treatment of the diffuse layer of the electrical double layer is based on the following assumptions [12]: (1) the charge density of the particle surface is assumed to be uniform across the particle surface, (2) the particle surface is assumed to be infinite and flat in geometry, (3) the charge distribution surrounding the particle is assumed to be governed by a Boltzmann distribution, (4) the only influence the solution has on the diffuse region is through the characteristic dielectric constant, which is also assumed to remain constant through the bulk of the medium, and (5) the electrolyte in the bulk medium is assumed to have a fixed single charge number, z. Figure 4 illustrates the assumed surface geometry with a fixed

surface charge, in this case, positive, having the characteristic Boltzmann distribution of ions. Given the concentration of positive and negative ionic species at a potential, Ψ, is expressed as [12,14]:

$$n(+) = n_o \exp[\frac{-ze\psi}{kT}] \tag{1}$$

and

$$n(-) = n_o \exp[\frac{+ze\psi}{kT}] \tag{2}$$

where n_o = concentration of ionic species in the bulk, $ze\psi$ is the electric potential energy created by each ionic specie, and k and T are Boltzmann's constant and temperature respectively. The net volume charge density, ρ, is given by:

$$\rho = ze[n(+) - n(-)] \quad . \tag{3}$$

The volume charge density can be related to the surface potential by considering Poisson's equation for a geometry of a flat plate, given by:

$$\frac{d^2\psi}{dx^2} = -\frac{\rho}{\varepsilon} \tag{4}$$

where ε is the permittivity of the particle. By combining equations (3) and (4), the

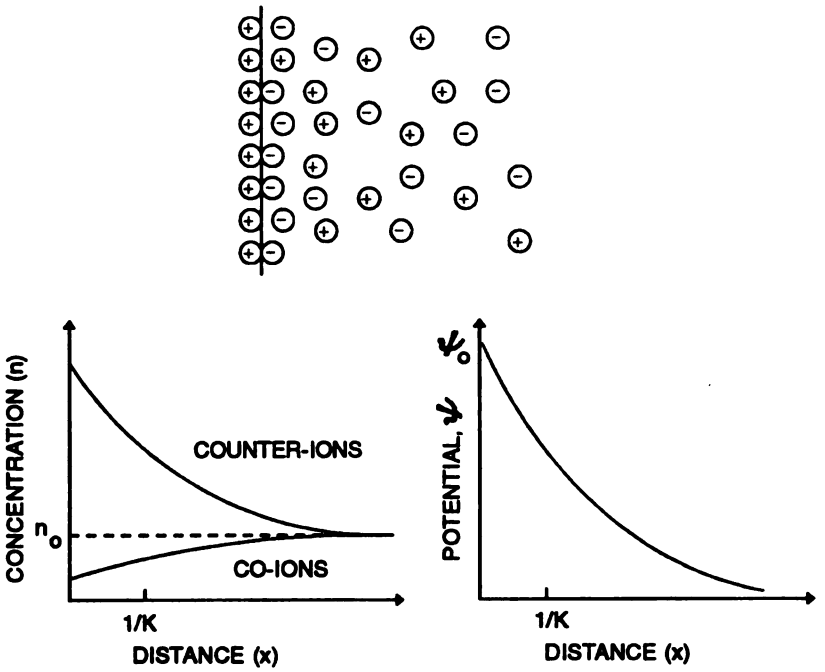

Figure 4. Illustration representing the diffuse electrical double layer.

following expression for relating the surface potential is found:

$$\frac{d^2\psi}{dx^2} = \frac{2zen_o}{\varepsilon}\sinh\frac{ze\psi}{kT} \quad . \tag{5}$$

From this equation, the appropriate boundary conditions can be applied. Using the assumptions of the Gouy and Chapman treatment of the electrical double layer, the appropriate boundary conditions for Equation (5) are as follows: $\psi = \psi_o$ as $x \rightarrow 0$ and $\psi = 0$ as $x \rightarrow \infty$. Applying these conditions to the Laplacian form of equation (5) yields the following relationship:

$$\ln\left[\frac{[\exp\frac{(ze\psi)}{2kT}+1][\exp\frac{(ze\psi_o)}{2kT}-1]}{[\exp\frac{(ze\psi)}{2kT}+1][\exp\frac{(ze\psi_o)}{2kT}+1]}\right] \quad . \tag{6}$$

This equation can then be simplified to the expression for the Gouy-Chapman expression for the variation of the particle potential with respect to distance within the double layer[12]:

$$\gamma = \gamma_o \exp[-\kappa x] \qquad where: \gamma = \frac{[\exp(\frac{ze\psi_o}{2kT})-1]}{[\exp(\frac{ze\psi_o}{2kT})+1]} \quad . \tag{7}$$

For small potentials, i.e. if $ze\psi_o/2kT << 1$, or kT/e = 25.7mV at 25°C, the Debye-Hückel approximation:

$$\exp[\frac{ze\psi_o}{2kT}] = 1 + [\frac{ze\psi_o}{2kT}] \tag{8}$$

can be used to obtain the following relationship

$$\psi = \psi_o \exp(-\kappa x) \tag{9}$$

where:

$$\kappa = [\frac{2e^2 n_o z^2}{\varepsilon kT}]^{\frac{1}{2}} \quad . \tag{10}$$

Equation (8) describes the Debye-Hückel approximation for the Gouy-Chapman treatment of the diffuse double layer. This Arrhenius-type relationship describes the variation in particle potential with respect to distance from the surface. Using the Debye-Hückel approximation, the relationship given in equation (9) only holds for small potentials, $\psi \leq 25.7$mV [12].

The potential ψ_o can be related to the surface charge density by considering the condition of electroneutrality at an interface between the particle and the fluid medium. The total charge contained in a volume element of unit cross sectional area of the diffuse layer must contain the same magnitude of charge, (opposite sign) of that of a unit element of the surface [14]. In simpler terms, the net charge of the diffuse layer is equated with that of the net surface charge of the particle surface. Therefore:

$$\sigma_o = -\int_0^{\infty} \rho \, dx \quad . \tag{11}$$

Applying the Poisson-Boltzmann distribution function and assuming low potentials, Equation (11) reduces to the form:

$$\sigma_o = \varepsilon \kappa \psi_o \quad . \tag{12}$$

This treatment provides an adequate approximation for a distribution of an "ion-cloud" around a specific particle immersed in a fluid medium, but it does not account for a problem that arises due to the stated assumptions. Primarily, at increased magnitudes of surface potential, the net charge density calculations become so unrealistic that it can no longer be assumed that the ions may be effectively treated as point charges. As the charge density increases at the surface, it is then assumed that the ions have some characteristic ionic volume [12,14]. Stern [12,13,14] examined the problems associated with the assumption of point-charge ions and devised a new geometric interpretation of the diffuse layer model. He proposed a model which divided the aqueous fluid medium into two layers: the diffuse layer and the Stern layer.

The interface between the Stern layer and the diffuse layer arises from the stipulation that there are two basic types of ionic species present in the electrical double layer. These include physisorbed ions and chemisorbed ions. Physically adsorbed ions, or physisorbed ions, are classified as any ionic species which are held to the surface by relatively weaker, physical bonds. Chemically adsorbed ions, or

chemisorbed ions, are any ionic specie which is attached to the particle surface by stronger chemical bonds. Chemisorbed ions are also commonly known as specifically absorbed ions. Both ionic species as either potential determining ions or indifferent electrolyte ions. The Stern model holds that particles do not remain still while suspended in a fluid medium. Particle motion results from a variety of forces including: (1) gravitational forces obeying Stoke's law, (2) convective forces due to thermal gradients, and (3) particle-particle interactions caused by Brownian motion. Therefore, Stern was able to assume that due to the existence of two types of ionic species and given the unrealistic charge density values obtainable through the Gouy-Chapman treatment, there must exist a layer which separates those ions which are attached, (or which determine the potential) and those that remain behind as the particle moves through an aqueous medium. Stern also assumed that there existed a Langmuir adsorption isotherm [14] that adequately described the mono-layer (Stern layer) adsorption of specifically potential determining ions.

The major difference between the Gouy-Chapman and Stern treatments for the electric double layer is that the potential, ψ_o, is measured at the interface between the Stern layer and the diffuse double layer, whereas for the Gouy-Chapman treatment, the potential, ψ_o, is evaluated directly on the particle surface. This Stern/diffuse layer interface is located at a characteristic distance, δ, as shown in Figure 6. The characteristic potential at that interface is denoted as ψ_δ. Assuming that only the specific adsorption of counter-ions exists, the following equation can be generated which describes the surface charge density within the Stern layer [14]:

$$\sigma_s = \frac{\sigma_m}{1 + \frac{N_A}{n_o \nu_m} \exp\left[\frac{ze\psi_d + \phi_o}{kT}\right]} \tag{13}$$

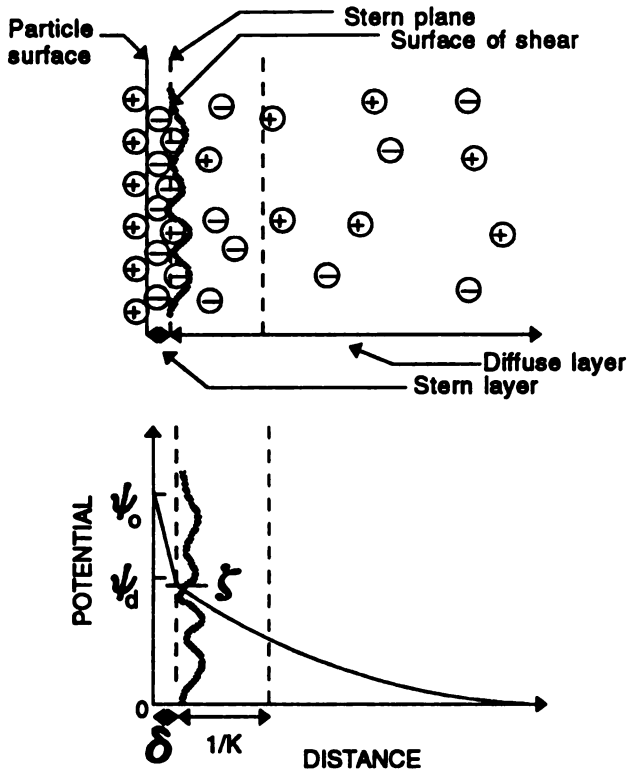

Figure 5. Illustration representing the electrical double layer with respect to Stern's Theory.

where σ_s is the surface charge density at the Stern layer, σ_m is the surface charge density associated with the Langmuir-type adsorption of counter-ions within a mono-layer, V_m is the molar volume of the solvent, and ϕ is the specific chemical interaction energy [12,13,14]. Therefore, assuming that electroneutrality exists throughout the entire double layer, the sum of each surface charge density, charge density for the particle surface, charge density for the Stern layer and the charge density for the diffuse layer will equal zero. Thus the following mathematical expression for the Stern model of the double layer can be obtained:

$$\frac{\varepsilon}{\delta}(\phi_o-\phi_d)+\frac{\sigma_m}{1+\frac{N_A}{n_o V_m}\exp[\frac{ze\phi_d+\phi_o}{kT}]}-(8n_o\varepsilon kT)^{\frac{1}{2}}\sinh\frac{ze\phi_d}{2kT}=0 \quad . \tag{14}$$

Heimenz [14] states that although the model proposed by Stern does accommodate the specific adsorption of ions, it also generates a number of difficulties. Most importantly, the complexity of the description of the variation of potential with respect to distance from the particle surface is dramatically increased when applying Stern's treatment to that of Gouy and Chapman for the electrical double layer. This is brought about by the added number of variables that must be considered during the treatment. In addition, it becomes unclear as to what exactly is physically defined by the characteristic distance, δ. Furthermore, it is uncertain as to where the potential, ψ is actually evaluated. In the design of the FED system, the main parameter of concern is this evaluated potential located somewhere within the Stern layer, known as the zeta potential (ζ).

As was previously illustrated, there exists a characteristic potential which is inherent to the electrical double layer surrounding a particle suspended in a fluid medium. The location and definition of this "potential" varies with respect to location from the particle surface. ψ_o is defined as the potential located at the particle surface. As was shown in Figure 5, there also exists a potential ψ_D which is defined as the potential at the plane separating the specifically adsorbed ions with those that are not. This plane of specifically adsorbed ions is also known as the Stern plane. Thus ψ_b is denoted as the Stern potential. In the same manner as the Stern plane was defined, the surface of shear is defined as the imaginary plane which separates the ions which remain attached to the particle surface and ions that are released as the particle moves through the fluid medium. The potential inherent to this "surface of shear" is defined as ζ, the zeta potential. As will be shown in the next section, it is the zeta potential, ζ, with which we are particularly interested in defining in order to ultimately characterize the degree of heterogeneous attraction between the Fe40Al intermetallic powder and the Al_2O_3 continuous fiber.

Electrokinetic Phenomena

In the previous section, it was shown that when a charged particle is immersed into a fluid medium, it acquires a characteristic "ionic cloud" which is defined as the electrical double layer. This double layer arises from the observation that the ionic distribution around the surface of the particle consists of differing types of ions. These ions are either specifically adsorbed to the surface and comprise the adsorbed layer or Stern layer surrounding the particle, or, they can reside in the a region beyond the Stern layer defined as the diffuse layer. The existence of particle motion within

the fluid medium, causes important changes to this entire ionic region surrounding the particle. As the particle moves through the fluid, attempts are made by the generated fluid forces to remove the ions from the specifically adsorbed layer surrounding the particle surface. As a result of this observation, four phenomena result which comprise what is generally referred to within colloidal theory as electrokinetic phenomena [14,15].

Electrokinetic phenomena is a result of the combination of particle motion and particle electrical effects. As applied to the previous discussion, this phenomena is more accurately defined as the combination of the theory describing the electrical double layer and that of fluid flow. There exists four separate situations which are adequately used to describe electrokinetic phenomena. These include:
(1) electrophoresis, (2) electro-osmosis, (3) streaming potential and (4) sedimentation potential [14]. Electro- phoresis is the phenomenon with which most of the attention has been given with respect to the results contained herein. Specifically, research was performed using electroacoustics which is very similar to electrophoresis.

Electrophoresis describes the movement of a charged particle and it attached ionic layer as is moves through a fluid medium. The movement associated with the particle is caused by the application of an electric field. The main stipulation of this phenomenon is that the velocity caused by the applied electric field is directly proportional to the magnitude of the electric field. The constant of proportionality is commonly defined as μ_e, the electrophoretic mobility. By measuring the electrophoretic mobility, it becomes possible to determine the potential characteristic of the adsorbed ionic layer, ζ, the zeta-potential. The calculation of the zeta potential depends on the shape of the double layer and how the charged particle and its

associated electrical double layer are treated [14].

The electrical double layer is defined by the parameter, $1/\kappa$ or κ^{-1}. This is known as the Debye length, or the distance over which the potential decreases by an exponential factor. Shaw showed that for low potentials the double layer has the same capacity as a parallel plate capacitor with a distance of κ^{-1} between the plates [12,13,14]. This parameter, κ^{-1}, is common referred to as the "thickness" of the double layer as shown in Figure 5. The shape of the double layer can be described by considering the radius of curvature of the particle surface, a, and the characteristic thickness of the double layer, κ^{-1}. With respect to examining the phenomena of electrophoresis, there exist two treatments which account for the different shape that the double layer can have and how this effects the calculation of the zeta potential, ζ. The first case deals with a experimental scenario where κa, the ratio of the radius of curvature to the double layer thickness is small and the second case deals with the inverse of this. For κa small, i.e. a much smaller than $1/\kappa$, the particle may be treated as a point charge. For κa large, i.e. a much larger than $1/\kappa$, the particle surface may be treated as a flat plate. For the case where κa is small, it is considered that Stoke's Law is still applicable even though the particle size is very small.

For κa small, the particle size is much smaller than the length of the double layer. In order to treat this case and generate an expression for the zeta potential as a function of electrophoretic mobility, the physical nature of the motion of the particle through a fluid medium must be considered. By equating the electrical forces with the particle/fluid frictional forces, the following expression is obtained [12,15]:

$$(Q_{NET})E = 6\pi\eta v_e a \qquad (15)$$

where Q_{NET} is the net charge on the particle, E is the magnitude of the applied electric field, η = viscosity, v_e is the electrophoretic velocity and "a" is the radius of curvature. Simplifying eq. (15) gives the following result for the electrophoretic mobility [12,15]:

$$\mu_e = \frac{v_e}{E} = \frac{Q_{NET}}{6\pi\eta a} \tag{16}$$

The zeta potential, ζ, is the calculated resultant between the charge on the particle, $+Q_{NET}$, and the charge on the adsorbed layer, $-Q_{NET}$. Since κa is assumed to be << 1, the following equation is obtained [12,15]:

$$\zeta = \frac{1.5\mu_E\eta}{\varepsilon_o\varepsilon_r} \tag{17}$$

where ε_o and ε_r are the permittivity in vacuum and relative permittivity respectively. Eq. (17) is known as the Hückel equation and is applicable to electrophoresis of non-aqueous media which has a low conductivity. As shown by Shaw, this inapplicability is due to the fact that extremely low electrolytic concentrations are required when using small particle sizes.

For ka large, i.e. for particle size much larger than the thickness of the double-layer, the same basic principles that were previously applied can be used to obtain the Helmholtz-Smoluchowski equation for zeta-potential as a function of electrophoretic mobility. This is achieved by equating the electrical and viscous forces generated by the motion of the liquid through the diffuse layer relative to the particle surface.

Thus, as shown by Shaw [12], the expression:

$$E\varepsilon\zeta = \eta v_e \tag{18}$$

or simplified:

$$\mu_e = \frac{v_e}{E} = \frac{\zeta\varepsilon}{\eta} \tag{19}$$

thus the Helmholtz-Smoluchowski equation for zeta potential is obtained:

$$\zeta = \frac{\mu_e \eta}{\varepsilon_o \varepsilon_r} \quad . \tag{20}$$

This equation is valid for aqueous suspensions. It should be pointed out that since there is some discrepancy as to the exact location where the "potential" is measured and to which potential is actually used to characterize the particle, ζ_{shear} is assumed equal to ζ at the Stern/diffuse layer interface.

As applied to the research project specifically, the phenomena examined is known as electroacoustics. The mechanisms by which the zeta-potential is determined are basically concurrent with those which define electrophoresis. The only major difference is that the motion the particle experiences due to the application of an electric field generates a measurable sound wave with a characteristic frequency. The technique commonly used to evaluate the electroacoustical phenomenon is known as Electrokinetic Sonic Amplitude or ESA [17,18,19]. The ESA technique consists of the application of an electric field of some known magnitude, E, to a fluid suspension.

An acoustic wave is generated by the back-and-forth motion of the particles though the electric field. This motion is caused by the charge and density differences between the particles and the fluid medium. The ESA then measures the amplitude of the pressure generated per unit electric field. This measured quantity is given in terms of the calculated dynamic mobility, $\mu_D(\omega)$, such that:

$$\mu_d(\omega) = \frac{ESA(\omega)}{\phi \Delta \rho c} \tag{21}$$

where ESA(ω) is the measured angular frequency, ϕ is the volume fraction of particles, $\Delta\rho$ is the density difference and c is the speed of sound within the suspension. The zeta potential is then determined using μ_d and an added correlation factor:

$$\zeta = \frac{\mu_d \eta}{\varepsilon_o \varepsilon_r} |G(\alpha^{-1})| \tag{22}$$

where:

$$\alpha = \frac{\omega a^2 \rho}{\nu} \quad . \tag{23}$$

From this technique, it is possible to characterize the zeta potential in terms of dynamic mobility associated with the sound wave generation. Once an understanding has been achieved regrading the determination of the zeta potential, this parameter, ζ, which is inherent to the particular solution and conditions surrounding it, can be used

to further describe the solution. This description extends to the determination of the attractive and repulsive forces which dictate the stability and lack-there-of for all colloidal suspensions. By ultimately understanding the forces present within the suspension, it becomes possible to control these parameters in order achieve the goal of producing a binder-less composite material. Before proceeding into a discussion regarding the forces present within a colloidal suspension, attention must be given to the understanding of suspension stability.

The most important property associated with colloidal processing is the stability of the suspension. The stability of the suspension is characterized by the amount of coagulation that takes place within the system. Coagulation can be defined as the formation of agglomerates, or bundles, comprised of the individual particles. If these agglomerates form, the system is considered to be unstable. Colloidal coagulation is considered a rate process, therefore it is important to analyze and understand the rate of coagulation of a colloidal system, rather than being concerned as to whether the agglomerates form or not.

With respect to suspension stability, there exists two classifications of suspension solutions, or, sols. These are lyophilic and lyophobic sols [12]. Lyophilic sols include all sols which are stabilized by and have a strong affinity for the liquid medium within which it is dispersed. On the other hand, lyophobic solutions refer to sols which have little affinity for and are not stabilized by the liquid medium within which they are dispersed. As pertaining to the processing of IMCs, the solutions or sols used are lophobic. Therefore, the stabilizing of the suspension must be achieved by modeling the forces inherent to the dispersed particles. The exists two basic force regimes which affect the stability of a colloidal system. These forces include an

attractive forces, which results from the existence of universal long-range forces known as van der Waals and London forces, and a repulsive force, generated by the interaction and overlapping of electrical double layers. The theories based on the existence of these two force regimes is commonly grouped in a cumulative theory known as the DLVO theory. The DLVO theory, named for the persons responsible for its development, Deraguin, Landau, Verwey, and Overbeek, is the culmination of individual research combined to describe to effects of interaction between two particles. The basis for the theory is the evaluation of the total interaction energy in terms of interparticle distance. In order to apply this theory to the situation of a multicomponent system, a model for representing two unequal spheres will be presented at the conclusion of the discussion regrading the DLVO theory [12,13,14,21,33].

The first principle of the DLVO theory is that the particles have a characteristic double layer. This double layer is the combination of a rigidly held inner layer, known as the Stern layer, and a diffuse "outer" layer both of which obey a Boltzmann distribution of point-like charges. The second principle of the DLVO theory is that the total particle interaction energy is described by following relation:

$$V_T = V_R + V_A \tag{24}$$

where: V_T = the total energy associated with the particle interaction, V_A = energy of attraction, and V_R = energy of repulsion. Therefore, an evaluation of each of these terms is required in order to produce a relation between the total particle energy and the relative distance between them.

As pertaining to attraction between particles, there exist three basic forces which are encountered in colloidal theory. These include Debye, Keesom, and London interaction [14]. It is the relative contribution of these forces which comprise the energy of attraction V_A. An expression for V_A was developed by Hamaker in 1937. Hamaker was able to assume that at very close ranges the London attractive forces would predominate. This is due to the fact that at close range the attractive force varies inversely to a power of 6 with respect to interparticle separation. Therefore the following equation was generated by Hamaker:

$$V_A = \left(\frac{-Aa}{12H}\right) \tag{25}$$

where A = Hamaker constant, a = particle radius, and H = interparticle distance. The DLVO theory generates an expression for the repulsive energy of interaction for two identical spherical particles by using the poisson equation for the flow of an electric field in a dielectric medium, given by [12]:

$$\nabla^2 \phi = -\frac{\rho}{\varepsilon_0 \varepsilon_r} \tag{26}$$

where ρ is the net charge density and ε_o and ε_r are the permittivities in a free space and a vacuum respectively. By applying the previously defined Boltzmann equation for the distribution of charges within the diffuse double layer, given by:

$$n_i = n_i^o \exp\left[\frac{-\omega_i}{kT}\right] \quad . \tag{27}$$

With $\omega \cong z_i e\psi$, the net charge density,ρ, becomes [12]:

$$\rho = \sum n_i^{\circ} \exp[\frac{-z_i e\psi}{kT}] \quad . \tag{28}$$

Combining equations (26) and (28), and simplifying using the previously defined Debye-Hückel approximation, ($\psi \leq 25$mV @ 25°C), gives [12]:

$$\nabla^2\psi = -\frac{1}{\varepsilon_o \varepsilon_r} \sum n_i^{\circ} z_i e - \frac{\sum z_i^2 e^2 n_i^2 \psi}{kT} \quad . \tag{29}$$

Assuming electroneutrality in a bulk medium:

$$\nabla^2\psi = \frac{1}{\varepsilon_o \varepsilon_r} [\frac{\sum z_i^2 e^2 n_i^{\circ} \psi}{kT}] \quad . \tag{30}$$

Assuming boundary conditions which describe a one dimensional, linear situation:

$$\psi \to \phi_o \; as \; x \to 0 \; \wedge \; \psi \to 0 \; as \; x \to \infty \quad . \tag{31}$$

An expression for the potential, ψ, is obtained:

$$\psi = \psi_o \exp(-\kappa x) \tag{32}$$

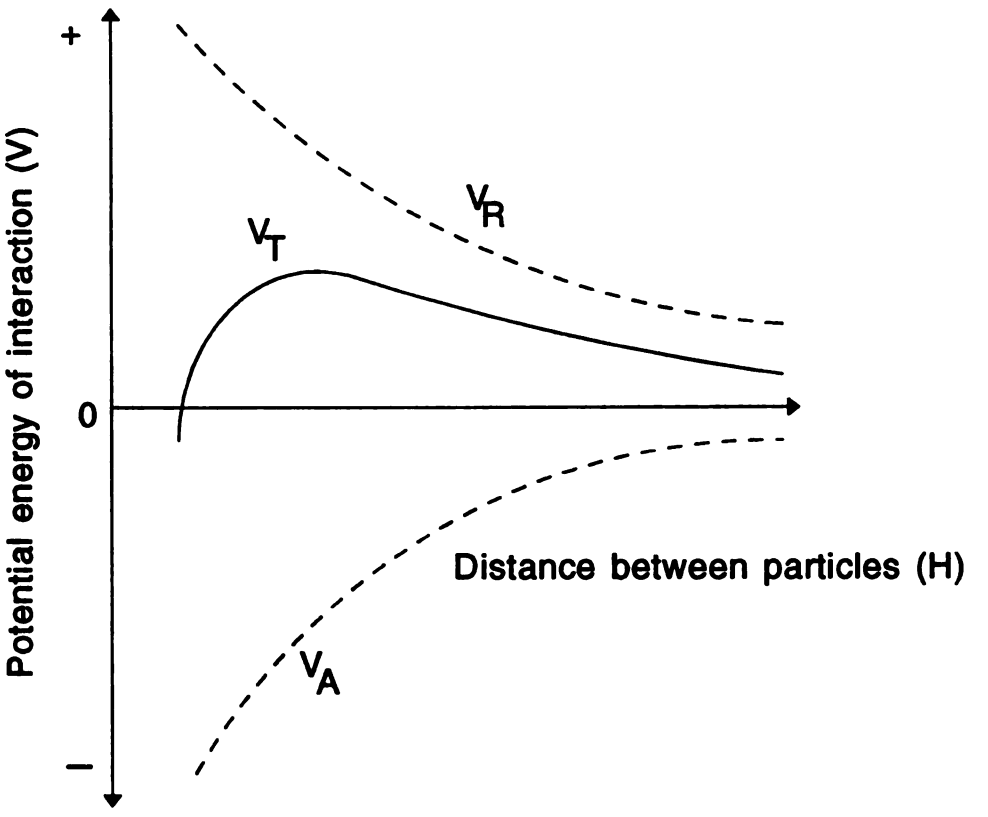

Figure 6. Graphical representation of the total energy of interaction, V_T, obtained by the summation of the energy of repulsion and attraction curves, V_R and V_A.

where:

$$\kappa = \sqrt{\frac{e^2 \sum n_i^o z_i^2}{kT}} \quad . \tag{33}$$

Deraguin used this result to obtain the following expression for the repulsive energy of interaction, V_R:

$$V_r = 2\varepsilon_o \varepsilon_r \psi^2 \ln[1 + \exp(-\kappa H_o)] \tag{34}$$

where H_o is the shortest interparticle distance. By combining the previously derived expression for V_A and V_R, and expression for the total energy of interaction is obtained for a single component system. Stability of the system is then indicated by graphing the potential energy, V_T, versus the particle separation, H. The condition of stability is indicated by the existence of a potential barrier, V_T, of at least 20-25kT.

Expanding the results of the DLVO theory, Hogg, Healy, and Furstenau developed a quantitative kinetic theory for stability for multicomponent systems. This theory is commonly referred to as the HHF theory for stability [20]. The HHF theory assumes that only small separations exist and that the particle potentials remain constant. The expanded equation for the attractive energy is given as:

$$V_A = \frac{-A a_1 a_2}{6 a_1 a_2 H} \tag{35}$$

where A = Hamaker constant and a_1 and a_2 are the particle radii of species 1 and 2

respectively. Therefore, evaluation of the Hamaker constant provides the energy associated with interparticle attraction. HHF showed that the ψ_i values are actually considered valid up to 50-60 mV as opposed to ≤25mV as indicated by the DLVO theory. In the same manner as the DLVO showed, Hogg, Healy, and Furstenau generated a relation for the energy of interparticle repulsion, V_R, by solving the Laplacian given in equation (30) and applying the following boundary conditions:

$$\psi = \psi_{o1} \; as \; x \rightarrow 0 \; \wedge \; \psi = \psi_{o2} \; as \; x \rightarrow 2d \tag{36}$$

By solving the Laplacian, the following relation for potential is obtained:

$$\psi = \psi_{o1} cosh(\kappa x) + \frac{(\psi_{o2} - \psi_{o1} cosh(2\kappa d))}{sinh(2\kappa d)} \tag{37}$$

Therefore using the equation given by Deraguin [21] for the interparticle repulsion energy for a single component system:

$$V_R = \varepsilon_o \varepsilon_r \pi \frac{a_1 a_2}{(a_1 + a_2)} (\psi_{01}^2 + \psi_{02}^2)[\frac{2\psi_{o1}\psi_{o2}}{\psi_{o1}^2 \psi_{o2}^2} \ln \frac{1 + \exp(-\kappa H)}{1 - \exp(-\kappa H)} + \ln(1 - \exp(-2\kappa H))] \tag{38}$$

The combination of the two components, V_A and V_R, gives and expression for the total energy of the system.

The stability for a system of non-identical particles is indicated by the stability ratio of the system. The stability ratio, W_T, is defined as the ratio of particle collisions to collisions resulting in coagulation. For a single component system:

$$W = 2a\int_{2a}^{\infty}\exp(\frac{V_T}{kT})\frac{dr}{r_2} \tag{39}$$

Expanding to include a multicomponent system:

$$W_{ij} = (a_i + a_j)\int_{2a}^{\infty}\exp(\frac{V_T}{kT})\frac{dR}{r^2} \tag{40}$$

Hogg, Healy, and Furstenau [20] integrated and applied this to show:

$$W_T = [\frac{n^2}{W_{11}} + \frac{(1-n)^2}{W_{22}} + \frac{2n(1-n)}{W_{12}}]^{-1} \quad . \tag{41}$$

HHF theory provides the best quantitative prediction for the stability of a multicomponent system. This is primarily attributed to the ability to make adjustments to improve the stability prediction. As applied to the analyzed multi-component system contained herein, it is possible to use the zeta-potential, ζ, to characterize the the component interaction. The only requirements for determining the ζ-potential are prior knowledge of the particle size and the surface charge density. Therefore, with respect to the research contained within, the H^+ and OH^- ions are considered the potential determining ions and the ζ-potential is measured as a function of the relative change in pH. For a change in concentration, the surface charge changes and therefore the ζ-potential changes. By calculating the ζ-potential and then assuming

that $\zeta=\psi$, the stability of the system can be characterized. A system is considered stable for W_T values $\geq 10^{10}$ or for log(W) = 10 [13].

Material Selection

The demand for high-performance materials which can accommodate the requirements for high temperature aerospace applications has steadily increased over the last decade. The immergence of high performance materials represents a new age of materials applications, where weight savings and increased structural integrity are primary design criteria. With this increasing demand, intermetallic alloys have become possible candidates. The majority of ongoing research has focused on the intermetallic aluminides, specifically the $L1_2$ ordered aluminides, titanium aluminides, and the B2 ordered aluminides. Of particular interest to high performance applications is the B2 ordered intermetallics, due to their low densities, high melting temperatures, and good environmental resistance.

A few alloys which are included within the B2 intermetallic system are FeAl, NiAl and CoAl. Each of these alloys exhibits the B2 crystal structure or ordered BCC, where the Al atom occupies the body-centered position and the Fe, Ni and Co atoms occupy the corner atoms for each of their respective systems. The most advantageous characteristic of the B2 aluminides is that they have relatively low densities and high melting temperatures as shown in Table 1.

In addition to these characteristics, the B2 aluminides also exhibit excellent oxidation resistance. Although these materials exhibit very desirable properties, as monolithic materials, they do not represent the complete solution to high performance applications. In addition to lacking high strength characteristics at elevated

Table 1. Component Properties

Material	Density (g/cc)	Melting Temp. (K)
FeAl	5.56	1724
NiAl	6.07	1921

temperatures, the B2 aluminides also lack ductility, toughness and creep strength at low temperatures. Due to the intrinsic brittle behavior of these materials, it has been of major research interest to investigate the effects of alloying additions such as Zr and B to improve the ductility [22,23,24]. Aoki and Izumi showed that by adding up to 1000ppm of boron to Ni_3Al provides up to 50% elongation [25]. Therefore, the main focus in intermetallic research is the improvement of the materials strength and toughness over the wide range of possible operating temperatures. In order to accomplish this, a reinforcement material is required to alleviate the problems associated with the monolithic intermetallics.

There exists two major criteria for selecting a suitable reinforcing material to be incorporated to form a composite system. These criteria include the need for both chemical compatibility and a suitable coefficient of thermal expansion, CTE, between the fiber and the matrix. The need for chemical compatibility arises due to the expected high temperature environments that can provide for extreme changes in the reaction rate kinetics subsequently degrading the reinforcing material and altering the composite properties [8]. The need for an acceptable match between the CTE's for both the fiber and the matrix is apparent since the associated operating range and

thermal gradients are very large. Improperly matched components can generate thermal stress cracking and cause system degradation.

At elevated temperature conditions, the reinforcement can exhibit three basic types of behavior. These include: highly reactive, partially reactive and non-reactive behavior [26]. A highly reactive reinforcement will allow a large amount of reaction product to form. Subsequently, a partially reactive product will also allow a reaction product to form, but the extent to which this happens is significantly less. This is due to the reduction in the reaction rate kinetics. Both of these types of reinforcement behavior produce detrimental effects due to the degradation and reduced effectiveness of the reinforcement. The non-reactive behavior prohibits any interdiffusion of constituents or the formation of reaction products [26]. The reaction rates and chemical compatibility are not only a concern with respect to the operating temperatures of the material but they are also a concern during processing where elevated temperatures are characteristic of many consolidation processes.

Shah, Anton and Musson [22] performed a compatibility study which examined several possible intermetallic matrix materials coupled with several reinforcing candidates. Some of the intermetallics examined included NiAl from the B2 aluminide group and (Nb, Ti)$_2$Al and (Nb, Ti)Al$_2$ from the ternary titanium aluminide group. The several reinforcing candidates used included Al_2O_3, SiC, TiC, Si_3N_4 and Y_2O_3. The primary objective of the compatibility study was to vacuum hot press several fiber/matrix samples and characterize each microstructure in terms of porosity, fiber damage, uniformity and the matrix/reinforcement reaction zone. From their work, Shah et al concluded that in terms of chemically stable reinforcing material, Dupont FP Al_2O_3 and Saphikon fibers represented the best possible candidates for use with

most intermetallic systems [22].

Draper, Gaydosh and Nathal performed a similar study which examined the chemical and thermodynamic stability of various fibers with an Fe-40at%Al matrix material. Using thermodynamic calculations to determine the reaction mode of the system, Draper et al were able to determine whether the selected reinforcement was compatible with the Fe-40Al matrix. A summary of results from the thermodynamic calculations can be found in Table 2 [23].

Table 2. Thermodynamic Calculations and Compatibility Results

Fiber	Reaction Mode	Compatible?
SiC	Forms FeSi and Al_4C_3	No
B_4C-B	Forms FeB and free Carbon	No
Al_2O_3	No reaction	Yes
W	Solubility of W in Fe-40Al = 2% at 1500K Solubility of Al, Fe in W = 2.7%Al, 0.5% Fe	Yes
MoHfC	Forms Mo_3Al	No

Upon performing a heat treatment and microstructural analysis of each system, the Al_2O_3 fibers produced no reaction product with the Fe-40Al matrix even at a heat treat of 1500K at 25 hours, thus agreeing with the corresponding thermodynamic calculations. Of the possible reinforcements examined, only the W and Al_2O_3 fibers provided chemical compatibility. The existence of Kirkendal porosity and high density of W limits the usefulness of W in the W/Fe-40Al composite system. Therefore, the

most suitable reinforcing fiber for use with Fe-40Al is Al_2O_3 due to its chemical compatibility and low density. Al_2O_3 also exhibits a high CTE ($9.4 \times 10^{-6}\ K^{-1}$) as compared to W ($5.3 \times 10^{-6}\ K^{-1}$). The CTE for Al_2O_3 also more closely matches that of Fe-40Al ($21.8 \times 10^{-6}\ K^{-1}$) [23]. Although the expected operating range of most IMC applications will be ~1273k, the mismatch in CTE between Fe-40Al and Al_2O_3 may still be large enough to limit its cyclic thermal fatigue properties. It should be noted here that it is beyond the scope of this research project to provide a solution to the CTE mismatch problem. The focus of this work is to select the most qualified reinforcing candidate to be incorporated into a composite system which utilizes electrokinetic phenomena to provide a binder-less, continuously reinforced, multi-component system. A summary of the selected materials is given in Table 3.

Table 3. Selected Materials

Material	Melting Temp. (C)	CTE (1000 C)
Al_2O_3	2050	$9.4 \times 10^{-6}\ K^{-1}$
Fe-40Al	1451	$21.8 \times 10^{-6}\ K^{-1}$

Filament Winding

As was previously discussed, there exists a variety of methods for the manufacture and consolidation of intermetallic matrix composites. The selection and implementation of a particular method depends on several variables associated with each components of the composite system. Since the application presented here involves the design and manufacture of a continuously reinforced IMC, the selection process becomes limited. A widely accepted method for the manufacture of

composites which incorporate the use of continuous reinforcement is that of filament winding [7,27]. Filament winding basically consists of a fiber source which is wound continuously around a mandrel, whose motion is controlled by a movable cross-head. The basic instrumentation of a typical winding system is illustrated in Figure 7. The filament winding process consists of two different method in which composites are formed. These include dry and wet filament winding. Dry filament winding consists of winding a fiber or tow which has previously been processed in order to attach the matrix material onto the fiber. This process is commonly referred to as pre-impregnation and consequently the winding medium is referred to as a preimpregnated tow, or "prepreg-tow." The general purpose for using this type of method is to provide specific geometries and shapes of parts by adjusting the variables associated with traditional winding principles. Wet filament winding consists of incorporating the impregnation process and the winding process into one system in order to produce a composite green body for manufacture using a variety of consolidation process mentioned previously. The system which has been designed for the manufacture of IMCs using fiber electrophoretic deposition will implement the principles associated with wet filament winding since it is the purpose of this project to incorporate a novel technique for generating a pre-impregnated tow with traditional winding practices.

The most important variables associated with the wet filament winding process are the rotational speed of the mandrel and the relative speed of the cross-head. The degree to which the fiber is impregnated depends on the length of time it is allowed to remain in the impregnation chamber. It is necessary to control the winding speed in order to produce sufficient impregnation of the fiber prior to being wound onto the

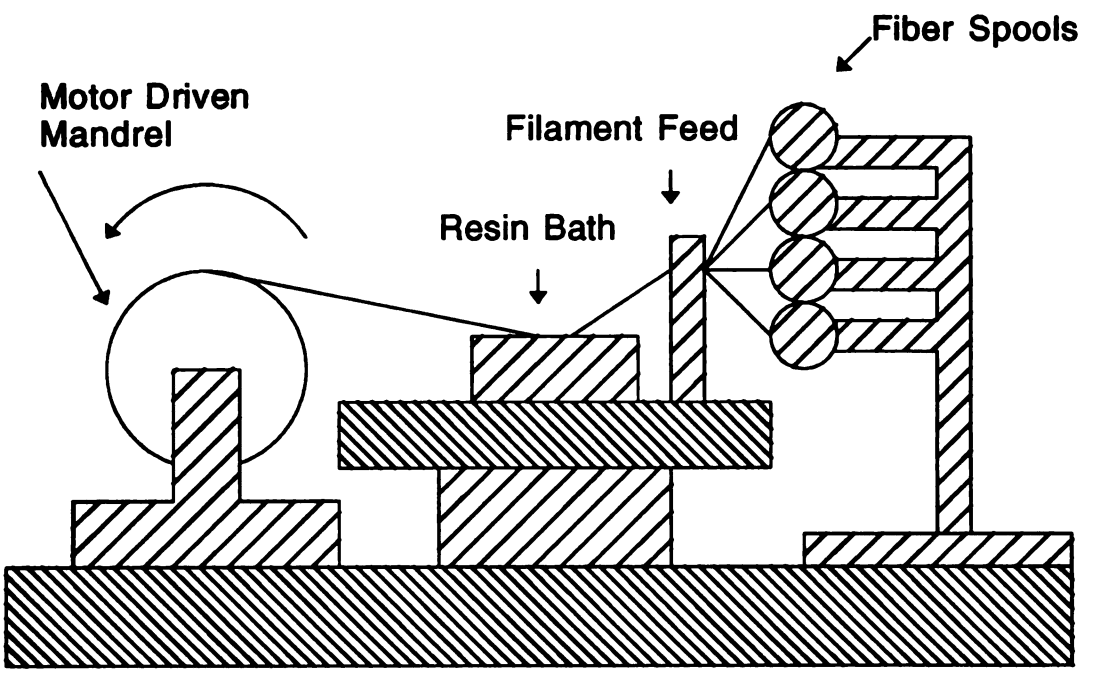

Figure 7. Basic filament winding system.

mandrel. The geometry and properties of the composite are controlled by the relative size and shape of the mandrel onto which the tow is wound. The typical size range for composite parts produced via filament winding can be as small as 1" (25mm) or as large as 20'(6m) [27]. The specific details associated with these controlling parameters will be given more detailed attention when the design of the winding system is presented later.

EXPERIMENTAL PROCEDURE

In order to design and develop an acceptable process for the production of IMC specimens utilizing the FED process previously described, it is necessary to consider the parameters involved. The outline for developing the FED technique includes five experimental topics. These include: (1) particle size analysis, (2) evaluation of the processing parameters involved, (3) comparison of system component behavior using the electrophoretic Sonic Amplitude (ESA) measurement technique, (4) experimental examination of the FP Al_2O_3 continuous fiber with the FeAl intermetallic matrix, and (5) design and development of the FED continuous winding system.

Particle Size Analysis and Reduction

During the course of this research project two batches of Fe-40Al intermetallic particles were utilized. The preliminary results for this project were obtained using a powder that was produced by Alloy Metals, Inc. of Troy, MI and supplied by Professor K.M. Vedula at Iowa State University. The powder provided was a gas atomized raw powder in an 80-mesh (150μm > diameter > 0.1μm) size range. Upon initial examination, it was readily apparent that due to the fact that the FP fiber strands consisted of individual fibers with an average diameter of 20-30 microns, adequate coating could not be achieved using the FeAl powder in its raw form. Previously, an

attempt had been made by Glime to reduce the particle size via a dry sieving technique which implemented the use of a ro-tap shaker and standard 3 inch ASTM screens supplied by Endecotts, Ltd., London, England, in sizes of 63, 38, 15 and 5μm. This method proved inadequate due to the large time commitment and relatively low yield percentage. A new technique was then developed for reducing the particle size in a more efficient manner.

With the use of the raw Fe-40Al powder a suitable size range had to be chosen. The range chosen for this powder was $10\mu m > d > 0.1\mu m$. This particular range was chosen for a variety of reasons. First an upper limit had to be established which would guarantee that the gravitational forces involved would not offset the colloidal forces which are required for adequate coating of the fiber. Second, a size distribution had to be chosen that would provide a narrow distribution so that not only would the particle/fiber interactions be maximized, but the stability problems associated with having a wide size range avoided. In addition to this, a more uniform coating of the particles around the fiber could be achieved. Therefore, since the average fiber diameter for the FP fiber is 20-30μm, it was assumed that a ceiling limit of 10μm for the matrix particle size range would be suitable for this particular raw powder. This limit met both the demands for a small enough particle for coating and a size range narrow enough for maximizing interactions. The specifics associated with the selection of this size range will be expanded during the discussion of the composite processing parameters.

The particle size reduction technique developed for this project incorporated the use of natural sedimentation coupled with high frequency sonication and vacuum

assisted filtering. The following equation was used which describes the motion of a particle in a fluid medium, as given by Stoke's Law [28]:

$$V = \frac{g(\rho - \rho_f)x^2}{18\eta} \tag{42}$$

where V = particle velocity, g = gravitational constant, ρ = particle density, ρ_f = fluid density, η = viscosity of fluid medium, and x = particle diameter
The following values were then used to determine the velocity of a 10μm particle in a fluid medium of doubly-deionized water:

ρ_{WATER} at 25°C = 0.99707 g/mL

ρ_{Au} = 5.56 g/cc

η_{WATER} = 0.8904cp (cp = centipoise = gm/[(9cm)(sec)(10^2) .

From Equation 42, V = 2.79 x 10^{-4} m/s. Once the particle velocity is known for the particular fluid medium, an average falling depth, y_{AVE} and sedimentation time, t, can be calculated relative to the size of the container used. This was accomplished by incorporating the result from Equation 42 and performing the following calculation:

y_{AVE} = 40 x 10^{-2}m

$V = (y_{AVE})/(t)$

t = 143.37s .

It should be noted that y_{AVE} is defined as half of the total falling height for a particle that begin sedimentation at the surface of the container. The value for y_{AVE} is used instead of y (total falling height) because the settling time, t, must not only account for particles which begin their decent somewhere between the surface and the bottom of the medium, but also those particles which begin their decent at the surface. This is a safety measure to insure that once the sedimentation time, t, for a 10μm has elapsed, there will exist no particles larger than those specified within the given falling length, y_{AVE}.

Once the values for y_{AVE} and t are known, a suspension with a desired amount of powder is then mixed and sonicated using a high frequency ultrasonic probe. The ultrasonic probe is used in conjunction with any mixing steps performed within this research project. The sonication provides an initial even dispersion by eliminating any flocculation which may have been present prior to the mixing operation. Once the sonication has been performed, the sedimentation time, t, is allowed to elapse. The amount of suspension corresponding to y_{AVE} is then drained into a cellulose membrane filter container. The de-ionized water is then draw off by applying a vacuum of approximately 3.3 - 4.0kPa. The remaining solution is then re-suspended and the process is repeated until it becomes apparent that the re-suspended solution has become supernatant and the solution no longer contains a significant amount of fines, i.e. the amount of solution corresponding to y_{AVE} is essentially clear in appearance. The collected fines are then dried using a tube furnace at a temperature of 110°C for 1 hour and then stored in a vacuum desiccator. Figure 8 gives a schematic illustration of the particle sizing sedimentation process. The powder provided by Alloy Metals, Inc. was previously referred to as raw Fe-40Al powder. Since two powder samples

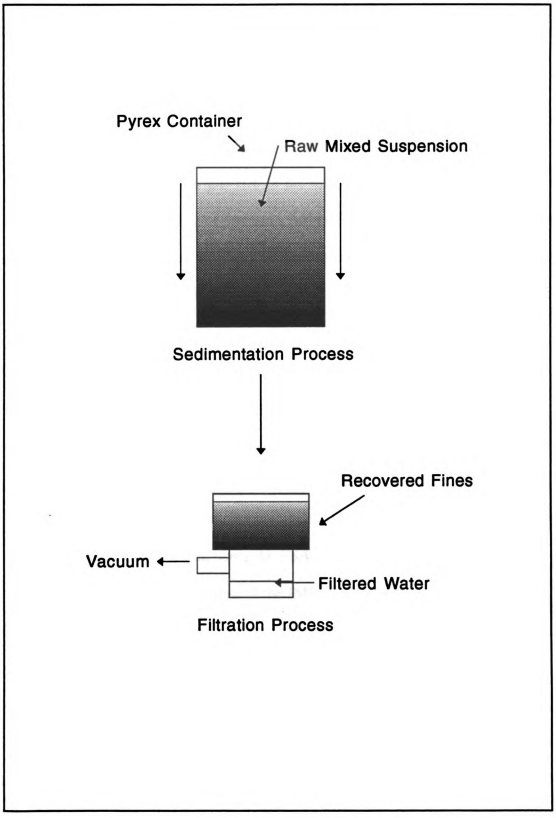

Figure 8. Schematic illustrating the particle size sedimentation technique.

were used during the project, the sedimented powder will be referred to herein as Fe-40AlSED.

For reasons which will be discussed later, it became necessary to implement another Fe-40Al powder for primary use in the composite processing. This specific Fe-40Al powder was donated by Mr. R. Noebe at NASA Lewis Research Center, Cleveland, Ohio. The initial particle size of the as-received was -325 mesh. This corresponds to a screen opening of 44.5μm. Although this particle size is larger than that of the desired size previously stated, it allowed for the continuation of experimental work to include other aspects which had not been possible with the use of the Fe-40AlSED. The reasons surrounding this fact will be discussed in a later section. In order to avoid confusion between the two different powder samples, the Fe-40Al received in the -325 mesh form will be referred herein as Fe-40Al325.

Processing Parameters

Before being able to accurately examine the colloidal forces which are inherent to an aqueous particle suspension using the ESA measurement technique, two main parameters associated with processing of the IMC composite system had to be evaluated. Two major processing parameters are related directly to the colloidal application within this system. The first parameter which was evaluated was the critical coagulation concentration or c.c.c. of the suspended Fe-40Al matrix particles. The second parameter which was analyzed was the "effective" particle size of the Fe-40Al matrix particles. The term "effective" refers to the size of the particles while they are suspended in the aqueous solution. By examining these two parameters, the conditions under which the experimental data is taken are optimized.

The procedure used for determining the c.c.c. for the Fe-40Al aqueous suspension was derived from the commonly known Shultz-Hardy Rule [13]. The critical coagulation concentration refers to the concentration of the electrolyte in the aqueous solution that will give way to rapid coagulation. As was discussed in the section on colloidal theory, a pair or more of particles will flocculate or attract when the force of attraction between them is greater than the force of repulsion. Furthermore, it was stated that the force of repulsion that prevents the flocculation of particles is directly related to the length, $1/\kappa$, of the double layer inherent to the individual particles. If the length of the double layer is less extensive than the curvature of the surface, the particle will have a small repulsive force and be susceptible to rapid coagulation or rapid flocculation. Rapid coagulation refers to the elimination of the electrical barrier that previously existed between the particles. Therefore, without this barrier, every collision which is a result of the Brownian motion of the particle, will form a combination of particles, or "floc". By adding a common ion source such as an electrolyte to a solution, the length of the double layer surrounding the particles can be controlled. The higher the concentration of electrolyte, the more compressed the characteristic double layer becomes, thus the probability for coagulation increases. If a solution experiences rapid flocculation, the particles will adhere to one another and "fall-out" of the suspension at a rate far exceeding that given by Stoke's law as related to a single particle. The exact value of the c.c.c. depends on the nature of the sol, the temperature of the environment in and around the sol, the nature of the electrolyte and the electrical charge on the surface of the particles.

The procedure for the determination of the c.c.c. for the Fe-40Al aqueous system was performed by selecting 4 different electrolyte concentrations. These included 0.0001N, 0.001N, 0.01N, and 0.1N. The electrolyte chosen was potassium nitrite or KNO_3 with an atomic weight of 101.1032 g/mole. 200mL solutions of de-ionized water and the corresponding electrolyte concentrations were mixed. The following table lists the concentration and relative amounts of KNO_3 added to the solution:

Table 4. Electrolyte Concentrations

Concentration	Grams needed
0.1N	2.0221g
0.01N	0.2022g
0.001N	0.0202g
0.0001N	0.0020g

Once the four different electrolyte concentrations are mixed the same concentration of powder is added to each 200mL electrolyte solution. For this experiment a 2%o Fe-40Al325 (22.24g/196mL DI H_2O) was added to each solution. After the powder is added, the solution is sonicated, poured into 80 mL glass test tubes, and then allowed to stand in a fixed support for a period of 2 hours. Once the solution has remained undisturbed for the specified time period, it is then re-shaken and returned to its fixed support. Time lapse photographs of the four test tubes are then taken at 5 second intervals. The c.c.c. is then estimated to be between the test tubes for which one attains a supernatant or "clear" state while the other contains particles which remain suspended.

By evaluating the c.c.c., it becomes possible to determine the amount of allowable time in which the processing of the composite can take place. For example, if a solution with a given amount of electrolyte remain suspended then the flocculation kinetics are at a minimum and therefore the matrix suspension will remain dispersed and the settling kinetics can then be estimated by simply considering the upper limit of the matrix particle size distribution and combining with Stoke's law [28]. In addition, the value of the c.c.c. is extremely important when calculating the potentials associated with the system components using the ESA measurement technique. By knowing what concentration of electrolyte to use for a specific component which will produce a stable and dispersed suspension, a greater accuracy in the values obtained from the ESA measurement is achieved due to the minimization of flocculation kinetics. This is primary due to the fact that a major variable involved in the measurement of zeta-potentials using ESA is particle size and if flocculation kinetics are not kept to a minimum, the particle size will change due to the formation of flocs within the system. This particle size change that can occur once a dry powder is dispersed into solution results in a different particle size from that of the dry powder. The particle size of the suspended powder is known as the "effective" particle size. The effective particle size of the suspension is not only a function of c.c.c. but it is also a function of the size range of the particles.

As was stated in the section on colloidal theory, the stability of a system is very dependent on the size range of the particles within the system. For a wide size range, any collisions between very large and very small particles will result in coagulation, thus producing stability ratio with respect to the two particles does not apply. With respect to the systems examined, Fe-40AlSED and Fe-40Al325, the

possibility for even a small amount of flocculation exists between the upper and lower limits of the size ranges. It was also previously stated that since the zeta-potential of a suspension also varies with respect to pH of the suspension the stability of the system, i.e. the number of collision which result in flocculation, is indicated by the change in the effective particle size. Therefore, by being able to evaluate the size of the particles in suspension, an accurate representation of the particle size can be obtained which will subsequently increase the accuracy of the zeta-potential data which will ultimately determine the ideal processing range.

The Malvern Mastersizer provided by the Hydrocyclone Development Consortium was selected to generate the particle size data for both the Fe-40AlSED and the Fe-40AL325. The Malvern obtains its measurement by analyzing the diffracted light from an emitted laser beam through a sample cell which contains an aqueous or non-aqueous suspension. The purpose of this experiment is to not only attempt to examine the flocculation behavior and kinetics associated with changing electrolyte concentration and changing pH values, but also to get an accurate representation of the particle size for use in the ESA measurement of the solution for which the c.c.c. is used. An experiment was set-up in which both powder batches would be analyzed at the same electrolyte concentrations as the c.c.c. calculation was performed at. 3 different pH values (3, 5.5, 8.0) were also selected in an attempt to gain additional understanding of the flocculation kinetics over a range of pH values. The following tables list the different samples measured and give a sample number for each for comparison with the results later. The experimental runs were performed by adding a small amount of Fe-40Al to premixed 200mL solutions containing each different variable mixed with de-ionized water. Prior to the measurement each sample

was sonicated for 1 min.

Before any ESA testing can be performed an accurate particle size has to be generated for each of the components which are to be analyzed. As was stated previously the Fe-40AlSED and Fe-40Al325 samples were analyzed using the Malvern Mastersizer. The particle size for the FP Al_2O_3 was obtained by implementing a simple line intercept technique. The fiber was initially ball-milled for 4 hours in a mixture of Borudum grinding media, provided by Stoneware, Inc., and propanol. At the completion of the milling operation, a 6mm x 6mm piece of carbon tape was inserted into the milling container and a sample of the sized FP Al_2O_3 was taken. This sample was then attached to a metal stage and microscopic examination was performed using the Hitachi S-2500C Scanning Electron Microscope. A grid analysis was performed which produced an array of micrographs which were then analyzed using a line intercept method for determining particle size. The reasons for using a different method for measuring the fiber will be discussed in a later section.

Table 5a. Measurement Variables for Fe-40AlSED

Specimen Number	Variable
FEAL1A	0.0001N KNO_3
FEAL2A	0.001N KNO_3
FEAL3A	0.01N KNO_3
FEAL4A	0.1N KNO_3
FEAL5A	pH = 3.0
FEAL6A	pH = 5.5
FEAL7A	pH = 8.0

Table 5b. Measurement Variables for Fe-40Al325

Specimen Number	Variable
FEAL1B	0.0001N KNO_3
FEAL2B	0.001N KNO_3
FEAL3B	0.01N KNO_3
FEAL4B	0.1N KNO_3
FEAL5B	pH = 3.0
FEAL6B	pH = 5.5
FEAL7B	pH = 8.0

ESA Measurement of System Components

The ideal pH range for processing of the IMC was determined by applying a potentiometric titration using the ESA measurement system from Matec Applied Sciences. During a potentiometric titration the zeta-potential, ζ, is measured with respect to specific pH value. The pH of the system is varied by adding small amounts of nitric acid, HNO_3, to make the suspension more acidic or by adding small amounts of potassium hydroxide, KOH^-. This allows for the measurement to take place over a range of pH values. Once ζ-potential versus pH curves have been generated for both components of the composite system, the stability is calculated using a computer simulation so that an estimation as to the proper pH range for processing can be made.

The potentiometric titration is performed by mixing a specified volume percent of suspension and then selecting a phase reference material. This preliminary operation is performed so that the sign (+,-) of the zeta-potential values obtained during the experiment can be correctly interpreted. For the ESA potentiometric

titration the following criteria regarding the sign interpretation with respect to phase difference of single point zeta-potential values is as follows:

If phase is between:

- -15 to 15 then material is same sign as reference material.
- 165 to 180 or -165 to -180 then the material is of opposite sign.

If the phase measured meets neither of the requirements listed above, then a different reference material must be chosen and the single point measurement repeated until a proper interpretation can be made. Once a proper reference has been chosen, the parameters required for the ESA potentiometric titration can be entered into the system. The following table summarizes the required information and the corresponding values used to perform the potentiometric titration for both the Fe-40AlSED, Fe-40AL325, and FP Al_2O_3.

Table 6. Potentiometric Titration Data

Material	Particle Density	Particle Size	v/o of sample
Fe-40AlSED	5.56g/cc	1.90μm	.2v/o
Fe-40Al325	5.56g/cc	11.90μm	.5v/o
FP Al_2O_3	3.965g/cc	0.53μm	.2v/o

Once these material parameters are entered, the ESA potentiometric titration can take begin. For the components analyzed here, the following tables list the sets of data that were obtained in the terms of ζ-potential versus pH. Each table list the sample numbers of each of the data set(s) and the corresponding titration(s) performed.

The data compiled from the potentiometric titration was then entered into a stability prediction program developed by Wilson and Crimp [15]. The basis for the program is to predict the state of flocculation of the system components. The resulting data from the computer run is compiled in the form of the stability ratios, W_{11}, W_{22}, and W_{12}, where the subscripts 1 and 2 correspond to the different system components. The values for the stability ratios are then plotted graphically with respect to their corresponding pH values. At the completion of both the potentiometric titration and the stability prediction data runs, an estimation can be made of the pH range within which the greatest instability exists between dissimilar materials while at the same time exhibiting stability with respect to like components.

Table 7a. Potentiometric Identification for Fe-40AL325

Sample Numbers	Titration Performed (pH)	Comments
510, 511, 512	3.0⇒10.0, 10.0⇒3.0, 3.0⇒10.0	Mixed at pH = 3.0
513, 514	10.0⇒3.0, 3.0⇒10.0	MIxed at pH = 10.0
515, 516	10.0⇒3.0, 3.0⇒10.0	Redispersed S.N. 523, 514
500, 501, 502	3.0⇒8.0, 8.0⇒3.0, 3.0⇒8.0	Mixed at pH = 7.0
503, 504, 505	3.0⇒12.0, 12.0⇒3.0, 3.0⇒12.0	Redispersed S.N. 500-502

Table 7b. Potentiometric Identification for Fe-40AlSED

Sample Number	Titration Performed (pH)	Comments
550-559	4.0⇒11.0, 11.0⇒4.0	Mixed at pH = 7.0
560, 561	4.0⇒8.3, 8.3⇒4.0	Mixed at pH = 7.0
562-567	4.0⇒7.0, 7.0⇒4.0	Mixed at pH = 7.0

Table 7c. Potentiometric Identification for FP Al_2O_3

Sample Number	Titration Performed (pH)	Comments
530, 531	4.0⇒11.0, 11.0⇒4.0	Mixed at pH = 7.0
532, 533	4.0⇒11.0, 11.0⇒4.0	Mixed at pH = 7.0

Fiber Coating

By using the data obtained from the ESA measurements, an approximate pH range was established for which maximum coating of the FP Al_2O_3 fiber by the Fe-40Al matrix could be achieved. Upon determining this ideal pH range, it was necessary to experimentally verify the results. This was accomplished by performing a series of experiments in which attempts were made to physically coat the fiber strands with the powder matrix. These experiments were initially performed using the Fe-40AlSED powder. The usage of the Fe-40AlSED had to be superceeded, though, due to an extreme shortage of sedimented powder. Preliminary results include the coating experiments using the Fe-40AlSED powder, but the majority of the data includes results from experiments performed using the Fe-40Al325. This was primarily due to the availability and the adequacy of the powder with respect to the experimental work.

The coating experiments were performed by initially cutting 70mm strands of the FP Al_2O_3 fiber. Each individual fiber was approximately 25-30μm in diameter and each bundle contained approximately 70 fibers. A long fiber was laid out on a plexiglass sheet where adhesive was placed over the fiber at 70mm increments. Upon drying the fibers were cut and stored in a vacuum desiccator. A 25v/o suspension was then prepared in a 150mL Pyrex beaker using 166.80g of Fe-40Al in 90mL of de-ionized H_2O. The beaker was then placed on a Corning stirring plate and allowed to

mix using a 1" magnetic stir bar. At this time the pH of the system was monitored using a Fisher Scientific Model Accumet 915 pH meter.

For alteration of the pH value of the suspension, different normalities of acid and base were used. The specific acid and base used for these experiments was nitric acid, (HNO_3), and potassium hydroxide, (KOH^-). For determining the relative weights needed for each of the different normalities, the following conversion was used:

$$molarity \rightarrow \frac{moles\ of\ solute}{liters\ of\ solution}\ x\ atomic\ weight\ x\ liters\ of\ solvent = grams\ of\ solute\ needed$$

To obtain the normality of the solution multiply the molarity by the number of equivalents of the substance or the mass that exactly reacts with the equivalent of another reactant. For each of the reactions for HNO_3 and KOH^-, the number of equivalents is equal to 1 so the number of grams required for a specific normality is equivalent to the weight required by the same molarity. The following table lists the different normalities used of acid and base and the grams needed per 200mL solution. Once the pH of the suspension had stabilized, small quantities of acid were added to bring the pH down to a starting point between pH3.0-pH3.5. Specific pH values were not targeted due to slight variations in the pH values. Prior to the coating of the fibers, the solution was sonicated using a Branson Model 950 sonifier to break any agglomerates that may have formed at the point of mixing. An individually cut fiber bundle was then taken and bent into a semicircular shape and immersed into the suspension for a time period of 20 seconds. The fiber was then placed on a glass slide and labeled. This process was repeated for the entire range of pH = 3.0 to pH = 11.0. Each of the fibers were placed on glass slides and photographed using a 35mm lens to

examine the amount of powder matrix which was carried out of solution by the fiber bundle.

The next experiment performed implemented the use of the Hitachi Model S-2500C Scanning Electron Microscope to characterize the coated fibers at different pH ranges. The procedure for coating the fibers is exactly the same as stated above for the residual coating experiment. Instead of placing the previously immersed fibers onto glass slides, the fibers were clipped at one end and allowed to dry before being placed on a 2" diameter SEM stage. The "dipped" fiber were secured to the stage by first adhering a glass slide to stage using Plyabond brand adhesive. SPI 5006 brand carbon paint was then used to cover the corners of the slide. The fiber(s) were then placed on the glass slide and secured to the stage using Plyabond and carbon paint on the ends of each strand. The stage was then given a 40nm thick gold coating using a gold coating device provided by the Composite Materials and Structures Center,

Table 8. Acid and Base Normalities

Normality	Grams of HNO_3	Grams of KOH^-
0.0001N	0.0013	0.0011
0.001N	0.0126	0.0112
0.01N	0.1260	0.1122
0.1N	1.2603	1.1221

Michigan State University. Pictures characterizing both sufficiently and poorly coated fiber specimens were then taken using the Hitachi Model S-2500C Scanning Electron Microscope.

Fiber Electrophoretic Deposition Winding System Design

In order to successfully produce intermetallic composite green bodies for consolidation, a laboratory-scale winding system was developed. The design and development of this system was dependent on many factors. These factors stemmed from both traditional composite winding practices and those specifically inherent to the electrodeposition procedure. The following procedure will outline those factors which were identified as having the greatest impact in the design and development of the FED winding system.

The behavior of the multi-strand FP filament used in this process is synonymous with most winding process which employ the use of a multiple fiber bundles. The key element in attaching, or impregnating, the desired component to the fiber strand is to allow each of the fiber to act individual, or more simply, to allow the fiber strand to become temporarily separated from the bulk of the filament bundle. The easiest way to insure that this will happen is to provide a means by which the fiber bundle can effectively "lay-down" or spread out during the impregnation process. The most common method for achieving this goal is to allow the fiber bundle to traverse across a series of rolling surface. The more rollers that are included in the system, the more effective the system will be in spreading the fibers out. Thus, the first step in the design of the FED winding system was to produce a roller system which exhibited the configuration shown in Figure 9. The rollers provided were cut from extruded UHDP (Ultra-High Density Polyethylene). This material was chosen due to its availibility, cost and very low coefficient of friction. Stainless steel sealed bearings were countersunk into each end of the rollers and a 5/16" drill rod was used to provide the support at each end. Aluminum supports were then machined and three

fixed

posit

that

exer

this

asse

supp

cho

to t

roll

des

pur

thr

and

the

Th

sup

eas

to t

fixed supports and 1 adjustable support were implemented as illustrated in Figure 9.

Another factor which is required for proper fiber lay-down is the use of positive tension on the fiber tow during operation. It is important to consider the fact that the individual FP fiber strands are relatively fragile and that caution must be exercised when planning to apply a positive tension. A simple method for providing this important variable is accomplished within the design of the filament cartridge assembly shown in Figure 10. 19mm stainless steel bearings were inserted into the support arms which house the 1/2" threaded rod assembly. These bearings were chosen in a larger configuration than normal so as to provide a slight amount of drag to the system thus enhancing the ability for the fibertow to spread out across the rollers.

The third factor considered in developing the FED winding system is the design of a rolling system which can be integrated within the suspension bath. The purpose for integrated roller system is to not only keep the tow constantly flowing through the powder bath but also to aid in guiding the impregnated tow out of the bath and onto a take-up device. The roller cradle designed is shown in Figure 11. Each of the integral rollers are full adjustable with complete angular rotational capabilities. The material used to construct each of the rolling assemblies was virgin Teflon supplied by Almac Plastics Inc., Grand Rapids, Michigan, and was selected due to its ease of cleaning, non-reactivity, and low coefficient of friction. Springs were attached to the corners of [illegible]y in order to provid a convenient means to remove the roller carriage [illegible]eaning, etc.

[illegible]on taken in the design is the take-up device unto which [illegible]s wound. The main objective in the take-up device or

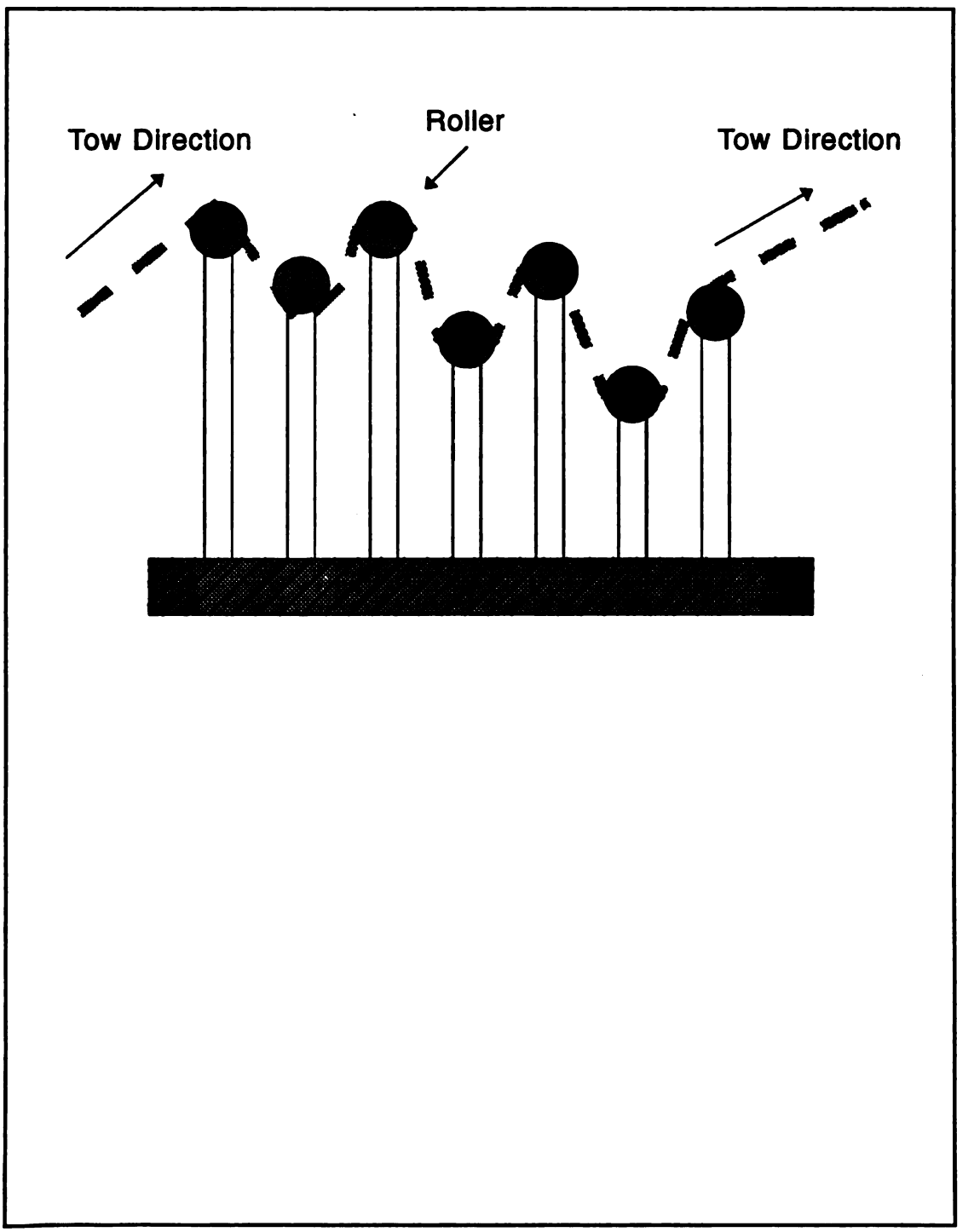

Figure 9. Hypothetical roller setup.

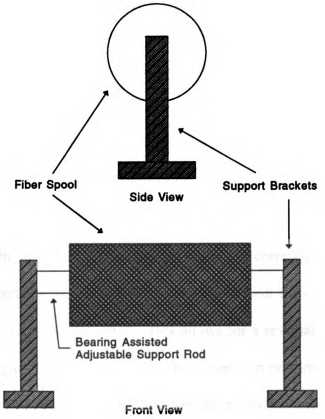

Figure 10. Filament carriage assembly design.

mandrel design is to provide transverse as well as rotational freedom. This insures that the fiber strand can be wound completely around the mandrel in desired interfiber spacings. Virgin Teflon was employed as the mandrel material, for the same reasons as stated above for the other applications, i.e. non-reactivity, low coefficient of friction, etc. The mandrel is supported by a 1/2" bearing supported tool-steel shaft. The rotational movement of the mandrel is provided by a Dayton 0.35A, 12V D.C. motor. The entire rotational assembly is mounted to a plate which is supported by a threaded base. The threaded base, or cross-head provides the transverse motion, which coupled with the rotational motion of the mandrel, generates the necessary winding action. The threaded cross-head is also powered by a 0.35A, 12V D.C.motor providedby Dayton, Inc. To make the production of multi-layer composites, a switching track was installed which takes advantage of the movement of the cross-head by employing the use of two polarized switches. By correctly positioning the switches along the track, the movement of the cross-head will activate each switch every time a transverse run is completed. This allows for a reversal in the polarity of the motors thus changing the direction of the cross-head and provides another complete wind in the opposite direction. A schematic of the proposed mandrel design is shown in Figure 11.

The power for the system is provided by an HPE3612A Dual Range Digital Power Supply. Located on the face plate of the system are the system controls. These include two variable resistors to provide fine adjustment of the rotational and cross-head speed. Another switch is supplied which, when activated, will provide a reversal in the transverse motion, identical to that provided by the two polarized

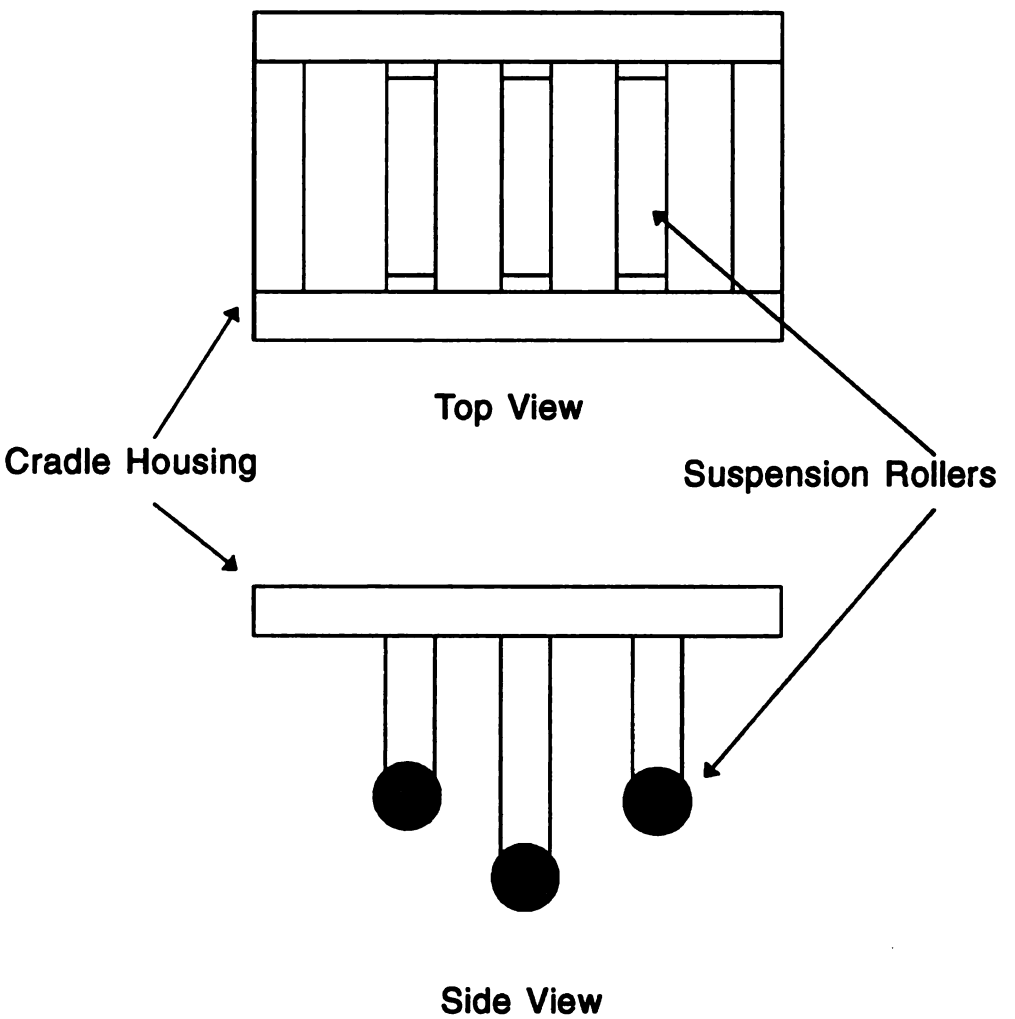

Figure 11b. Fiber cradle assembly.

switches previously discussed. The only remaining switch on the face-plate is an intermediate power switch which allows for the adjustment of the HP power supply prior to the engagement of the motors.

RESULTS AND DISCUSSION

Particle Size Reduction

During the course of this research project, two intermetallic powders were employed. The composition for both intermetallic powders is Fe40Al with 40 atomic percent of aluminum present. The differences between the two powders include the as received condition and small additions of Zr and B used to influence the mechanical deformation behavior. At the outset of the research project the only available intermetallic powder was the raw powder supplied in the by Alloy Metals, Inc. of Troy, MI. This gas atomized pre-alloyed powder was received with a characteristic particle size of 150μm > diameter > 0.1μm. As was previously discussed, the need arose for the reduction of this nominal size to a range more suitable for the electrophoretic deposition of the particle matrix on to the continuous fiber reinforcement. The range initially chosen was 10μm > diameter > 0.1μm. A smaller particle size allows colloidal forces to dominate over the gravitational forces which become a significant factor with the use of large particle sizes. In order to effectively reduce the particle size of the raw Fe-40Al powder, a sedimentation technique was developed and is discussed in detail in the previous section. The SEM micrographs in Figures 11 and 12 show the as-received Fe-40Al powder and the sedimented Fe40Al

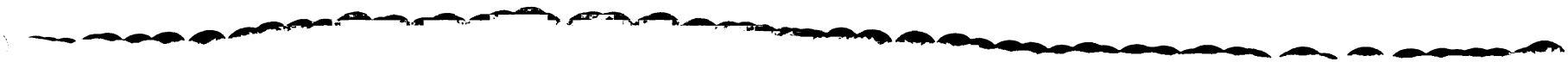

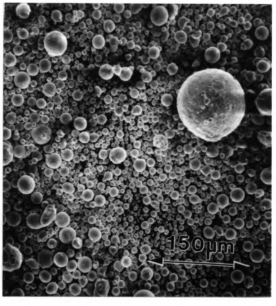

Figure 11b. SEM micrograph of Fe-40AlSED as-received powder.(800X)

Figure 12. SEM micrograph of sedimented Fe-40AlSED powder sample.

powder. The specimens used in the SEM analysis were produced by applying 6mm x 6mm double-sided carbon tape to the powder sample and then removing the excess via compressed air. This sample preparation technique provided for a well grounded system which would prevent charging during examination. In order to determine if a proper particle size range was achieved, a grid analysis was performed. The verification of the correctparticle size was obtained by locating a large sample area in the SEM. This large area was then sectioned into a smaller area in a grid fashion. Each of the smaller areas were then visually examined using the micron marker on the SEM video monitor to verify that the largest particles encountered were within the specified size limit of 10μm. The grid method is illustrated in Figure 13 and two of the eight micrographs which comprise the grid are shown in Figures 14 and 15. As is observed in Figures 14 and 15, the particle size achieved was below the intended size range limit of 10μm.

Although success was achieved and an accurate distribution of Fe-40Al particles was obtained, the developed particle sizing method encountered a number of potential problems. Initially, the sedimented powder was allowed to remain hydrated for extended periods of time, e.g. t > 24hours, and this resulted in a significant color change in the powder. The fact that the powder surface had been altered in some way became readily apparent when immersing the sedimented powder in doubly deionized water and attempting to stabilize the pH. Upon mixing, the suspension would exhibit a consistent tendency to stabilize in the more basic range of pH 10 to pH 11. Any attempts to lower this value to the acidic range would result in the pH of the suspension increasing again towards values of pH10 and pH11. An identical experiment was performed on the raw powder and immediate stabilization was

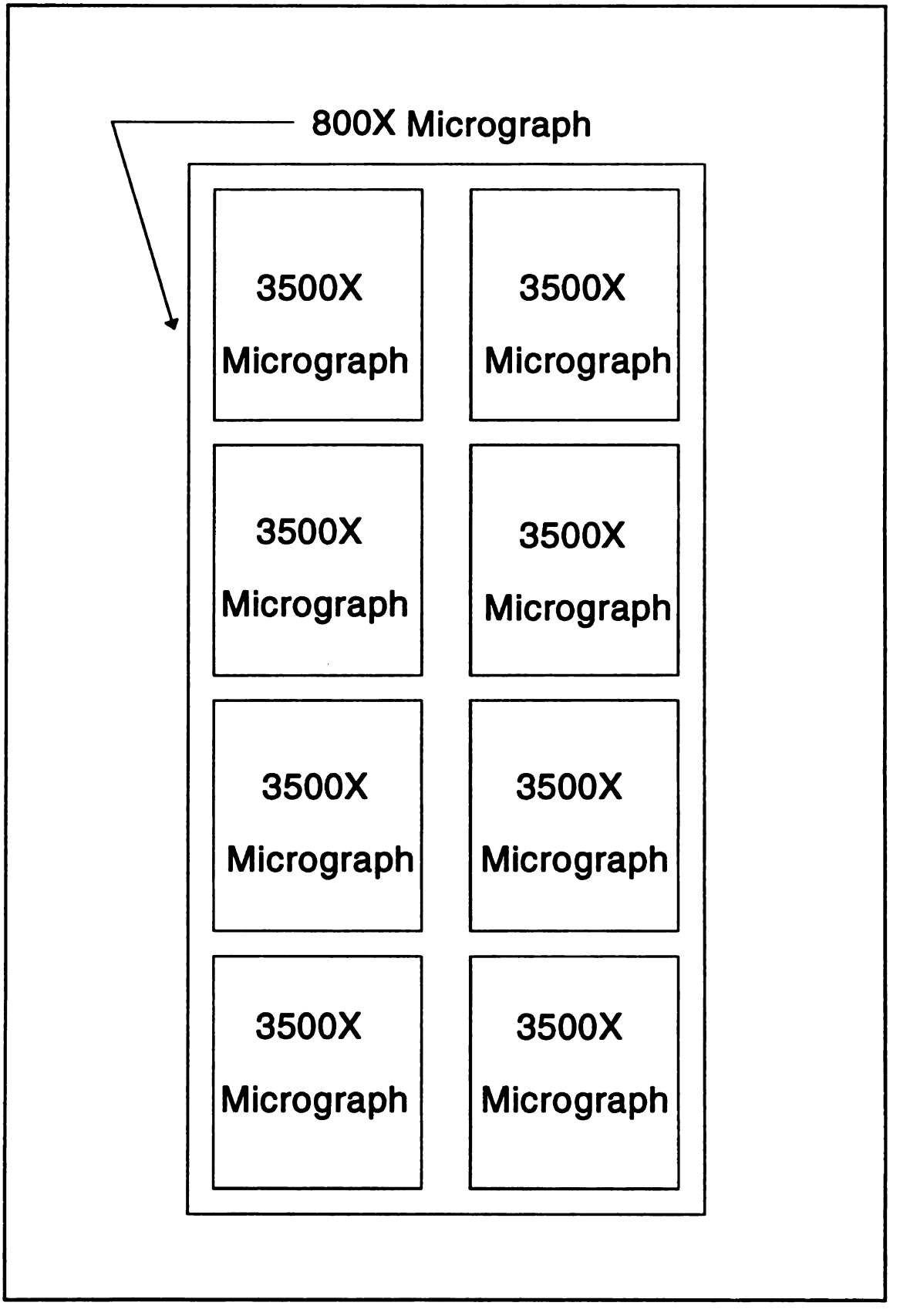

Figure 13. Illustration of grid analysis used to determine maximum particle size.

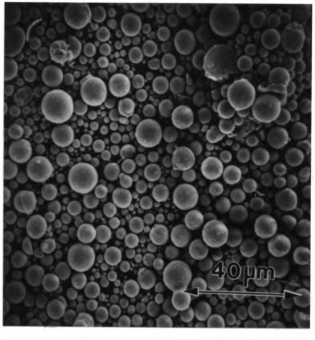

Figure 14. SEM micrograph of Fe-40AlSED. (850X).

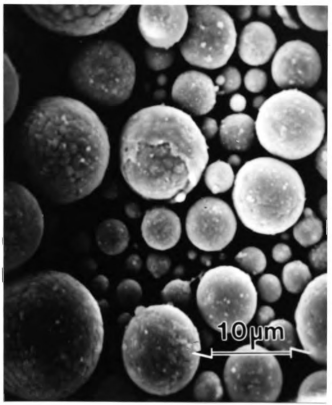

Figure 15. SEM micrograph of Fe-40AlSED. (3500X).

obtained for a wide range of pH values. It was then concluded that possible surface reactions had taken place by allowing the surface to remain hydrated in an nonprotective atmosphere.

An attempt was made to remedy the surface change problem previously encountered. A furnace treatment was employed which would attempt to dehydrate the powder. The variables selected for the furnace operation included a 2 hour furnace treatment at a temperature of 110°C. Table 9 provides the relative weight of the powder sample with respect to operation time.

Table 9. Wet Powder Furnace Treatment Data

Average Weight (g)	Furnace Time Elapsed (min)
54.2096	30
53.9378	60
53.9242	90
53.9372	120

As can be seen in the previous table, the weight of the sedimented powder sample no longer decreases after a 2 hour furnace operation, thus showing that the sample is no longer hydrated. At the conclusion of the furnace operation, the specimen still exhibited some degree of instability when suspended and the pH monitored, as seen previously. It was concluded that the specimen may have undergone further surface damage during the furnace operation, possibly oxidation. In light of the previous observations, the furnace operation was negated as a possible solution to the instability

problem encountered. The solution to the instability problem was ultimately produced by developing a vacuum assisted desiccating system in order to completely dry the powder immediately after it was sedimented. Upon performing this type of dehydration process, the Fe-40Al powder exhibited a vast decrease in the observed instability. The remaining instability resulted in a much slower increase of the pH level with respect to time. The small degree of instability may have resulted in adsorbed ions present on the particle surface which will become active when re-wetted by an aqueous solution.

The other intermetallic Fe-40Al powder was supplied by the NASA/Lewis research Center, Cleveland, Ohio. This powder was obtained in a -325 mesh form which corresponds to the largest screen opening of 44μm. The same grid analysis procedure for verifying the expected particle size range was used. Since it was initially assumed that the as-received particle size was acceptable, no addition reduction methods were employed. Therefore an instability problems observed while using the previous reduction technique could be avoided. The SEM micrographs are shown in Figures 16a and 16b.

Processing Parameters

The next major area of experimentation involved the determination and examination of two processing parameters. These included the calculation of the critical coagulation concentration (c.c.c.) and the determination and examination of the effective particle sizing. Both of these parameters are extremely important with

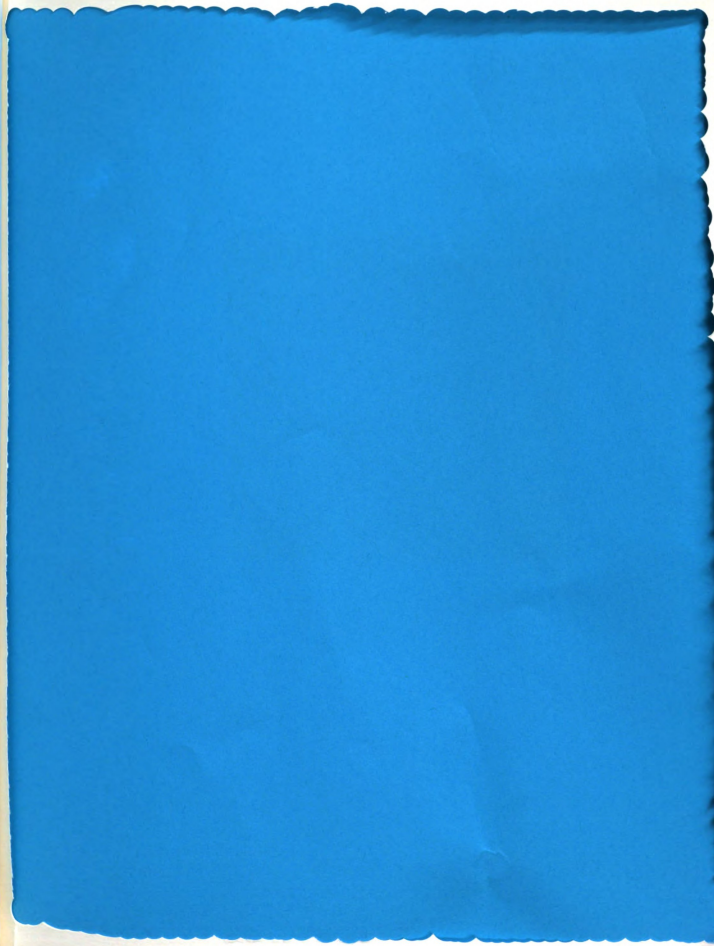

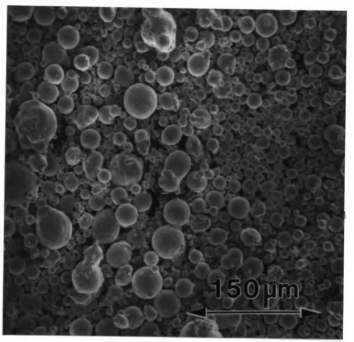

Figure 16a. SEM micrograph of Fe-40Al325. (200X).

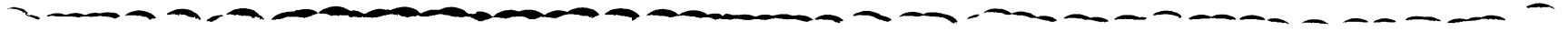

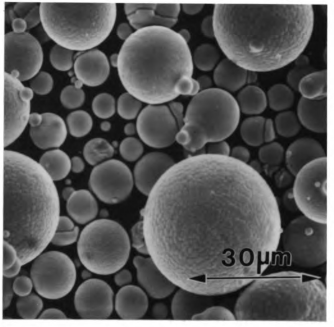

Figure 16b. SEM micrograph of Fe-40Al325. (1100X).

respect to the generation of the characteristic potentiometric titration data and the subsequent stability prediction. Therefore the accuracy of the ESA and stability data is dependent on the accuracy of the values obtained for the two parameters listed above.

The c.c.c. value is defined as the specific concentration for which the suspension coagulates and forms flocs which fall out of the system in a rapid manner, and the concentration at which the suspension exhibits stable behavior. During thecourse of the experiment it was originally intended to provide c.c.c. data for the Fe-40AlSED powder. Instead, the Fe-40AlSED was not included as acceptable data for the calculation of the c.c.c.. This was primarily due to the previously explained fact that when powder is hydrated and then dried, the adsorbed ions, which were present when the particles were wet, become active upon rehydration of the particle surface. During the attempt to calculate the c.c.c. using 2^{v}/o suspensions containing Fe-40AlSED powder, the time-lapse sedimentation utilizing the different concentrations were initially successful. Due to the limited supply of the Fe-40AlSED powder, the powder used for the initial c.c.c. calculation was wet-filtered through a cellulose membrane. Since a proper washing technique was not employed, the electrolyte ions which were present in solution during the first run of the c.c.c. experiment were reactivated during the second time-lapse sedimentation. This resulted in equal settling in each test tube so no differentiation can be made as to which should settle out and which should not. The result of this initial c.c.c. experiment verified the existence of adsorbed ions since each test tube suspension exhibited the same behavior.

At the conclusion of the initial attempt to determine the c.c.c. for the Fe-40Al system it was decided that further endeavors in its determination should employ the

use of the Fe-40Al325 powder instead of the Fe-40AlSED powder. This is primarily due to the abundance of the Fe-40Al325 and the realization that this particular powder would most likely be employed in the processing of the IMC. The c.c.c. was determined in the same manner as previous attempts. The procedure for the calculation of the c.c.c. is given in detail in the previous section. The time lapse photos for the calculation of the c.c.c. for the Fe-40Al325 system are shown in Figures 17, 18, and 19. The end result of the experiment is dependent on each stage of the experiment. Initially, the solutions are mixed to the specifications present earlier and sonicated with an ultrasonic probe. This sonication procedure ensures that any flocs which form as a result of initial mixing are broken up and act as individual particles. The solutions are then shaken and allowed to stand for 2 hours. This stage of the experiment allows for the formation of the flocs. The suspensions are then resuspended and allowed to stand. This is the most important step within the experiment. This provides an actual representation of the effect of a particle floc as it falls through a suspension. The floc will not only cause the particles comprising it to fall out of the suspension, but also those particles which get pushed to the bottom by the moving floc. As can be seen from the following figures, the suspensions containing the 0.1N and 0.01N KNO_3 electrolyte concentrations virtually settle out completely. The suspensions with values of 0.0001N and 0.001N KNO_3, negating the effects that Stoke's law has on the larger particles in the distribution, exhibit stable behavior. Therefore, the values of 0.0001N and 0.001N KNO_3 electrolyte concentration, are considered acceptable for use in the processing of the IMC.

The next parameter analyzed was the effective particle size of the powder in suspension. The scope of this experiment included the analysis of several variables.

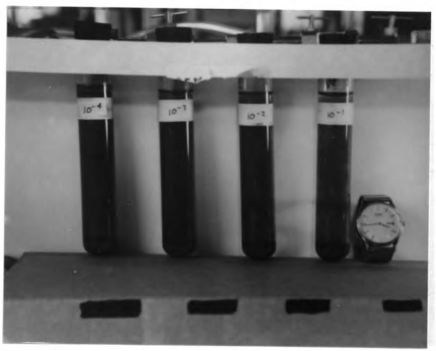

Figure 17. Time lapse photograph for c.c.c. determination. (time = 0 seconds).

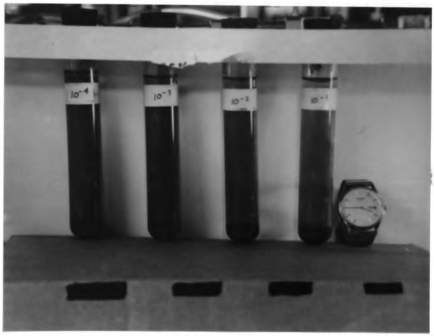

Figure 18. Time lapse photograph for c.c.c. determination. (time = 45 seconds).

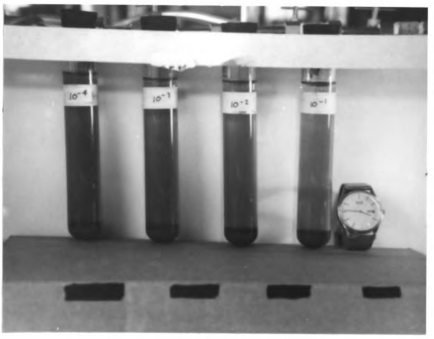

Figure 19. Time lapse photograph for c.c.c. determination. (time = 90 seconds).

The initial purpose of this experiment was to verify the previous experimental work performed which concluded that the particle size limits which were specified were accurate. Upon beginning the effective particle size measurements using the Malvern Mastersizer, it became possible to measure several other variables. Additional experimental variables examined included: (1) measuring the effective particle size with respect to different electrolytic concentrations and to compare those values with the experimental work performed to calculate the c.c.c. for the system, (2) examine the flocculation behavior of the suspension with respect to pH and electrolyte concentration, and (3) explore the possibility of examining flocculation kinetics.

The first experiment performed utilizing the determination of effective particle sizing included comparing the data gathered from performing the calculation of the c.c.c. with values obtained for the effective particle size at the same electrolyte concentrations. After the data for the effective particle size was completed using the Malvern Mastersizer, several results are given which were then used to interpolate different types of information. With respect to comparing the values from the Mastersizer and the c.c.c. time-lapse photo experiment, the results used to characterize the data include the mean particle size, (measured in μm), of the entire distribution and the specific surface area, (measured in m^2/cc) of the suspension sample. The results for the four particle sizing data runs are presented in Tables 10 and 11 on the following pages. By examining the data, the following values were obtained for the Fe-40AlSED powder with respect to electrolyte concentrations of 0.0001N, 0.001N, 0.01N, 0.1N KNO_3:

D[v,0.5] = mean p.s. = 5.32μm for 0.1N KNO_3.

= 4.89μm for 0.01N KNO_3.

= 5.30μm for 0.001N KNO_3.

= 5.53μm for 0.0001N KNO_3.

Specific S.A. = 1.2746m^2/cc for 0.1N KNO_3.

= 1.3846m^2/cc for 0.01N KNO_3.

= 1.2867m^2/cc for 0.001N KNO_3.

= 1.2292m^2/cc for 0.0001N KNO_3.

By examining the values listed above and on page 84, no differentiation or correlation can be generated from the patterns exhibited. The most reasonable explanation for the inconclusiveness of the data taken for the Fe-40AlSED is that the particle size range is so narrow that there exists minimal flocculation since there is not an over abundance of very large and very small particles. This eludes to the explanation presented by Hogg, Healy and Furstenau [20], where it was stated that the prediction for stability within a multicomponent system does not apply for particles in which there is such a large size difference. Therefore for a system where very large and very small particles exist, these particles will tend to attract more readily than those which are more equal in size. It is difficult to evaluate any flocculation that may be present because the interaction of large and small particles do not adhere to the governing stability and may flocculate. Therefore, the amount the Mastersizer laser beam is defracted is so small that the results obtained do not outweigh those values associated with the standard deviation. Flocculation does exist in some capacity if the previous grid analysis for particle size limits is used as a benchmark for comparing the data obtained

Table 10. Particle Size Data for 0.1N KNO_3 Fe-40AlSED

HIGH SIZE	% UNDER	HIGH SIZE	% UNDER	HIGH SIZE	% UNDER	HIGH SIZE	% UNDER	HIGH SIZE	% UNDER	HIGH SIZE	% UNDER	Span 1.14
180	100	64.4	100	23.0	100	8.25	85.7	2.95	9.7	1.06	0.2	D[4,3] 5.77μm
164	100	58.7	100	21.0	99.9	7.51	80.0	2.69	6.9	0.96	0.1	
149	100	53.4	100	19.1	99.8	6.84	73.1	2.45	4.8	0.88	0.1	D[3,2] 4.71μm
136	100	48.7	100	17.4	99.7	6.23	65.0	2.23	3.3	0.80	0.1	
124	100	44.3	100	15.9	99.4	5.67	56.2	2.03	2.3	0.73	0.0	D[v,0.9] 9.02μm
113	100	40.4	100	14.4	99.0	5.17	47.3	1.85	1.5	0.66	0.0	
103	100	36.8	100	13.2	98.4	4.71	38.7	1.68	1.0	0.60	0.0	D[v,0.1] 2.98μm
93.6	100	33.5	100	12.0	97.3	4.29	30.9	1.53	0.7	0.55	0.0	
85.2	100	30.5	100	10.9	95.8	3.91	24.0	1.40	0.5	0.50	0.0	D[v,0.5] 5.32μm
77.6	100	27.8	100	9.94	93.5	3.56	18.2	1.27	0.3			
70.7	100	25.3	100	9.05	90.2	3.24	13.4	1.16	0.2			Shape =OFF
Source = :Sample Focal Length = 100mm Presentation = std				Beam Length = 14.3mm Residual = 1.827% Obscuration = 0.1829 volume Distribution				Model indp Volume Conc. = 0.0020% Sp. S.A. = 1.2746 m^2/cc				

Table 11. Particle Size Data for 0.01N KNO_3 Fe-40AlSED

HIGH SIZE	% UNDER	HIGH SIZE	% UNDER	HIGH SIZE	% UNDER	HIGH SIZE	% UNDER	HIGH SIZE	% UNDER	HIGH SIZE	% UNDER	Span 1.12
180	100	64.4	100	23.0	100	8.25	90.1	2.95	12.8	1.06	0.2	D[4,3] 5.28μm
164	100	58.7	100	21.0	100	7.51	85.3	2.69	9.2	0.96	0.1	
149	100	53.4	100	19.1	99.9	6.84	79.7	2.45	6.4	0.88	0.1	D[3,2] 4.33μm
136	100	48.7	100	17.4	99.9	6.23	72.5	2.23	4.5	0.80	0.1	
124	100	44.3	100	15.9	99.8	5.67	64.1	2.03	3.1	0.73	0.1	D[v,0.9] 8.24μm
113	100	40.4	100	14.4	99.5	5.17	55.2	1.85	2.1	0.66	0.0	
103	100	36.8	100	13.2	99.2	4.71	46.3	1.68	1.4	0.60	0.0	D[v,0.1] 2.75μm
93.6	100	33.5	100	12.0	98.5	4.29	37.8	1.53	1.0	0.55	0.0	
85.2	100	30.5	100	10.9	97.5	3.91	30.0	1.40	0.7	0.50	0.0	D[v,0.5] 4.89μm
77.6	100	27.8	100	9.94	95.9	3.56	23.1	1.27	0.4			
70.7	100	25.3	100	9.05	93.6	3.24	17.4	1.16	0.3			Shape =OFF
Source = :Sample Focal Length = 100mm Presentation = std				Beam Length = 14.3 mm Residual = 2.254% Obscuration = 0.1348 volume Distribution				Model indp Volume Conc. = 0.0013% Sp. S.A. = 1.3846 m^2/cc				

Table 12. Particle Size Data for 0.001N KNO_3 Fe-40AlSED

HIGH	%	HIGH	%	HIGH	%	HIGH	%	HIGH	%	HIGH	%	Span
180	100	64.4	100	23.0	100	8.25	85.9	2.95	10.1	1.06	0.2	D[4,3] 5.73µm
164	100	58.7	100	21.0	99.9	7.51	80.2	2.69	7.3	0.96	0.1	
149	100	53.4	100	19.1	99.9	6.84	73.3	2.45	5.1	0.88	0.1	D[3,2] 4.66µm
136	100	48.7	100	17.4	99.8	6.23	65.2	2.23	3.6	0.80	0.1	
124	100	44.3	100	15.9	99.5	5.67	56.5	2.03	2.5	0.73	0.0	D[v,0.9] 8.97µm
113	100	40.4	100	14.4	99.1	5.17	47.6	1.85	1.7	0.66	0.0	
103	100	36.8	100	13.2	98.5	4.71	39.0	1.68	1.2	0.60	0.0	D[v,0.1] 2.94µm
93.6	100	33.5	100	12.0	97.5	4.29	31.3	1.53	0.8	0.55	0.0	
85.2	100	30.5	100	10.9	95.9	3.91	24.4	1.40	0.6	0.50	0.0	D[v,0.5] 5.30µm
77.6	100	27.8	100	9.94	93.6	3.56	18.6	1.27	0.4			
70.7	100	25.3	100	9.05	90.4	3.24	13.9	1.16	0.3			Shape =OFF
Source = :Sample Focal Length = 100mm Presentation = stnd				Beam Length = 14.3mm Residual = 2.120% Obscuration = 0.1481 Volume Distribution				Model indp Volume Conc. = 0.016% Sp. S.A. = 1.2867 m^2/cc				

Table 13. Particle Size Data for 0.0001N KNO_3 Fe-40AlSED

HIGH SIZE	% UNDER	HIGH SIZE	% UNDER	HIGH SIZE	% UNDER	HIGH SIZE	% UNDER	HIGH SIZE	% UNDER	HIGH SIZE	% UNDER	Span 1.12
180	100	64.4	100	23.0	99.9	8.25	82.6	2.95	8.81	1.06	0.1	D[4,3] 6.06µm
164	100	58.7	100	21.0	99.8	7.51	76.4	2.69	6.3	0.96	0.1	
149	100	53.4	100	19.1	99.7	6.84	69.2	2.45	4.4	0.88	0.1	D[3,2] 4.88µm
136	100	48.7	100	17.4	99.4	6.23	61.0	2.23	3.0	0.80	0.0	
124	100	44.3	100	15.9	99.1	5.67	52.4	2.03	2.1	0.73	0.0	D[v,0.9] 9.59µm
113	100	40.4	100	14.4	98.4	5.17	43.7	1.85	1.4	0.66	0.0	
103	100	36.8	100	13.2	97.5	4.71	35.6	1.68	1.0	0.60	0.0	D[v,0.1] 3.06µm
93.6	100	33.5	100	12.0	96.1	4.29	28.3	1.53	0.7	0.55	0.0	
85.2	100	30.5	100	10.9	94.1	3.91	21.9	1.40	0.4	0.50	0.0	D[v,0.5] 5.53µm
77.6	100	27.8	100	9.94	91.3	3.56	16.6	1.27	0.3			
70.7	100	25.3	100	9.05	87.5	3.24	12.2	1.16	0.2			Shape =OFF
Source = :Sample Focal Length = 100mm Presentation = stnd				Beam Length = 14.3 mm Residual = 1.753% Obscuration = 0.0971 Volume Distribution				Model indp Volume Conc. = 0.0011% Sp. S.A. = 1.2292 m^2/cc				

for the effective particle size. As can be seen from the histogram data in Tables 10 and 11, between 7.5% and 8.7% of the samples tested were above the upper limit of 10μm. Therefore, those particles which are measured as being greater than 10μm can be considered as the result of flocculated particles. The pick-up lens of the mastersizer, which produces the diffracted data for the measurement, is unable to tell the difference between particles which are a single entity or an entity which is made up of a collection of particles. Therefore, the computer pick-up lens will report a floc as a larger particle rather than a collection of small particles.

The flocculation behavior for the Fe-40AlSED was more apparent when comparing the effective particle size values over a range of pH values. This is shown by examining Tables 12, 13, and 14. Each of the data acquisition runs was performed at a pH 3.0, pH, 5.5 and pH 8.0 respectively. Again, the variable which provided the most revealing information was the amount of fines which were below the project 10μm limit. These values are listed as follows:

pH 3.0 ⇒ for a high size = 9.94μm ⇒ 96.0% of sample below

pH 5.5 ⇒ for a high size = 9.94μm ⇒ 96.4% of sample below

pH 8.0 ⇒ for a high size = 9.94μm ⇒ 89.3% of sample below.

This result indicates that the flocculation behavior is excited at the higher levels of pH due to the amount of fines below the project 10μm limit decreases as the pH of the suspension increases.

Table 14. Particle Size Data for 0.0001N KNO_3 pH 3.0 Fe-40AlSED

HIGH SIZE	% UNDER	HIGH SIZE	% UNDER	HIGH SIZE	% UNDER	HIGH SIZE	% UNDER	HIGH SIZE	% UNDER	HIGH SIZE	% UNDER	Span 1.12
180	100	64.4	100	23.0	100	8.25	90.0	2.95	12.7	1.06	0.2	D[4,3] 5.29µm
164	100	58.7	100	21.0	100	7.51	85.3	2.69	9.1	0.96	0.1	
149	100	53.4	100	19.1	99.9	6.84	79.6	2.45	6.4	0.88	0.1	D[3,2] 4.34µm
136	100	48.7	100	17.4	99.9	6.23	72.3	2.23	4.5	0.80	0.1	
124	100	44.3	100	15.9	99.8	5.67	63.8	2.03	3.1	0.73	0.1	D[v,0.9] 6.24µm
113	100	40.4	100	14.4	99.6	5.17	55.0	1.85	2.1	0.66	0.0	
103	100	36.8	100	13.2	99.2	4.71	46.1	1.68	1.4	0.60	0.0	D[v,0.1] 2.76µm
93.6	100	33.5	100	12.0	98.6	4.29	37.6	1.53	1.0	0.55	0.0	
85.2	100	30.5	100	10.9	97.6	3.91	29.8	1.40	0.6	0.50	0.0	D[v,0.5] 4.91µm
77.6	100	27.8	100	9.94	96.0	3.56	23.0	1.27	0.4			
70.7	100	25.3	100	9.05	93.6	3.24	17.3	1.16	0.3			Shape =OFF
Source = :Sample Focal Length = 100mm Presentation = stnd				Beam Length = 14.3mm Residual = 2.306% Obscuration = 0.1261 Volume Distribution				Model indp Volume Conc. = 0.0012% Sp. S.A. = 1.3818 m^2/cc				

Table 15. Particle Size Data for 0.0001N KNO_3 pH 5.5 Fe-40AlSED

HIGH SIZE	% UNDER	HIGH SIZE	% UNDER	HIGH SIZE	% UNDER	HIGH SIZE	% UNDER	HIGH SIZE	% UNDER	HIGH SIZE	% UNDER	Span 1.12
180	100	64.4	100	23.0	100	8.25	90.8	2.95	13.1	1.06	0.2	D[4,3] 5.21µm
164	100	58.7	100	21.0	100	7.51	86.2	2.69	9.4	0.96	0.1	
149	100	53.4	100	19.1	100	6.84	80.7	2.45	6.6	0.88	0.1	D[3,2] 4.29µm
136	100	48.7	100	17.4	99.9	6.23	73.5	2.23	4.6	0.80	0.1	
124	100	44.3	100	15.9	99.8	5.67	65.1	2.03	3.2	0.73	0.1	D[v,0.9] 6.09µm
113	100	40.4	100	14.4	99.6	5.17	56.2	1.85	2.1	0.66	0.0	
103	100	36.8	100	13.2	99.3	4.71	47.2	1.68	1.5	0.60	0.0	D[v,0.1] 2.73µm
93.6	100	33.5	100	12.0	98.8	4.29	38.6	1.53	1.0	0.55	0.0	
85.2	100	30.5	100	10.9	97.9	3.91	30.7	1.40	0.7	0.50	0.0	D[v,0.5] 4.85µm
77.6	100	27.8	100	9.94	96.4	3.56	23.7	1.27	0.4			
70.7	100	25.3	100	9.05	94.2	3.24	17.9	1.16	0.3			Shape =OFF
Source = :Sample Focal Length = 100mm Presentation = stnd				Beam Length = 14.3 mm Residual = 2.450% Obscuration = 0.1453 Volume Distribution				Model indp Volume Conc. = 0.0014% Sp. S.A. = 1.3981 m^2/cc				

Table 16. Particle Size Data for 0.0001N KNO_3, pH 8.0 Fe-40AlSED

HIGH SIZE	% UNDER	HIGH SIZE	% UNDER	HIGH SIZE	% UNDER	HIGH SIZE	% UNDER	HIGH SIZE	% UNDER	HIGH SIZE	% UNDER	Span 1.34
180	100	64.4	100	23.0	99.7	8.25	80.8	2.95	11.4	1.06	0.4	D[4,3] 5.14µm
164	100	58.7	100	21.0	99.5	7.51	75.2	2.69	8.5	0.96	0.3	
149	100	53.4	100	19.1	99.3	6.84	68.5	2.45	6.3	0.88	0.2	D[3,2] 4.66µm
136	100	48.7	100	17.4	98.8	6.23	61.2	2.23	4.6	0.80	0.2	
124	100	44.3	100	15.9	98.2	5.67	53.4	2.03	3.4	0.73	0.1	D[v,0.9] 10.13m
113	100	40.4	100	14.4	97.4	5.17	45.5	1.85	2.4	0.66	0.1	
103	100	36.8	100	13.2	96.1	4.71	38.0	1.68	1.8	0.60	0.1	D[w,0.1] 2.83µm
93.6	100	33.5	100	12.0	94.5	4.29	31.0	1.53	1.3	0.55	0.1	
85.2	100	30.5	100	10.9	92.3	3.91	24.9	1.40	1.0	0.50	0.0	D[w,0.5] 5.45µm
77.6	100	27.8	99.9	9.94	89.3	3.56	19.5	1.27	0.7			
70.7	100	25.3	99.9	9.05	85.6	3.24	15.0	1.16	0.5			Shape =OPP
Source = :Sample Focal Length = 100mm Presentation = stnd				Beam Length = 14.3mm Residual = 1.705% Obscuration = 0.1342 Volume Distribution				Model indp Volume Conc. = 0.00.14 Sp. S.A. = 1.2871 m^2/cc				

The initial experiment performed on the Fe-40AlSED for comparing the time-lapse c.c.c. results with the effective particle size data was also performed on the Fe-40Al325 powder. Similar suspensions were mixed and sonicated prior to measuring with the Mastersizer. The results for each of the data runs are given in Tables 15, 16, 17, and 18. By examining the data, the following values were obtained for the Fe-40Al325 powder with respect to electrolyte concentrations of 0.0001N, 0.001N, 0.01N, 0.1N KNO_3:

D[v,0.5] = mean p.s. = 27.67µm for 0.1N KNO_3.

= 23.32µm for 0.01N KNO_3.

= 23.18µm for 0.001N KNO_3.

= 23.71µm for 0.0001N KNO_3.

Table 17. Particle Size Data for 0.1N KNO_3 Fe-40Al325

HIGH SIZE	% UNDER	HIGH SIZE	% UNDER	HIGH SIZE	% UNDER	HIGH SIZE	% UNDER	HIGH SIZE	% UNDER	HIGH SIZE	% UNDER	Span 2.06
600	100	203	96.0	68.5	90.7	23.1	40.4	7.82	7.5	2.64	0.5	D[4,3] 46.61µm
544	99.6	184	95.9	62.1	88.7	21.0	35.7	7.08	6.1	2.39	0.4	
493	99.1	166	95.8	56.2	86.0	19.0	31.3	6.42	5.0	2.17	0.3	D[3,2] 18.35µm
446	98.4	151	95.7	50.9	82.6	17.2	27.3	5.82	4.0	1.97	0.3	
404	97.7	137	95.5	46.2	78.4	15.6	23.8	5.27	3.1	1.78	0.2	D[v,0.9] 66.06µm
366	97.2	124	95.3	41.8	73.5	14.1	20.6	4.77	2.5	1.61	0.2	
332	96.8	112	95.0	37.9	68.2	12.8	17.7	4.33	1.9	1.46	0.1	D[v,0.1] 9.08µm
301	96.5	102	94.6	34.3	62.5	11.6	15.2	3.92	1.5	1.32	0.1	
273	96.3	92.1	94.0	31.1	56.8	10.5	12.9	3.55	1.1	1.20	0.1	D[v,0.5] 27.67µm
247	96.2	83.4	93.2	28.2	51.1	9.52	10.9	3.22	0.9			
224	96.1	75.6	92.1	25.5	45.5	8.63	9.1	2.92	0.7			Shape =OPP
Source = :Sample Focal Length = 300mm Presentation = std				Beam Length = 14.3mm Residual = 0.418% Obscuration = 0.1054 volume Distribution				Model indp Volume Conc. = 0.0045% Sp. S.A. = 0.3269 m^2/cc				

Table 18. Particle Size Data for 0.01N KNO_3 Fe-40Al325

HIGH SIZE	% UNDER	HIGH SIZE	% UNDER	HIGH SIZE	% UNDER	HIGH SIZE	% UNDER	HIGH SIZE	% UNDER	HIGH SIZE	% UNDER	Span 2.06
600	100	203	96.8	68.5	93.6	23.1	49.6	7.82	9.7	2.64	0.7	D[4,3] 39.99µm
544	99.7	184	96.7	62.1	92.2	21.0	44.3	7.08	8.0	2.39	0.5	
493	99.2	166	96.7	56.2	90.3	19.0	39.3	6.42	6.4	2.17	0.4	D[3,2] 15.85µm
446	98.5	151	96.7	50.9	87.8	17.2	34.5	5.82	5.2	1.97	0.3	
404	97.7	137	96.6	46.2	84.6	15.6	30.2	5.27	4.1	1.78	0.3	D[v,0.9] 55.42µm
366	97.3	124	96.5	41.8	80.8	14.1	26.3	4.77	3.2	1.61	0.2	
332	97.1	112	96.4	37.9	76.3	12.8	22.7	4.33	2.5	1.46	0.2	D[v,0.1] 7.93µm
301	97.0	102	96.1	34.3	71.4	11.6	19.4	3.92	2.0	1.32	0.1	
273	96.9	92.1	95.8	31.1	66.2	10.5	16.6	3.55	1.5	1.20	0.1	D[v,0.5] 23.32µm
247	96.8	83.4	95.3	28.2	60.6	9.52	14.0	3.22	1.2			
224	96.8	75.6	94.6	25.5	55.0	8.63	11.8	2.92	0.9			Shape =OPP
Source = :Sample Focal Length = 300mm Presentation = std				Beam Length = 14.3mm Residual = 0.559% Obscuration = 0.0891 volume Distribution				Model indp Volume Conc. = 0.0033% Sp. S.A. = 0.3785 m^2/cc				

Table 19. Particle Size Data for 0.001N KNO_3 Fe-40Al325

HIGH SIZE	% UNDER	HIGH SIZE	% UNDER	HIGH SIZE	% UNDER	HIGH SIZE	% UNDER	HIGH SIZE	% UNDER	HIGH SIZE	% UNDER	Span 1.90
500	100	203	99.9	68.5	96.5	23.1	49.9	7.82	11.5	2.64	0.8	D[4,3] 27.41µm
544	100	184	99.9	62.1	94.8	21.0	44.9	7.08	9.5	2.39	0.6	
493	100	166	99.9	56.2	92.6	19.0	40.1	6.42	7.7	2.17	0.5	D[3,2] 14.98µm
446	100	151	99.9	50.9	89.7	17.2	35.7	5.82	6.2	1.97	0.4	
404	99.9	137	99.8	46.2	86.1	15.6	31.7	5.27	4.9	1.78	0.3	D[v,0.9] 51.43µm
366	99.9	124	99.7	41.8	81.9	14.1	28.0	4.77	3.9	1.61	0.2	
332	99.9	112	99.6	37.9	77.1	12.8	24.6	4.33	3.0	1.46	0.2	D[v,0.1] 7.27µm
301	99.9	102	99.4	34.3	71.9	11.6	21.5	3.92	2.3	1.32	0.1	
273	99.9	92.1	99.0	31.1	66.4	10.5	18.7	3.55	1.8	1.20	0.1	D[v,0.5] 23.18µm
247	99.9	83.4	98.5	28.2	60.8	9.52	16.1	3.22	1.3			
224	99.9	75.6	97.7	25.5	55.2	8.63	13.7	2.92	1.0			Shape =OPP
Source = :Sample Focal Length = 300mm Presentation = stnd				Beam Length = 14.3mm Residual = 0.623% Obscuration = 0.0879 Volume Distribution				Model indp Volume Conc. = 0.0030% Sp. S.A. = 0.4004 m^2/cc				

Table 20. Particle Size Data for 0.0001N KNO_3 Fe-40Al325

HIGH SIZE	% UNDER	HIGH SIZE	% UNDER	HIGH SIZE	% UNDER	HIGH SIZE	% UNDER	HIGH SIZE	% UNDER	HIGH SIZE	% UNDER	Span 2.05
500	100	203	98.0	68.5	93.6	23.1	48.6	7.82	10.2	2.64	0.8	D[4,3] 37.15µm
544	99.3	184	97.9	62.1	92.1	21.0	43.2	7.08	8.5	2.39	0.6	
493	98.8	166	97.8	56.2	90.0	19.0	38.2	6.42	7.0	2.17	0.5	D[3,2] 15.65µm
446	98.5	151	97.7	50.9	87.4	17.2	33.5	5.82	5.7	1.97	0.4	
404	98.3	137	97.6	46.2	84.1	15.6	29.3	5.27	4.6	1.78	0.3	D[v,0.9] 56.23µm
366	98.3	124	97.4	41.8	80.3	14.1	25.4	4.77	3.7	1.61	0.3	
332	98.2	112	97.1	37.9	75.8	12.8	22.0	4.33	2.9	1.46	0.2	D[v,0.1] 7.74µm
301	98.1	102	96.8	34.3	70.9	11.6	19.1	3.92	2.3	1.32	0.1	
273	98.1	92.1	96.3	31.1	65.6	10.5	16.4	3.55	1.8	1.20	0.1	D[v,0.5] 23.71µm
247	98.1	83.4	95.7	28.2	60.0	9.52	14.1	3.22	1.4			
224	98.0	75.6	94.8	25.5	54.3	8.63	12.0	2.92	1.1			Shape =OPP
Source = :Sample Focal Length = 300mm Presentation = stnd				Beam Length = 14.3mm Residual = 0.261% Obscuration = 0.0897 Volume Distribution				Model indp Volume Conc. = 0.0033% Sp. S.A. = 0.3785 m^2/cc				

Specific S.A. = $0.3269m^2/cc$ for 0.1N KNO_3.

= $0.3785m^2/cc$ for 0.01N KNO

= $0.4004m^2/cc$ for 0.001N KNO_3.

= $0.3834m^2/cc$ for 0.0001N KNO_3.

By initial examination of the mean and specific surface area values it is apparent that flocculation is present at an electrolyte concentration of 0.1N KNO_3 and not very apparent at the other levels of electrolyte concentration. Even with respect to the results generated for the mean and specific surface area, the values presented could be suspect and not necessarily represent flocculation since there exits no understanding as to the standard deviation of the measure. A qualitative estimate can be made though regarding the flocculation behavior with respect to pH if we consider the average particle size at the 90th percentile. This particular percentile is chosen since we are concerned with particles coagulating and forming flocs which will be represented at the upper end of the sizing spectrum. The values for the 90 percentile are given as follows:

D[v,0.5] = .90 particle size = 66.06μm for 0.1N HNO_3.

= 55.42μm for 0.01N HNO_3.

= 51.43μm for 0.001N HNO_3.

= 56.23μm for 0.0001N HNO_3.

From examination of these results it is a much more apparent comparison than that generated by the mean and specific surface area results. A further comparison can be made with the c.c.c. data by using the data representing the amount of the sample

which is less than the expected value of 44μm for the Fe-40Al325. This data is represented as follows:

0.1N KNO_3 ⇒ for a high size = 46.2μm ⇒ 78.4% of sample below

0.01N KNO_3 ⇒ for a high size = 46.2μm ⇒ 84.6% of sample below

0.001N KNO_3 ⇒ for a high size = 46.2μm ⇒ 86.1% of sample below

0.0001N KNO_3 ⇒ for a high size = 46.2μm ⇒ 84.1% of sample below

This data also confirms the fact that the flocculation behavior has increased for an electrolyte value of 0.1N KNO_3. Although this data show a correlation with the observed experimental results used in determining the c.c.c., it does not account for the fact that the c.c.c. visually determined is between 0.001N KNO_3 and 0.01N KNO_3. This observation can be attributed to the fact that the driving force for the determination of the critical coagulation concentration is the evolution of the flocculation kinetics inherent to the particular system. It became apparent during the conclusion of the effective particle sizing experiment that it was not feasible to examine the flocculation kinetics of either the Fe-40AlSED or Fe-40Al325 systems. Because the sample sizes required for the particle size measurement in the Malvern Mastersizer are so small, (sample size range 0.0011% to 0.0073), that the interactions of the individual particles is dramatically decreased, therefore the probability for the formation of floc will also decrease. Furthermore, the sample container and the area within which the laser beam acts is also so limited that the time required for measurement, (approximately 5 min. for 1000 sweeps = single data acquisition), far exceeds the settling time of a particle in an upper size region. Therefore, a majority

of the particles which actually do flocculate, have already settled out before the measurement takes place, so they are simply ignored when the final data is processed and the results are received. Therefore it is highly probable that the results presented here only indicate a fraction of the total flocs that are formed during the experiment.

Even though the data acquired does not give the desired representation that would allow for the examination of flocculation kinetics, it does present some insight as to the flocculation behavior with respect to pH. Fe-40Al325 samples were again prepared in a similar fashion as the Fe-40AlSED and an effective particle sizing run was performed for the same pH range. The complete particle size data with respect to pH is given in Tables 19, 20, and 21. A similar set of data is presented here which, again, represents the amount of powder which is below the specified of the upper size limit:

pH 3.0 $\Rightarrow$ for a high size = 46.2μm $\Rightarrow$ 79.4% of sample below

pH 5.5 $\Rightarrow$ for a high size = 46.2μm $\Rightarrow$ 80.6% of sample below

pH 8.0 $\Rightarrow$ for a high size = 46.2μm $\Rightarrow$ 89.2% of sample below

Therefore for a pH of 8.0 the amount of powder within specification exceed the other pH values by approximately 10%,thus indicating that flocculation is much more prevalent at the lower pH values. This point is can be emphasized even further by once again examining the 90 percentile particle size value for each of the pH ranges. This data is given as follows:

D[v,.90] = .90 particle size = 524.58μm for pH 3.0 .

= 111.05μm for pH 5.5 .

= 47.32μm for pH 8.0 .

Table 21. Particle Size Data for 0.0001 KNO, pH 3.0 Fe-40Al325

HIGH SIZE	% UNDER	HIGH SIZE	% UNDER	HIGH SIZE	% UNDER	HIGH SIZE	% UNDER	HIGH SIZE	% UNDER	HIGH SIZE	% UNDER	Span 21.27
600	100	203	86.2	68.5	84.7	23.1	47.2	7.82	8.7	2.64	0.6	D[4,3] 94.29µm
544	92.2	184	86.2	62.1	84.0	21.0	41.6	7.08	7.2	2.39	0.5	
493	87.7	166	86.2	56.2	82.9	19.0	36.2	6.42	5.9	2.17	0.4	D[3,2] 17.21µm
446	86.9	151	86.1	50.9	81.4	17.2	31.3	5.82	4.8	1.97	0.3	
404	86.5	137	86.1	46.2	79.4	15.6	27.0	5.27	3.8	1.78	0.3	D[v,0.9] 524.58m
366	86.3	124	86.1	41.8	76.7	14.1	23.2	4.77	3.0	1.61	0.2	
332	86.3	112	86.0	37.9	73.3	12.8	19.9	4.33	2.4	1.46	0.2	D[v,0.1] 8.41µm
301	86.3	102	85.9	34.3	69.1	11.6	17.0	3.92	1.8	1.32	0.1	
273	86.2	92.1	85.7	31.1	64.3	10.5	14.6	3.55	1.4	1.20	0.1	D[v,0.5] 24.27µm
247	86.2	83.4	85.5	28.2	58.8	9.52	12.4	3.22	1.1			
224	86.2	75.6	85.2	25.5	53.0	8.63	10.5	2.92	0.8			Shape =OFF
Source = :Sample Focal Length = 300mm Presentation = stnd				Beam Length = 14.3mm Residual = 0.605% Obscuration = 0.1746 Volume Distribution				Model indp Volume Conc. = 0.0073% Sp. S.A. = 0.3487 m²/cc				

Table 22. Patricle Size Data for 0.0001N KNO, pH 5.5 Fe-40Al325

HIGH SIZE	% UNDER	HIGH SIZE	% UNDER	HIGH SIZE	% UNDER	HIGH SIZE	% UNDER	HIGH SIZE	% UNDER	HIGH SIZE	% UNDER	Span 4.20
600	100	203	90.4	68.5	87.9	23.1	46.3	7.82	10.7	2.64	1.1	D[4,3] 72.92µm
544	95.2	184	90.4	62.1	86.8	21.0	40.9	7.08	9.2	2.39	0.8	
493	92.4	166	90.3	56.2	85.3	19.0	35.9	6.42	7.7	2.17	0.7	D[3,2] 15.77µm
446	91.6	151	90.3	50.9	83.3	17.2	31.4	5.82	6.5	1.97	0.5	
404	91.1	137	90.2	46.2	80.6	15.6	27.5	5.27	5.3	1.78	0.4	D[v,0.9] 111.1µm
366	90.8	124	90.1	41.8	77.3	14.1	24.1	4.77	4.3	1.61	0.4	
332	90.7	112	90.0	37.9	73.3	12.8	21.1	4.33	3.5	1.46	0.3	D[v,0.1] 7.47µm
301	90.6	102	89.8	34.3	68.7	11.6	18.6	3.92	2.8	1.32	0.2	
273	90.5	92.1	89.6	31.1	63.5	10.5	16.3	3.55	2.2	1.20	0.2	D[v,0.5] 24.66µm
247	90.5	83.4	89.2	28.2	57.9	9.52	14.3	3.22	1.7			
224	90.5	75.6	88.6	25.5	52.0	8.63	12.5	2.92	1.4			Shape =OFF
Source = :Sample Focal Length = 300mm Presentation = stnd				Beam Length = 14.3mm Residual = 0.561% Obscuration = 0.1051 Volume Distribution				Model indp Volume Conc. = 0.0039% Sp. S.A. = 0.3805 m²/cc				

Table 23. Particle Size Data for 0.0001 KNO_3 pH 8.0 Fe-40Al325

HIGH SIZE	% UNDER	HIGH SIZE	% UNDER	HIGH SIZE	% UNDER	HIGH SIZE	% UNDER	HIGH SIZE	% UNDER	HIGH SIZE	% UNDER	Span 1.79
600	100	203	99.7	68.5	97.0	23.1	52.2	7.82	11.2	2.64	0.9	D[4,3] 26.81µm
544	100	184	99.7	62.1	95.9	21.0	46.3	7.08	9.3	2.39	0.7	
493	99.9	166	99.6	56.2	94.2	19.0	40.8	6.42	7.7	2.17	0.6	D[3,2] 14.66µm
446	99.9	151	99.6	50.9	92.1	17.2	35.8	5.82	6.3	1.97	0.5	
404	99.9	137	99.5	46.2	89.2	15.6	31.3	5.27	5.1	1.78	0.4	D(v,0.9) 47.32µm
366	99.8	124	99.4	41.8	85.6	14.1	27.4	4.77	4.1	1.61	0.3	
332	99.8	112	99.3	37.9	81.3	12.8	23.9	4.33	3.2	1.46	0.2	D(v,0.1) 7.35µm
301	99.8	102	99.1	34.3	76.3	11.6	20.7	3.92	2.5	1.32	0.2	
273	99.8	92.1	98.8	31.1	70.7	10.5	18.0	3.55	2.0	1.20	0.1	D(v,0.5) 22.32µm
247	99.7	83.4	98.4	28.2	64.6	9.52	15.5	3.22	1.5			
224	99.7	75.6	97.8	25.5	58.4	8.63	13.2	2.92	1.2			Shape =OFF
Source = :Sample Focal Length = 300mm Presentation = std				Beam Length = 14.3mm Residual = 0.345% Obscuration = 0.1949 Volume Distribution				Model indp Volume Conc. = 0.0070% Sp. S.A. = 0.4093 m²/cc				

This data clearly shows that with respect to flocculation initially present at a pH 3.0 is far greater than that experienced during the measurements taken at pH 5.5 and pH 8.0. This also gives a better understanding as to the differences in flocculation at the various pH values. The specific importance of this data will be expanded upon when the data for the ESA measurement and subsequent stability prediction is presented.

By being able to measure the particle size of the powder as it "appears" in solution, an accurate determination of the effective particle size can be obtained. As was discussed previously, one of the most important input variables involved in both the ESA measurement and the stability prediction is the particle size. Even though an accurate particle size estimation can be made on a dry powder sample using a variety of techniques, the ESA measurement takes into account that the particle is in suspension and not dry. By using a particle size which is inaccurate, the zeta potential values obtained by the ESA measurement will change in magnitude. This was

experienced during previous work performed on the Fe-40AlSED [15,29]. Generally, particle sizes, entered into the computer prior to ESA measurement, which are greater than the actual in-situ value observed by the ESA will tend to shift the zeta-potential curves down in magnitude. Therefore, accurate curves can be obtained but they are limited to the accuracy of the measurement used for the input parameters.

ESA Measurement and Stability Prediction

The next step in the development of a technique for processing IMCs via electrophoretic deposition is the analysis of the zeta potential of each component of the system and the subsequent stability prediction associated with this. As was discussed in the section on colloidal theory the ESA technique can measure characteristic zeta potential values for a range of pH values. The specifics of this measurement include the micro-titration of acid or base in order to achieve different pH values. The ESA then takes individual measurements of potential at each of the pH values. Once this data is compiled, a stability prediction program, developed by Wilson, is used to give a theoretical prediction of the degree of homo- and heterocoagulation between the system components.

The first potentiometric titration performed include the Fe-40AlSED and the ball milled FP Al_2O_3. An SEM micrograph showing the ball milled Al_2O_3 is shown in Figure 20c. Both titrations were performed independently. Each titration consisted of mixing with a neutral solution of deionized water at a pH of 7. The 1.0N HNO_3 solution was then micro-titrated to lower the pH to a level of pH 4.0. Once this level was established the titration began and the zeta potential measurements were taken over the range from pH 4.0 to pH 10.0. The plot corresponding to the potentiometric

titration for the Fe-40AlSED and FP Al_2O_3 is shown in Figure 21. Upon examining the curves it is apparent that the Al_2O_3 exhibits expected behavior compared to data seen elsewhere [15]. The Al_2O_3 zeta potential curve shows that both positive and negative values are present and that the Al_2O_3 has an iso-electric point or i.e.p. at pH 8.5, where homocoagulation will be at a maximum. Recalling the previously established criteria that homocoagulation is minimized for higher values of pH, the curve indicates that the flocculation of FP Al_2O_3 with respect to itself is minimized for pH values less than approximately pH 8.0. Otherwise, theory dictates that the homocoagulation of Al_2O_3 will be maximized for those pH values which are within the range pH 7.5 surrounding the i.e.p.

The Fe-40Al curve presented in Figure 21 illustrates markedly different behavior than that showed by the potentiometric titration for Al_2O_3. Assuming again that theory is correct and that a like component will flocculate for zeta potential values which approach zero, one would expect flocculation to occur at all pH levels as show by the characteristic potentiometric titration. Although, theoretically, flocculation is known to exist over pH ranges which are near zero, (i.e. near the i.e.p.)and since no i.e.p. is shown for the Fe-40AlSED curve, it can also be stipulated that for positive zeta potential values, flocculation will be at a minimum for pH values where the zeta potential is maximized. Using this realization, a range for which the zeta potential is consistently maximized is between pH 5.5 and pH 8.5. In comparing the potentiometric titration data with the previous effective particle sizing experiment, the range identified as that of minimum attraction does not agree entirely with that shown by the Mastersizer data. The most apparent correlation between the two sets of data is that for a pH 5.5, the flocculation as shown by the particle sizing is at a minimum,

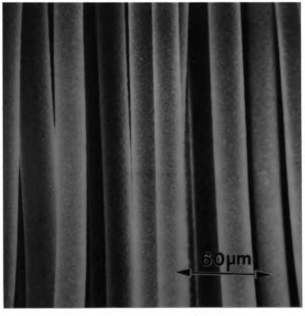

Figure 20a. SEM micrograph of FP Al_2O_3 Fiber bundle. (500X).

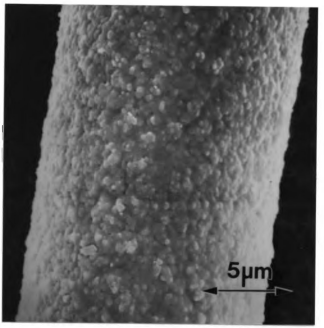

Figure 20b. SEM micrograph of FP Al_2O_3 single fiber. (4000X).

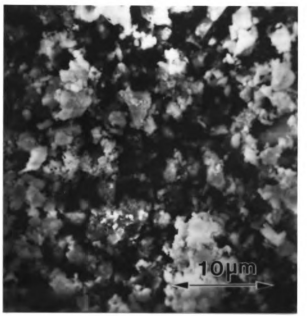

Figure 20c. SEM micrograph of ball-milled alumina. (800X).

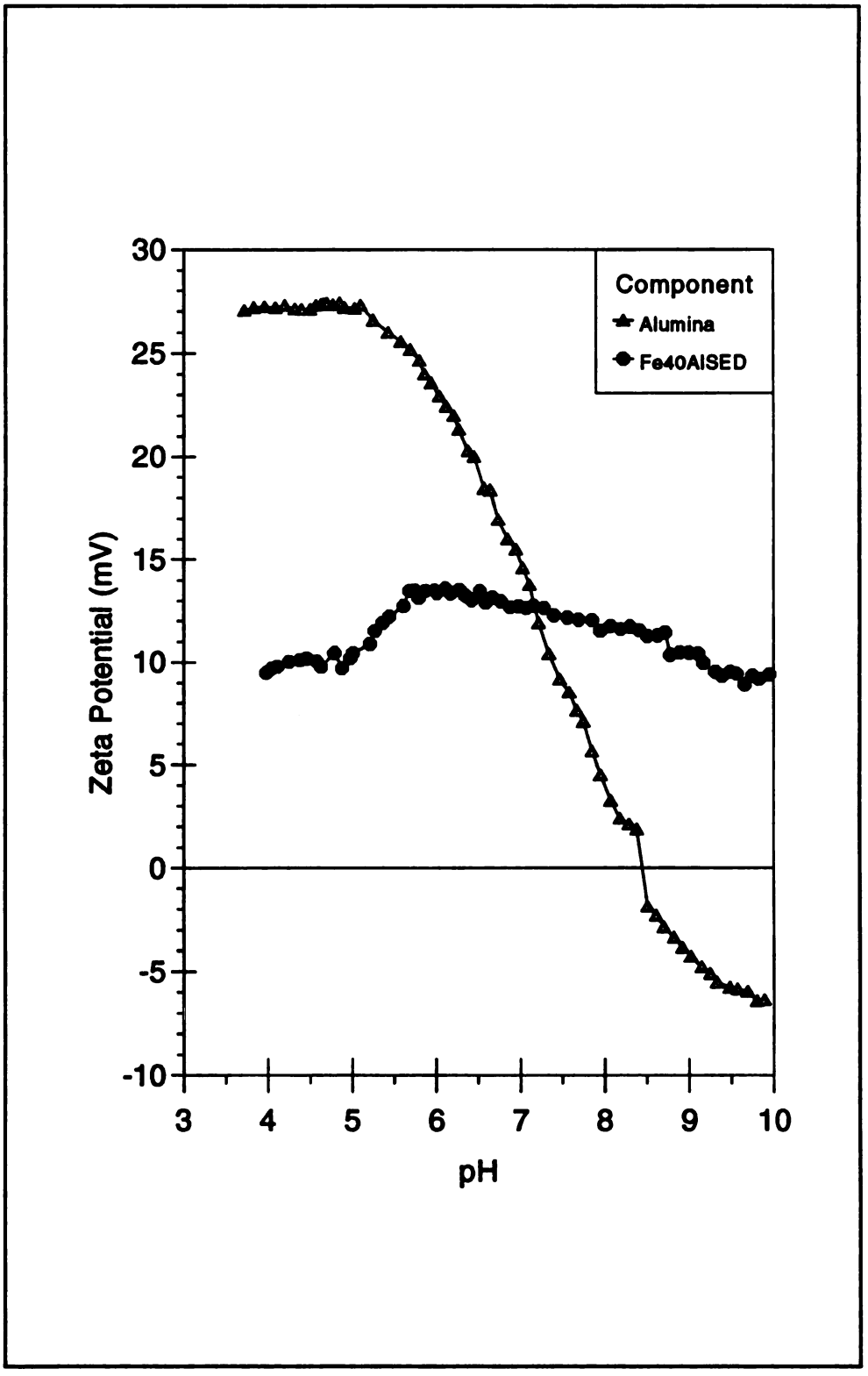

Figure 21. Zeta potential data for Fe-40AlSED and FP Al_2O_3. Titration from pH 4.0 to pH 10.0.

and the zeta potential is at a maximum, therefore also illustrating minimum flocculation.

The second potentiometric titration performed involved the Fe-40Al325 powder. The titration was performed over a range of pH 3.0 to pH 11.0. The data presented in Figure 22 includes the data for the FP Al_2O_3 that was previously obtained. This data is superimposed on the same plot as before for comparative purposes. As can be seen from the plot presented, the data points for the Fe-40Al325 are scattered in a much more exaggerated fashion than that exhibited by the Fe-40AlSED. This can be primarily attributed to the wider range in particle size for the -325 mesh sample. This identical phenomena was also exhibited in previous work [15,29]. Again, using the assumption that the flocculation is minimized for maximum values of zeta potential, the curve for the Fe-40Al325 sample in Figure 22 shows minimized flocculation to occur at pH levels above 5.5, because the zeta potential at these pH values is consistently maximized.

Once the ESA measurements were completed, the zeta potential vs pH values could then be imported into a computer program developed and written by Wilson and Crimp [15,30] which theoretically predicts the colloidal stability of multicomponent composite systems. As was shown in Figure 6, the there exists a total energy of interaction which varies with increasing interparticle distance. The interparticle distance, H, at which the total potential energy, V_T, is maximum is know as the distance at which the potential barrier exists. As was stated previously, the stability of a system is indicated by graphing the total potential energy of a system versus the interparticle distance. The condition of stability is accepted where the potential barrier is at least 20-25kT [15,20,31]. It was also previously introduced that the stability ratio

W of a system is equivalent to the ratio of the number of particles interactions and the number of particle interactions which result in flocculation. A stable or unflocculated dispersion is approximated by log(W) > 10 which corresponds to a potential barrier being at least as large as 20-25kT. Therefore, the ultimate goal of the ESA measurement and stability prediction is to generate a plot which illustrates the stability behavior of a multicomponent system by plotting the log(W) values versus the pH at which the corresponding zeta potential values were taken. From this plot, a prediction can be made as to the IMC processing pH range for the Fe-40Al / Al_2O_3 system.

The zeta potential data given in both Figures 21 and 22 was inputed into the stability prediction program previously described. The main goal for stability prediction program is to gather predicted data values for each component which makes up the total stability ratio, W_T. These include the stability ratio for components with respect to themselves, given by W_{11} and W_{22}, and with respect to each other, given by W_{12}. The value of most concern here is the stability ratio which predicts heterocoagulation, W_{12}. The purpose for using the experimentally determined data generated by the ESA, is to give a prediction as to the range of pH which may be suitable for the process and to compare the predicted processing range with that found by physically attempting to coat the Al_2O_3 fibers with Fe-40Al particles at various pH levels. This comparison not only reveals the actual desired coating range but also examines the accuracy of the stability prediction as applied to this particular system.

The zeta potential data for both the Fe-40AlSED/FP Al_2O_3 and the Fe-40Al325/FP Al_2O_3 systems was used to develop the stability prediction plots shown in Figures 23 and 24. Both plots show almost identical behavior for the heterocoagulation stability ratio, W_{12}. The prediction given by both plots shows that

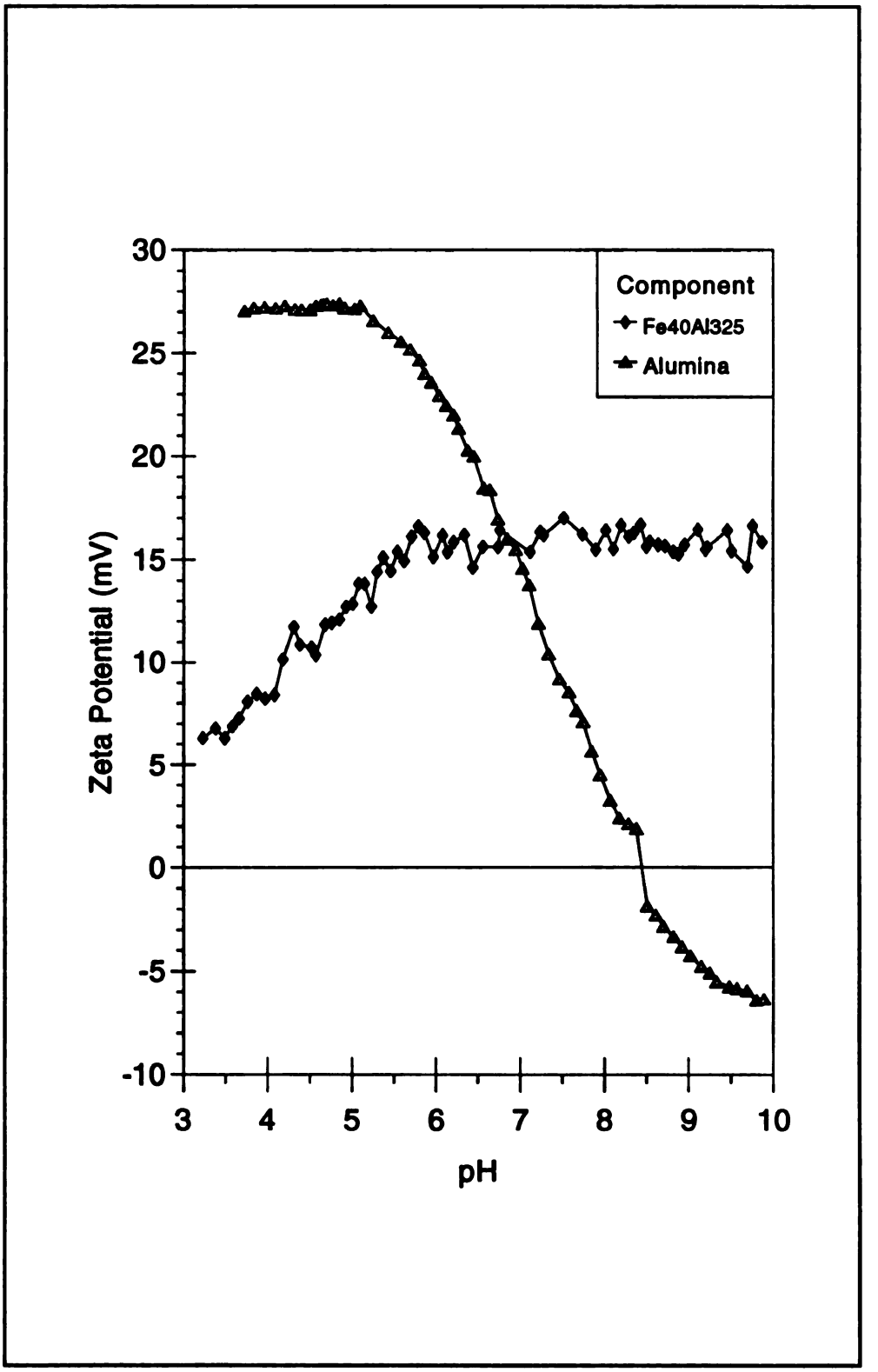

Figure 22. Zeta potential data for Fe-40Al325 and FP Al_2O_3. Titration from pH 3.0 to pH 10.0.

stability exists for pH values less than approximately pH 8.0. From this data, it is predicted that the desired processing range for which maximum heterocaogulation would occur is located at the higher pH values of pH 8.0, pH 9.0, and pH 10.0 from the stipulation that stability is assumed for log(W) values >10. The most promising aspect of these plots is shown in the stability prediction for the Fe-40Al325 / FP Al_2O_3 plot which shows that the Fe-40Al powder is stable with respect to itself for the range of pH 4.5 to pH 10.0 while the components exhibit instability for pH ranges in excess of pH 8.0, thus resulting in heterocoagulation.

By comparing Figures 21 and 22, the curves for both Fe-40Al appear to be different in shape and in magnitude. This discrepancy is magnified upon incorporating the zeta potential data into the stability prediction program. This can be seen by examining Figures 23 and 24. Given that both powder samples are approximately identical in terms of atomic weight, it was initially assumed that both samples would generate approximately the same prediction. Since the same prediction was not achieved, some possible explanations for the difference in the acquired data for both samples is given. First, as was stated before, there existed a fundamental difference between the sedimented powder and the as-received -325 mesh powder, in that the surface charge of the sedimented powder was affected by the adsorbed ions which were present as a result of the sedimentation procedure. Second, even though the powder samples were almost identical in terms of atomic percent, the -325 mesh sample contained small additions of B and Zr to enhance mechanical behavior of the intermetallic. The constituents of the Fe-40Al325 sample are (in atomic percent) 59.70% Fe, 39.80% Al, 0.10% Zr, and 0.41% B. This is compared to the Fe-40AlSED sample which contained (in atomic percent) 60.00% Fe and 40.00%Al.

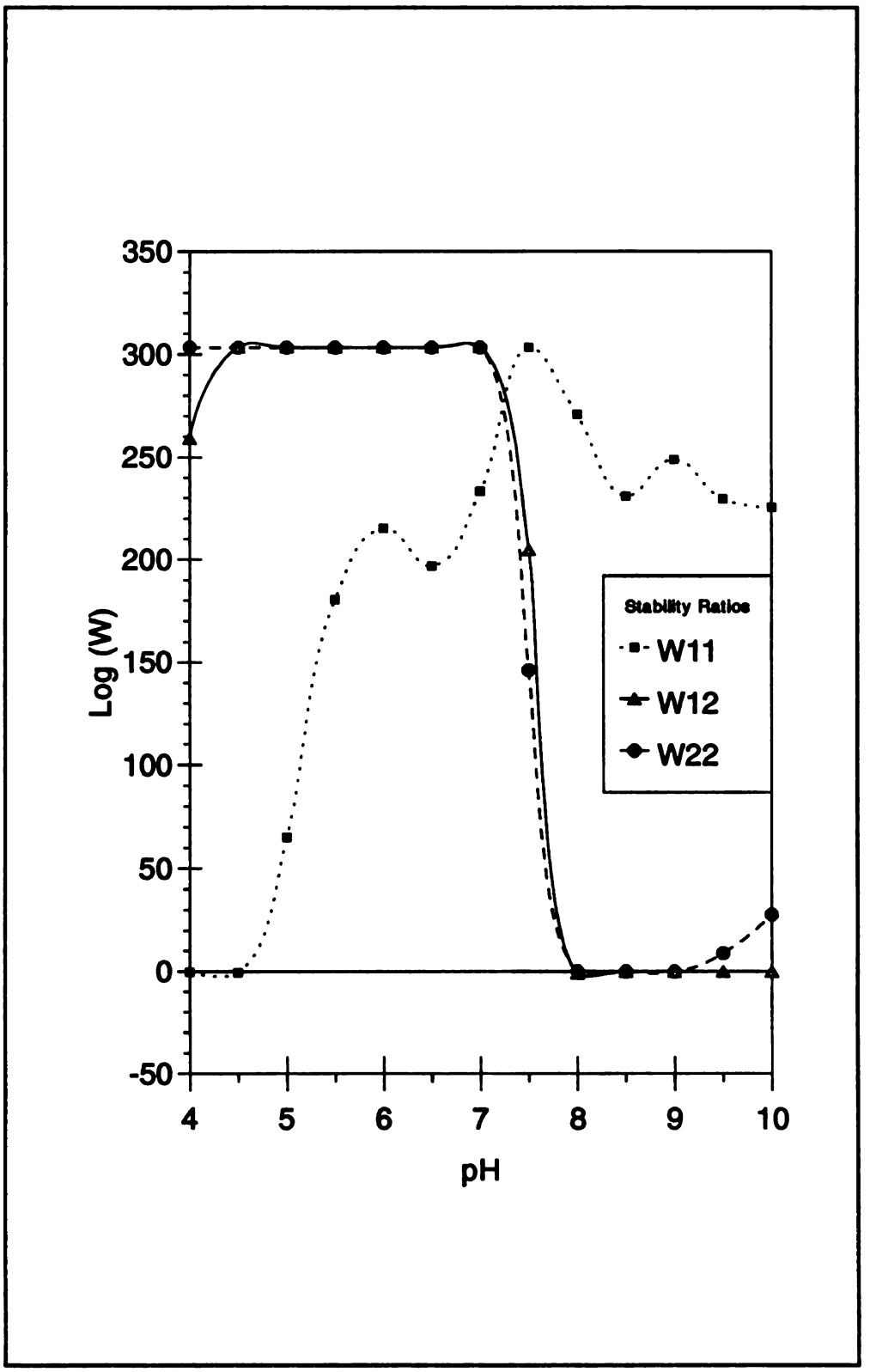

Figure 23. Stability prediction for Fe-40Al325 and Al_2O_3 multicomponent system.

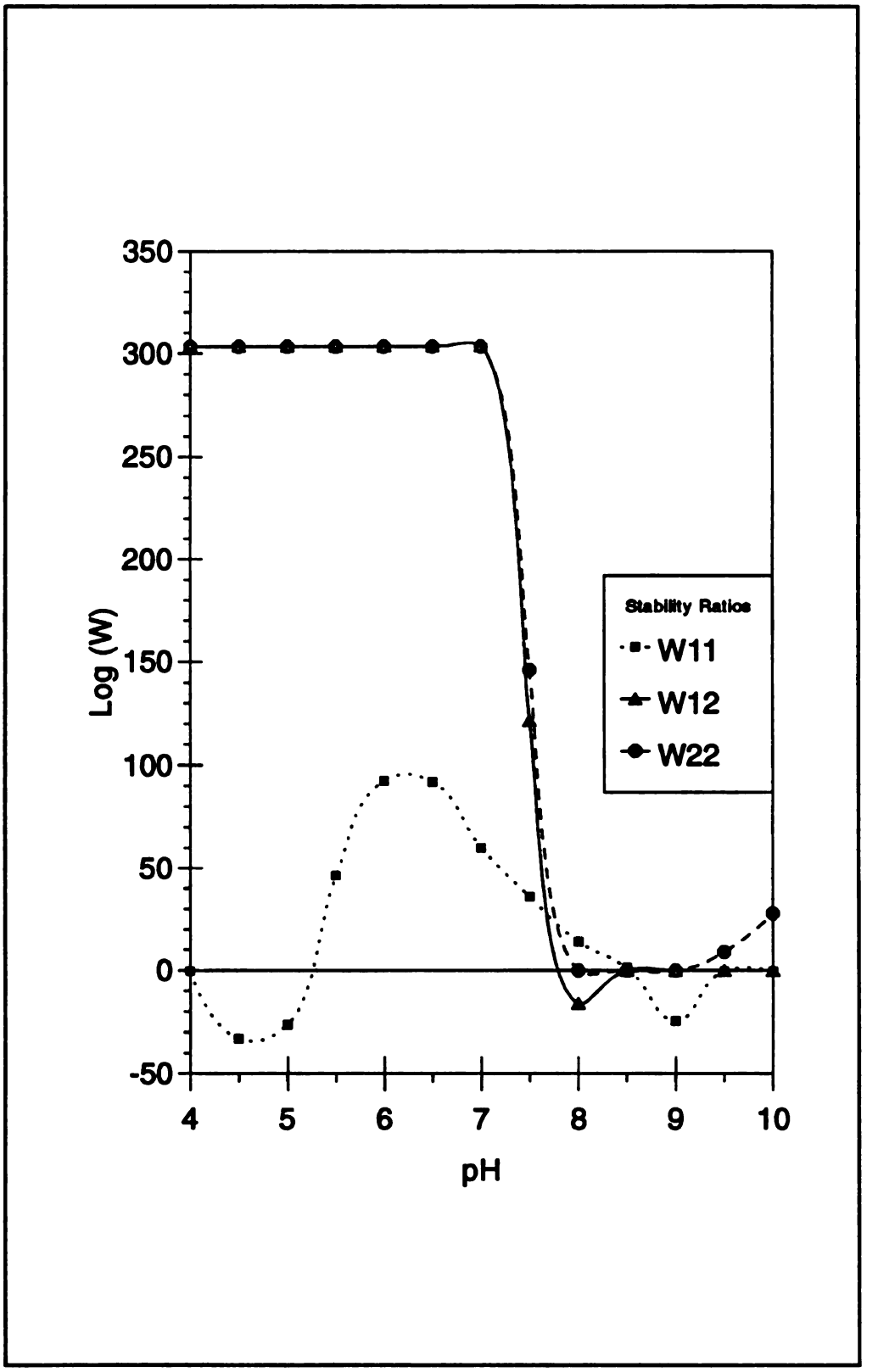

Figure 24. Stability prediction for Fe-40AlSED and Al_2O_3 multicomponent system.

Therefore, even thought the additions of Zr and B are so minimal, they should not be *disregarded* as having no effect on the chemical make-up of the powder surface. The third possible reason for the discrepancy in the two data sets is that the particle size range for each of the samples was markedly different, d < 10μm for the Fe-40AlSED and d < 44μm for the Fe-40Al325. This difference not only changes the zeta potential behavior but also significantly alters the stability ratio data describing homocoagulation of the Fe-40Al powder. This difference is primarily due to the settling out that occurs during the ESA measurement. For example, if a powder of relatively small size, d < 10μm, were suspended in a dilute concentration, 2v/o, the settling time for this suspension is relatively adequate with respect to the measurement time. Therefore the ESA system, is "told" that the average particle size is commensurate with the value obtained during the particle sizing. If, during the measurement, the powder remains suspended then the ESA will "see" an average particle size concurrent with the value that was initially used. On the contrary, if the system is given an average particle size value for a larger powder range, i.e. d < 44μm, and the powder sample experiences some significant settling effects during the measurement, then what the ESA "sees" as the average particle size and what that actual particle size is are two different values. The value that is inputed into the system will subsequently be larger than that which is actually "seen" by the ESA measurement system. Therefore with regard to the difference in data, the fact that there is some error experienced when using a larger particle size range explains the discrepancy in the data between the two powder samples.

This fact was illustrated by performing two additional stability prediction runs which would subsequently use reduce average particle size values. The first additional

stability prediction used an average particle size of d = 11.86μm, which corresponds to half the value used for the previous run. The second additional stability prediction used an average particle size of d = 2.46μm, which corresponds to the value used for the run using Fe-40SED. This allow for the generation of a series curves which can be examined to see if a trend exists for decreasing particle size. The stability predictions generated are shown in Figures 25 and 26. As can be seen from these plots the curve corresponding to the homocoagulation of Fe-40Al325 decreases considerably in magnitude and approaches the behavior exhibited by the curve for the Fe-40SED shown in Figure 23, as the particle size decreases. Therefore, this illustrated the importance in having an accurate correlation between the actual particle size of the material and the particle size that is used by the ESA to provide the zeta potential data.

Even in light of the differences which exist between the two powder samples, the predicted stability ratio curves for the heterocoagulation of Fe-40Al and Al_2O_3, i.e. W_{12}, change very little. Therefore, since it is the stability ratio describing heterocoagulation, W_{12}, that is of most concern, the discrepancy between the Fe-40Al powder samples can be disregarded. An additional experiment was performed which used the previous data for the Fe-40Al325 plot with exagerrated zeta potential values. This data is shown in Figure 27. Once the hypothetical potential values were compiled, a stability prediction was again performed to see if any changes would occur in the W_{12} stability ratio which governs the heterocoagulation. It should be noted here that the possibility exist for taking single point measurements using the

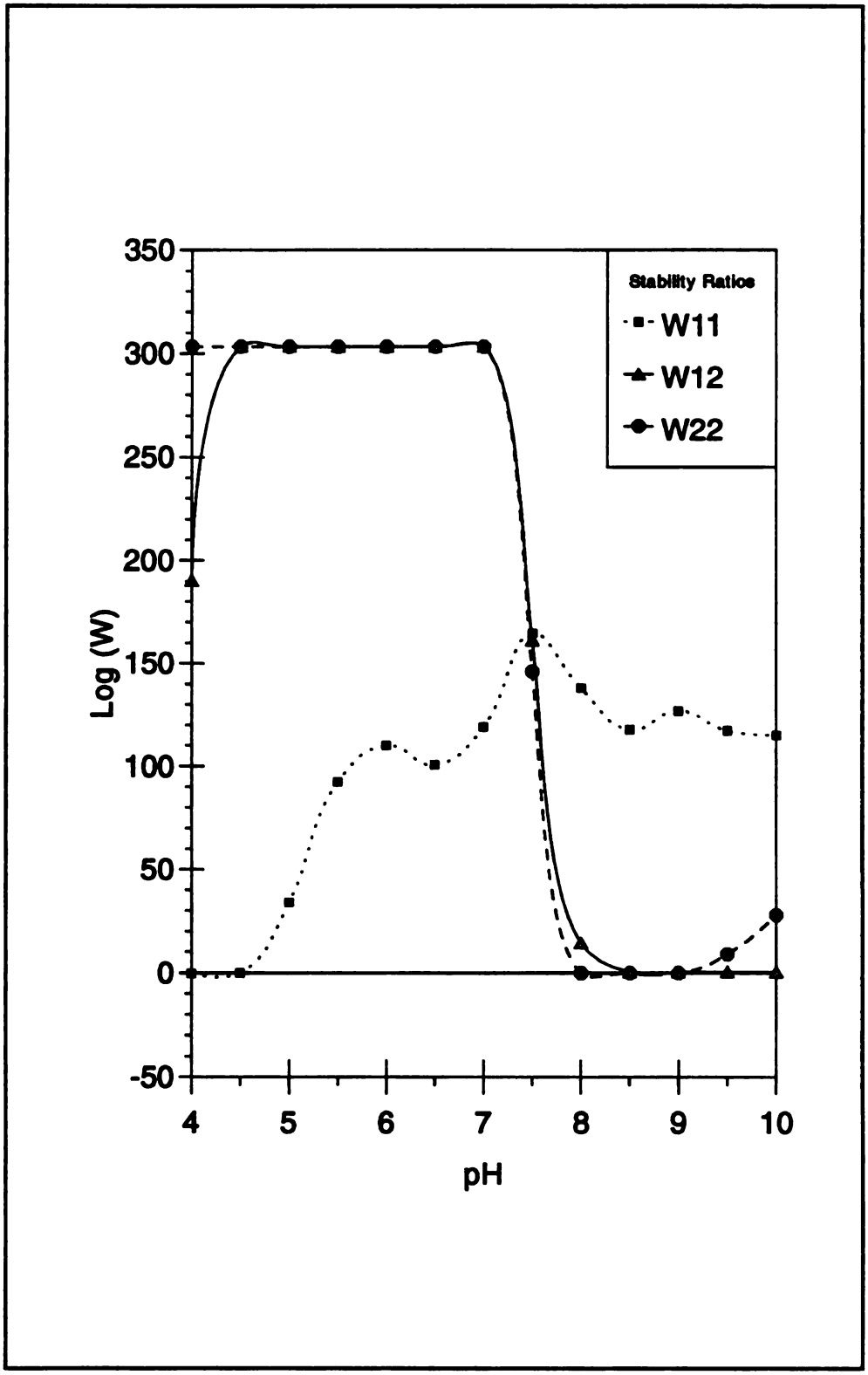

Figure 25. Stability prediction for the Fe-40Al325/Al_2O_3 system using p.s. = 1/2 simulation.

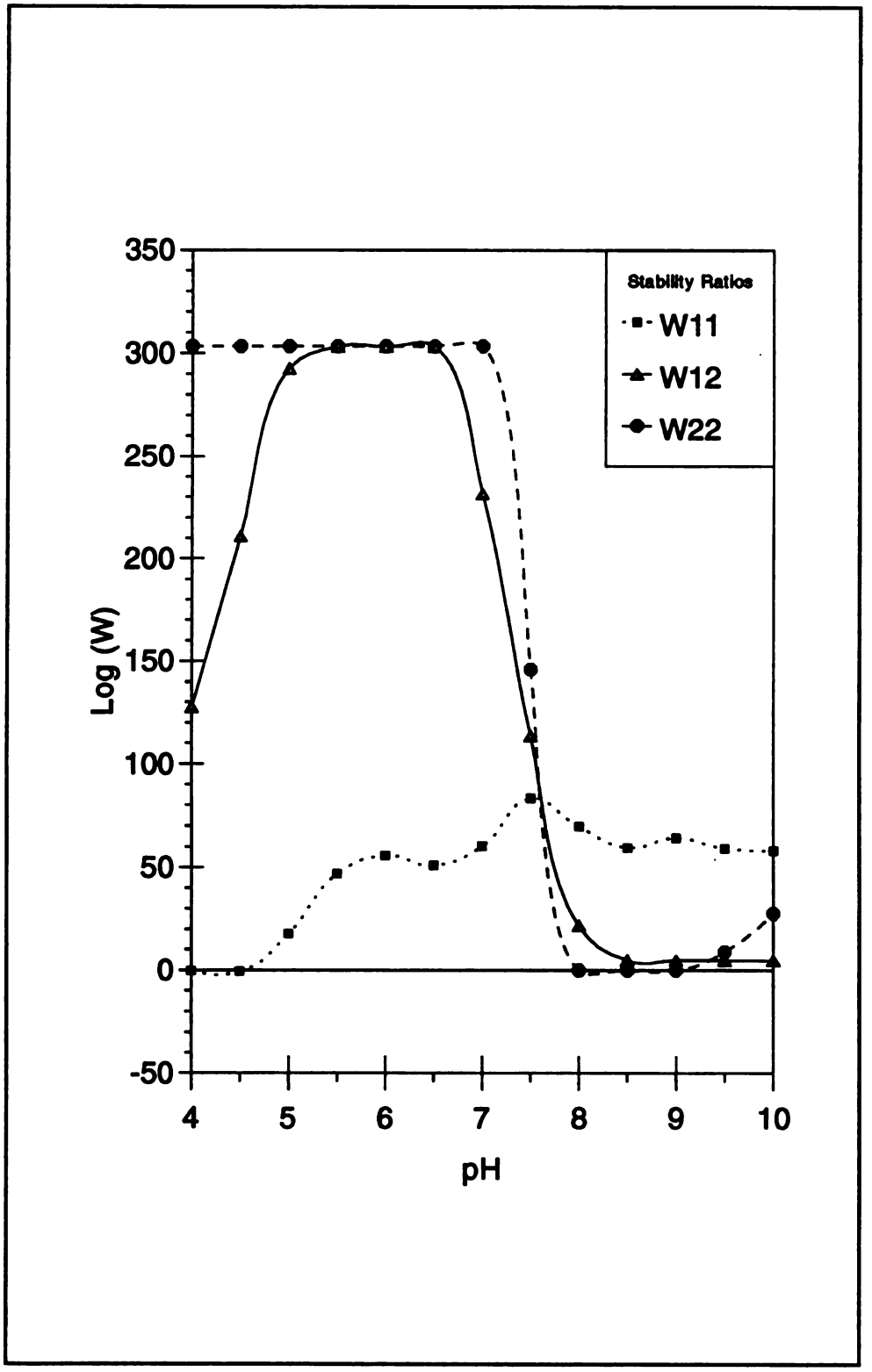

Figure 26. Stability Prediction for Fe-40Al325 / Al_2O_3 system using p.s. < 10μm simulation.

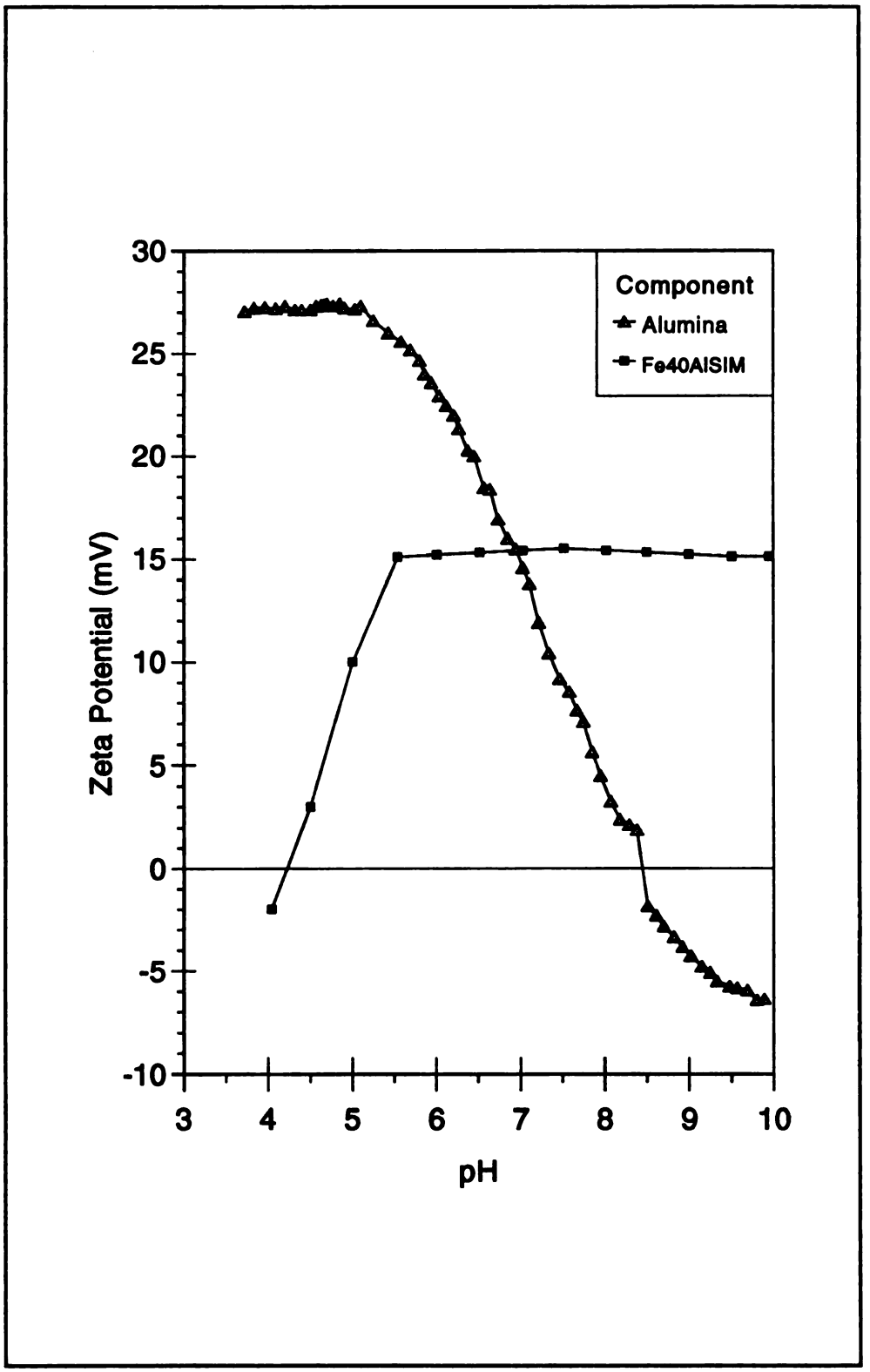

Figure 27. Zeta potential vs. pH data for the Fe-40Al325 Simulation (titration from pH 4.0 to pH 10.0).

ESA. One possible method for taking the flocculation kinetics into account is by performing point measurements using data from the Mastersizer for the same pH values. This would allow the zeta potential to be measured with repect to the particle size at that particular pH instead of assuming that the particle size remians constant over the entire pH range. The hypothetical stability prediction plot for the Fe-40Al325 / Al_2O_3 system is shown in Figure 28.

By examining the data it is apparent that the exaggerated zeta potential values have a significant affect on the W_{11} stability ratio behavior, as expected. These exaggerated values, however, do not provide any change in the stability ratio governing heterocoagulation, W_{12}. This result indicates that the heterocoagulation data is controlled by other factors such as particle size and flocculation kinetics. The significance of this result will be explained in the next section. Experimental verification utilizing the both of the Fe-40Al powders and the FP Al_2O_3 fiber is presented in the next section.

Fiber Coating

As was stated previously, the stability prediction program revealed that the ideal processing range for the Fe-40Al/Al_2O_3 system existed at pH vales greater than pH 8.0. The net set of experiments performed were designed to not only verify the accuracy of the prediction relative to the Fe-40Al/Al_2O_3 system but also to determine the actual ideal processing range by physical coating the FP Al_2O_3 fibers with the Fe-40Al matrix powder. Two experiments were set up for the characterization of particle-

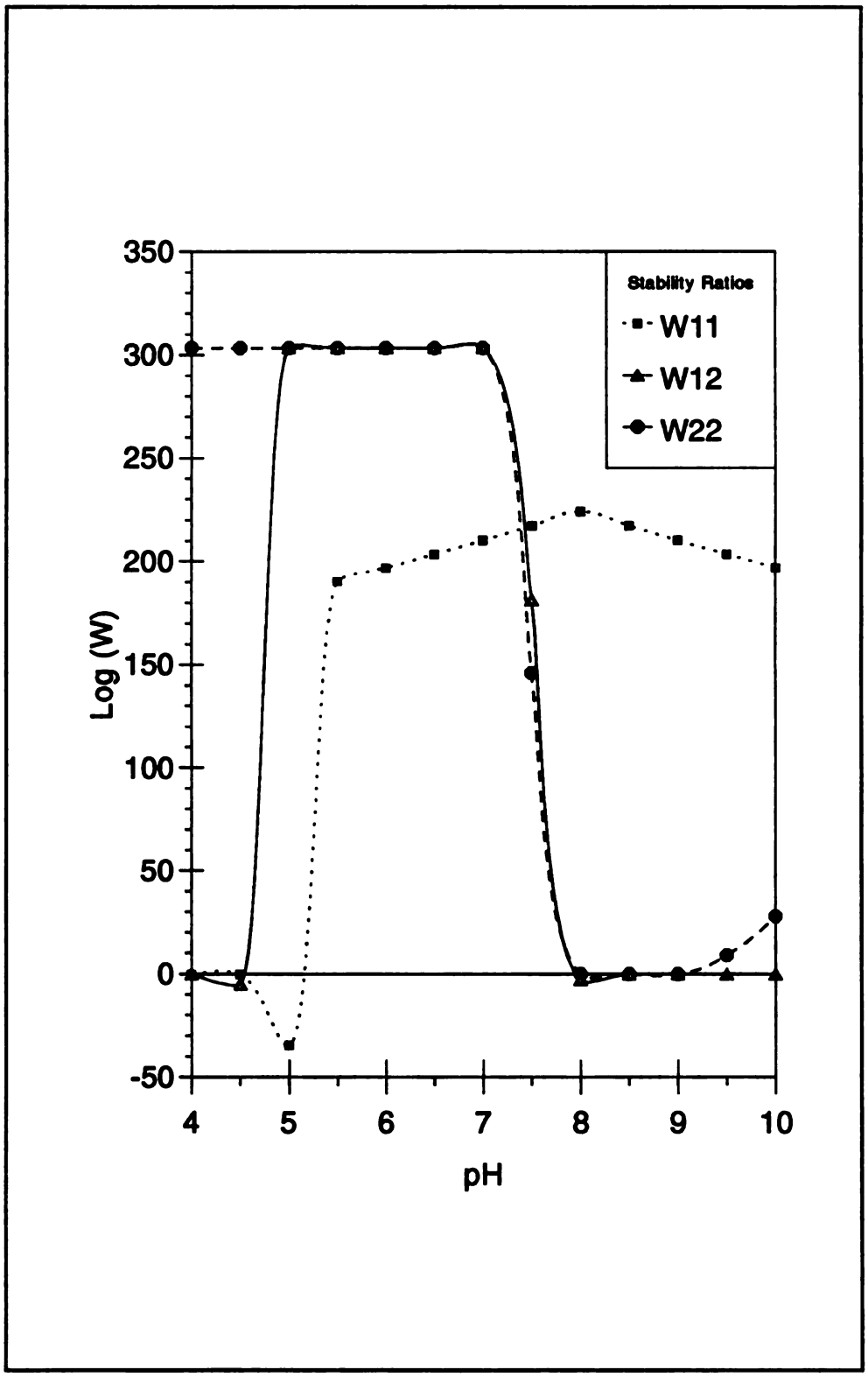

Figure 28. Stability prediction for Fe-40Al325 simulation.

coated fibers. The first experiment was designed to qualitatively evaluate the magnitude and distribution of coating with respect to varying pH values. The results were obtained by visually examining the residual coating of the fibers by the matrix particles at different pH values. The term "residual" is used to define the amount of matrix which is electrophoretically deposited onto the fiber when the fiber is immersed into the powder suspension. The residual coating experiment was primarily focused on using the Fe-40Al325 powder as the matrix instead of the Fe-40AlSED. For reasons that will be expanded upon later, in the best interest of the research project, it only became feasible to use the -325 mesh powder for the matrix. The second experiment performed expanded upon the results of the first experiment utilizing the scanning electron microscope to characterize the coated specimens.

The residual coating experiment was performed by mixing up a 25% Fe-40Al325 powder suspension. Once the desired pH of the suspension was obtained and stabilized, a previously cut 70mm fiber strand was immersed into suspension and then immediately placed on a glass slide and labeled. The basis for this experiment was to allow the surface tension of the water to remove the powder form the fiber surface by allowing the wet fiber strand to come into contact with the glass microscope slide. This allowed for the amount of "residual" powder to be visually characterized and subsequently the ideal processing value(s) identified. As was observed, the pH range which generates the highest magnitude of coating is between the ranges of 5.5 and 6.0. This differs slightly from the predicted values of pH 8.0 and higher. The values that each coating was performed at is actually represented by a small range. For example, the value of pH 5.5 was actually between the range of pH 5.5 and pH 6.0. this approach had to be taken as a result of the minor problems associated with

achieving a pH value and holding that value to an accuracy of two significant decimal places by titrating different normalities of acid and base.

Once the overall pH range was macroscopically characterized and the actual ideal processing range established, the second experiment could then be performed utilizing the SEM. Initial coating experiments were performed which utilized the Fe-40AlSED powder. An experiment similar to the residual coating experiment was performed by A. Martin revealed that the ideal processing range would also be between pH 5.0 and pH 6.0. Therefore, a 10^{w}/o suspension was prepared using the Fe-40ALSED and specimens were prepared over a range of pH's from pH 4.0 to pH 7.0. The major reason that the number of specimens prepared for SEM characterization was substantially less than those prepared for residual coating was due to the immense difficulty in preparing the SEM samples. Due to the relative sensitivity of individually coated fiber samples being handled. In addition to this, difficulty was consistently encountered in providing a conductive sample within the SEM. This was remedied by providing a 40nm thick gold coating using a sputter coating device. The work involving the Fe-40AlSED was eventually replaced by the Fe-40Al325 powder because of several problems encountered using the Fe-40AlSED.

The major problem encountered while using the Fe-40AlSED was the extremely limited supply of usable fines (i.e. d <10μm). In order to generate enough powder for a 5^{v}/o suspension of powder extensive preparation time was expended for the sedimentation. In addition to this, it was later noticed that in order for the coating to be effective, larger volume percentage suspension were required. Therefore, due to the shortage of Fe-40AlSED, this requirement became impossible to fulfill. Another additional problem encountered when coating the FP Al_2O_3 fibers with the

Fe-40ALSED powder was that due to the reactivation of the adsorbed ions once the suspension was formed. This made it extremely difficult to stabilize the pH in order to coat the fibers and record the conditions at which the process took place in an accurate manner. As pertaining to the formation of the SEM specimens, the major problem encountered here involved excess damage of the coated fibers via the electron beam. In light of many of these initial problems encountered, a successful coating of an FP Al_2O_3 using the Fe-40AlSED powder was achieved. The ideal coating was achieved within the range of pH 5.5 to pH 6.0. As can be observed from Figure 29, uniform coating of the FP fiber is achieved. Also evident from this picture is the existence of some homocoagulation between the very large and small particles which are active in the coating process. This attraction between like components can be eliminated by narrowing the working size range of the powder used. This will not only provide less homocoagulation but also aid in providing a more uniform distribution of matrix particles around the fiber. The photograph in Figure 29 was initially representative of the specimen itself prior to the electron beam damage which eventually destroyed the specimen.

Once the Fe-40Al325 was obtained, the Fe-40AlSED was replaced and the residual coating experiments were performed to provide an approximate processing range were the SEM characterization could take place, as explained previously. As shown in Figure 29, the range which produces the most residual powder is located at a pH of 5.5 to pH of 6.5. Therefore, an SEM characterization experiment was performed by coating three 70mm fiber strands at three different pH values. The values chosen, as dictated by the residual coatingexperiment, were pH 3.0, pH 6.0, pH 8.0. Contrary to the previous experiment, the specimens produced for the SEM

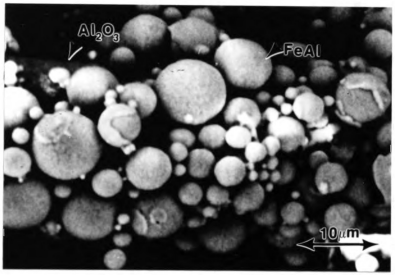

Figure 29. SEM micrograph of coated FP Al_2O_3 fiber with Fe-40AlSED matrix particles at pH 5.5 to 6.0.

characterization were submersed for 20 seconds in a 25v/o suspension in a "bow-like" manner. This geometry was provided by securing each end and then producing a bendin the fiber that produces a horse-shoe shape. This geometry is preferred over the initial configuration used which included simply dipping the fiber longitudinally into the suspension. This is because the geometry produced by forming a bend and securing the fiber at both ends more adequately approximates the interactions that the fibers and powder will experience in a continuous winding system. Once the fiber were immersed for 20 seconds, they were then hung vertically to allow for the water to run off the end of the fiber. This drying procedure was performed in this manner so as to imitate the scenario that the coated fiber will go through as it is pulled out of the suspension and wound onto the mandrel of the winding system. As will be shown in the following micrographs, the surface tension of the water was not great enough to remove the adhered powder along with it as it transversed the length of the fiber when hung vertically. Figures 30, 31, and 32 show the variability achieved in coating the fibers at pH 3.0, pH 6.0, and pH 8.0. As can be seen from both Figures 30 and 32, unacceptable coating of the fiber is exhibited. This is characterized by the absence of uniform coating and the small volume fraction of the matrix particles present. An example of an acceptable degree of coating is exhibited in Figure 31. From these micrographs it is apparent that the not only is uniform coating of the fiber achieved but there exists an adequate volume fraction of powder present. Also, infiltration is achieved between the fibers thus indicating that there is no homocoagulation between the fibers themselves which would prevent this. A higher magnification micrograph of the same specimen coated at pH 6.0 is shown in Figure 33. Upon examination it is apparent that homocoagulation between the powder

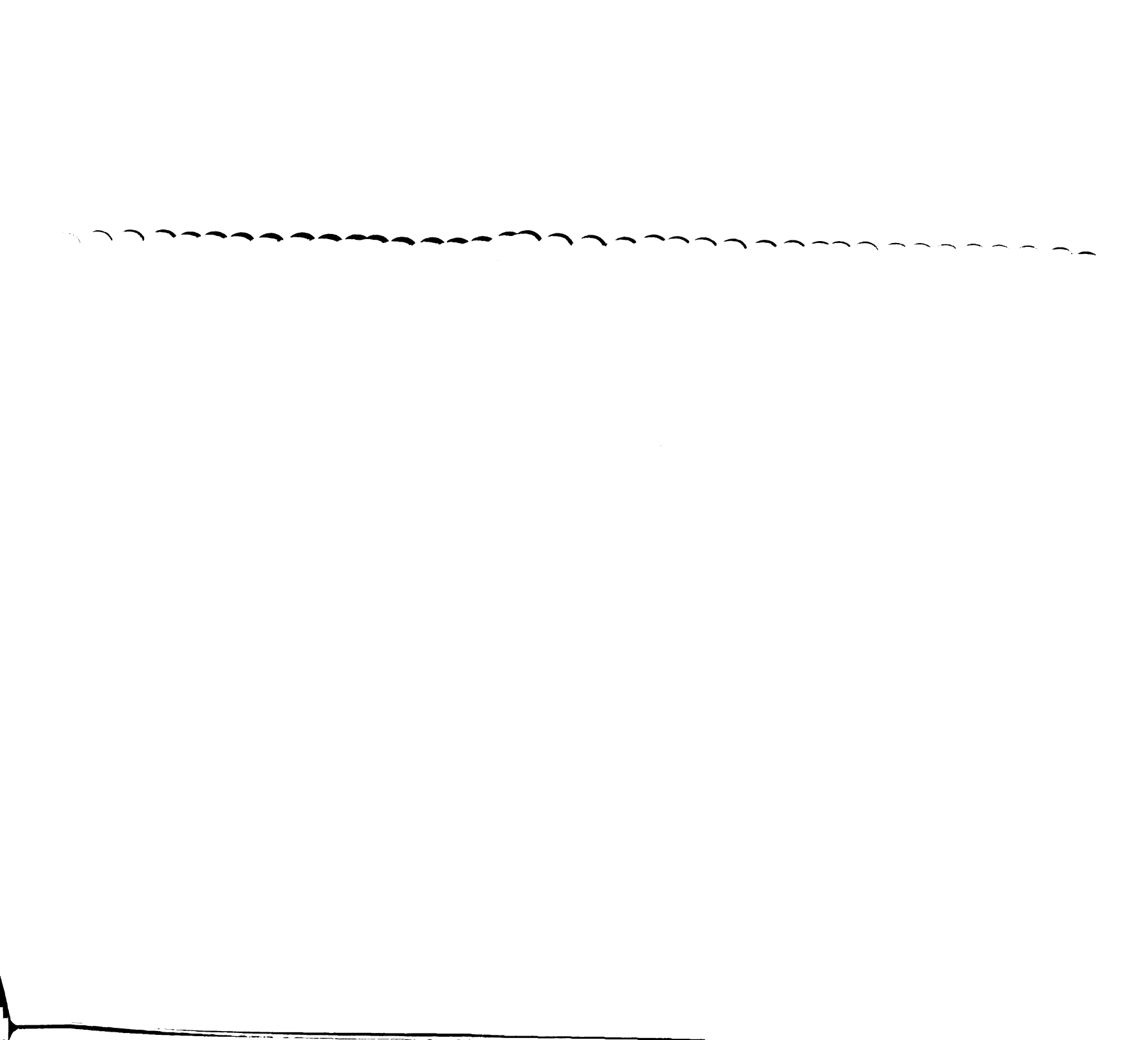

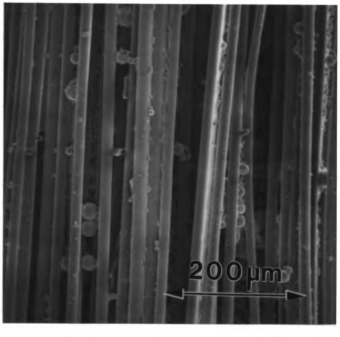

Figure 30. SEM micrograph showing the degree of coating at pH 3.0 for the Fe-40Al325 / FP Al_2O_3 system. (100X).

Figure 31. SEM micrograph showing the degree of coating at pH 6.0 for the Fe-40Al325 / FP Al_2O_3 system. (80X).

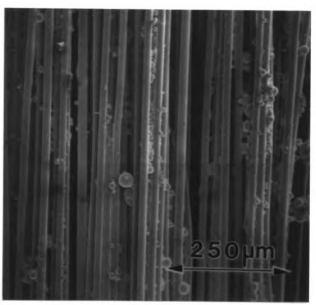

Figure 32. SEM micrograph showing the degree of coating at a pH 8.0 for the Fe-40Al325 / FP Al_2O_3 system. (100X).

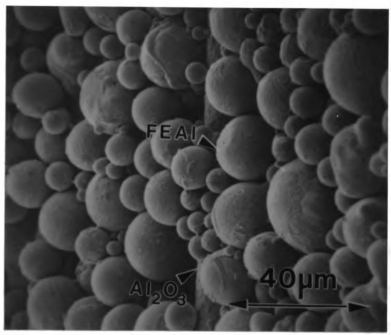

Figure 33. SEM micrograph showing the uniform structure of the Fe-40Al325 / FP Al_2O_3 system. (800X).

particles is limited and that an even distribution of powder around the reinforcing fibers is achieved.

From the previous two experiments performed, the actual range within which the IMCs should be processed at using fiber electrophoretic deposition method is located between pH 5.0 and pH 6.5. This is verified by the production of individually coated fiber specimens which show a uniform distribution of matrix particles and exhibit limited homocoagulation with respect to both components. Now attention will be shifted to present and discuss the Filament winding system developed for future implementation into the IMC production process.

Filament Winding System

The fundamental intent for the design of the Fiber Electrophoretic Deposition (FED) filament winding system was to develop a prototype winding system which would enable future processing of continuously reinforced IMCs. The basis for the design of the winding system followed the fundamental requirements pertaining to conventional winding systems in addition to those requirements generated by the use of electrophoretic deposition.

The overall design requirement was to provide a laboratory scale winding system which would generate IMC composite green bodies for consolidation into near-fully dense composites. Figure 39 shows the completed prototype in its current state. From this photograph, the several components necessary for a successful winding system are shown. These include: (1)the fiber delivery assembly, (2)successive multiple rollers, (3)suspension bath and roller/guide cradle, (4)take-up mandrel, and (5)system control panel. In addition to the global requirements already discussed,

there exists specific design requirements which pertain to each component of the system. The design of each of these components will be discussed in detail.

The main design requirement of the fiber delivery system was to force the multistrand fiber to spread-out or "lay down" prior to entry into the impregnating suspension bath. This is initially accomplished by providing a consistent drag force upon the fiber while it is being pulled through the system. This is accomplished by implementing a bearing assisted shaft though the multistrand filament spool. The specific bearings were selected such that the diameter was large enough to provide enough positive tension without the fiber breaking. Figure 35 shows the finished filament delivery assembly. The bearing rod is threaded along with the end caps so that the spool is secure during operation and can be easily changed when needed.

In addition to providing positive tension to the multistrand fiber, there exists additional requirement necessary for adequate fiber lay-down. This is accomplished by allowing the fiber to transverse over a succession of bearing assisted rollers which provide the curved surface over which the multistrand fiber will spread out. The specific multiple rolling assembly developed for this system included the use of 3 bearing assisted rollers made from ultra-high density polyethylene which have 2 dimensional rotational motion and 1 bearing assisted roller with both rotational and transverse motion. The purpose for the rotational and transfers motion in the last roller is to provide an multi-adjustable roller which will give proper alignment of the fiber into the suspension bath. The multiple rolling assembly is depicted in Figure 34.

Once the fiber has properly spread out, it is ready to be incorporated into the suspension bath were the matrix powder will infiltrate and electrophoretically deposit onto the fiber strands. Several design requirements were adhered to. The first

requirement involved providing enough space to accommodate an acid/base titration system, metering pumps and ultrasonic probe if necessary. Also, a cradle was designed to further the spreading out of the multistrand fiber which was previously done by the multiple rolling assembly. 3 rollers were fashioned from virgin Teflon and given rotational motion with the structure of the cradle. The cradle itself was provided with eyelets at each corner so that the entire assembly could be attached to the winding system base via tension springs. Figures 36 and 37 illustrate these design requirements. The remaining design requirement pertaining to the cradle assembly involved providing the ability to guide the impregnated fiber out of the suspension and onto the take-up mandrel. This was accomplished by cutting a 1mm wide square groove 3mm deep into the roller which resides closest to the mandrel assembly. This would groove controls the impregnated fiber onto the mandrel and allows the motion of the mandrel to dictate the geometry of the wound fiber. The major difference here, as compared to previously introduced design methods [27], is that the guide roller must remain within the suspension. Whereas with conventional winding techniques, there exists a guide roller directly atop of or even connected to the mandrel assembly [27]. This is illustrated in Figure 38.

The final step in the winding process involves collecting the impregnated fiber onto a mandrel for future consolidation using a variety of techniques [4-8]. The design anddevelopment for the mandrel in this winding system was adapted from previously done work by D. Maglaya [32]. The modifications performed on the existing assembly included providing independent rotational and transverse motion so that precise control can be achieved in producing an successfully wound IMC. This independent motion was provided by attaching a one Dayton D.C. motor to the

Figure 34. 35mm photograph showing the various components of the laboratory-scale FED filament winding system.

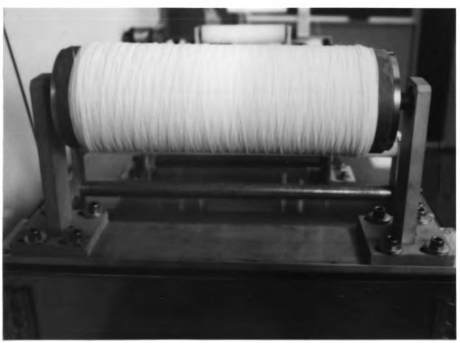

Figure 35. Multi-strand fiber delivery assembly.

mandrel assembly and another Dayton D.C. motor to threaded cross-head assembly. This is shown in Figure 39. Figures 40 and 41 show the complete mandrel assembly. Several components of the assembly include: (1)teflon mandrel, (2)reversible polarizing switches, (3)transverse motion cross-head assembly motor, (4)and mandrel rotation motor.

Once the fiber winding system was completed, physical runs were made in which a the Al_2O_3 was drawn through dry so that all imperfections and parameters could be adjusted to provide a mechanically sound system. From the runs performed the following judgements were made regarding the modifications for the FED winding system. First, the fiber delivery assembly needed to be relocated to a position much farther away than that originally anticipated due to the fact that the 11" fiber coil provided from the manufacturer contained a helical wind and this caused excess transverse motion of the fiber along the rolling assembly. In addition to this, the suspension bath itself had to be elevated to lessen the radius of curvature that the fiber experienced while going into and coming out of the suspension bath. The last modification is currently involving the re-shaping of the teflon mandrel due to the change in the foreseen consolidation requirements.

Figure 36. Cradle-roller guide and suspension bath assembly.

Figure 37. Rotational motion of cradle-roller assembly.

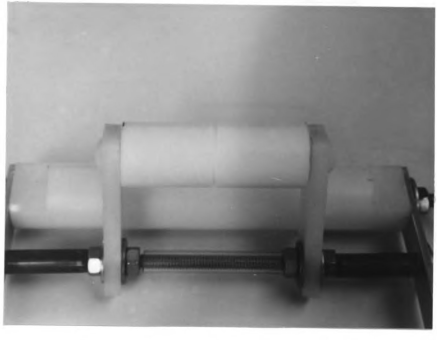

Figure 38. Fiber guide roller.

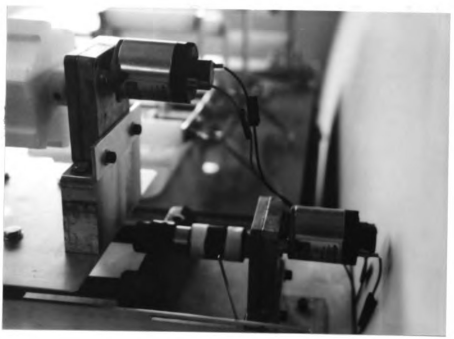

Figure 39. Rotational and transverse motor assembly.

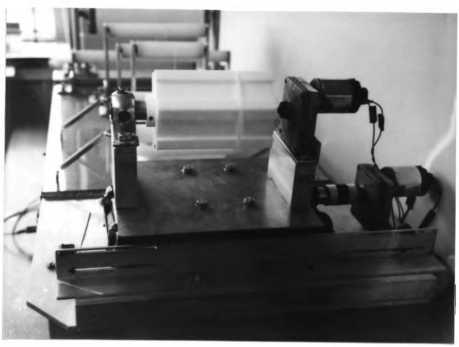

Figure 40. Mandrel assembly.

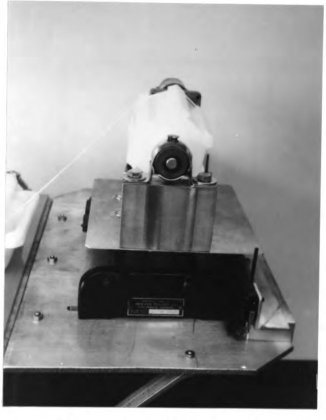

Figure 41. Side-view of mandrel assembly

CONCLUSIONS

Over the course of this research project several aspects relating to the development of a technique for the processing of intermetallic matrix composites were analyzed. These several aspects included determining a method for reducing the particle size, developing a means for determining both the actual and effective particle size, and correlating both theoretical and experimental results which describe the colloidal behavior of the multi component composite system. In addition to this a suitable mechanical winding system was also designed and developed for future implementation in to the processing scheme.

From the experimental work performed it was determined that an acceptable means for reducing the initial particle size of the as-received powder was developed. This technique involved combining sedimentation behavior and vacuum assisted dehydration. As was in the data presented, surface changes due to consistent hydration of the powder surface, which may include oxidation, contributed to the observed instability of the single component. Upon realizing which steps within the reduction method were unnecessary, the relative instability of the system improved. Nevertheless, since the powder was suspended in an aqueous solution during the process, the existence of adsorbed ions was apparent as revealed by the experiments to determine the relative stability of the system. Therefore, it became evident that the

only necessary step within the reduction process was a washing step which would remove the adsorbed ions and produce a reduced particle size with the same characteristics as the as-received supply.

It was also determined that the ideal particle size range for the matrix powder is relatively small (i.e. a few μm) and the size range as narrow as possible. This type of processing necessitates a small particle size in order that the colloidal forces can dominate over gravitational forces. This size range stipulation was made so that the previously observed large particle/small particle flocculation which indicated instability would be alleviated.

During the examination of the processing parameters which are important to the colloidal processing of IMC's it was determined that the ideal electrolyte concentration for the powder suspension was between 0.001N and 0.0001N KNO_3. The c.c.c. experiment that was performed using the Fe-40AlSED powder generated experimental verification that adsorbed ions existed as a result of the particles being suspended in an aqueous solution. The second parameter examined was the effective particle size. The purpose of this experiment was not only to provide particle size data which could be cross-referenced with particle size expectations from the grid analysis but also to generate an array of data which could aid in determing the flocculation behavior which is extremely important with respect to the determination of surface potential and stability. It was discovered over the duration of the particle size experiments that the possibility for obtaining a complete examination of the flocculation kinetics was not possible with the equipment that was utilized. Data was produced, though, which gave an excellent description as to the flocculation behavior for each matrix component analyzed. Although, the data provided inconclusive

flocculation evidence for the Fe-40AlSED sample over a wide range of pHs, it did provide information which revealed that maximum flocculation occurs at a pH 3.0 and pH 5.5 for the Fe-40Al325 sample. As was discovered during the ESA measurement and stability predictions, accuracy and knowledge of particle size is crucial in providing accurate results for the theoretical model.

During the ESA measurement for the Fe-40AlSED, it was determined that the maximum potential, which corresponds to minimum flocculation was achieved for a range of pH 5.0 - 6.5. A similar but more generalized result was obtained for the Fe-40Al325sample which showed maximum potential for pH greater than 5.5. The data scatter shown in the potentiometric titration plot can be primarily attributed to the large particle size range characteristic to the -325 mesh sample. This again reinforces the initial stipulation that not only is a small particle size desirable but also a narrow particle size range. Upon comparison with the effective particle size data, the behavior exhibited during the potentiometric titration was very consistent with the data complied from the particle size analysis. The discrepancies which existed between the Fe-40AlSED and the Fe-40Al325 zeta potential data were the resultant of several factors. These included: (1) Fundamental difference in the surfaces due to the sedimentation procedure, (2) Possible difference in the chemical make-up of the -325 mesh surface due to the minor additions of Zr and B, (3) Particle size range and accuracy of reported values, and (4) Inability to determine the true particle size due to flocculation kinetics.

By using the acquired zeta potential data, stability plots were generated utilizing a computer program which attempted to predict the most desirable processing range by maximizing the stability of like components and minimizing the stability of

dissimilar components, thus providing heterocoagulation of the powder to the fiber surface. Both stability plots which were provided yielded the same conclusion for both powder samples. The ideal range indicated from the stability data showed that stability was minimized (in both cases) for a pH value approximately greater that pH 8.0. Once this predicted range was established, physical coating experiments were then performed to generate actual pH processing range for which the results are most desirable. From the fiber coating experiments it was determined that the ideal range is located between pH 5.0 to pH 6.5. Since this result did not agree with the theoretical predictions from before, the validity of the computer model, as applied to this system, was in question. In order to determine whether the program itself did not apply to this system or whether inaccurate particle sizing was the cause for the conflicting results, a simulation was performed which utilized exaggerated zeta potential data so that any inaccuracies related to particle size changes caused by flocculation kinetics could be eliminated. This leads us to conclude that in order to generate more accurate zeta potential and stability data, the current standing of the ESA measurement, which assumes one constant particle size over the entire pH range, must be changed. This would allow for one particle size value to be specified per a single measurement, thus accounting for the flocculation kinetics present.

An adequate mechanical fiber winding system was also developed to eventually facilitate the processing of the IMCs. During the test runs which were performed, several modifications were implemented which were not previously introduced. The minor required modifications which were identified include: (1) the development of a different mandrel which eliminate high stress areas around its circumference and prevent fiber damage, (2) relocation of fiber delivery assembly to account for existing

helical wind on the provided fiber spool, and (3) implementation of a second power supply to make the D.C. motors independent of each other so that accurate and repeatable results can be obtained.

Upon completion of the experimental examination of the several aspects of FED processing, an excellent understanding as to the behavior of the system was gained. Several variables which were important to the validity of the testing procedure were identified and examined. From the gathered results such parameters as optimum pH processing range, critical coagulation concentration, and effective particle size were determined. Information from these experiments were then used to contrast the theoretical and experimental results. It was further shown that it is physically possible and feasible to produce a powder coated fiber tow without the use of expensive and contaminating binders. By understanding and controlling the parameters inherent to the FED processing scheme, it has become possible to produce uniformly coated continuously reinforced composites.

APPENDIX

```
CCCCCCCCCCCCCCCCCCCCCCCCCCCCCCCCCCCCCCCCCCCCCCCCCCCCCCCCCCCCCCCCCC
C                                Rev. 06-22-92                      C
C   MASTERS THESIS RESEARCH                                         C
C   BRETT A. WILSON                                                 C
C   MICHIGAN STATE UNIVERSITY                                       C
C   COLLEGE OF ENGINEERING                                          C
C   DEPARTMENT OF METALLURGY, MECHANICS,                            C
C       AND MATERIAL SCIENCE                                        C
C                                                                   C
CCCCCCCCCCCCCCCCCCCCCCCCCCCCCCCCCCCCCCCCCCCCCCCCCCCCCCCCCCCCCCCCCC

CCCCCCCCCCCCCCCCCCCCCCCCCCCCCCCCCCCCCCCCCCCCCCCCCCCCCCCCCCCCCCCCCC
C                                                                   C
C   THIS PROGRAM USES MEASURABLE MATERIAL DATA TO                   C
C   CREATE INFORMATION WHICH SHOULD PREDICT THE                     C
C   FLOCCULATION STATE OF TWO COMPONENT COLLOIDAL                   C
C   SUSPENSIONS.                                                    C
C                                                                   C
C   THE PROGRAM RELIES ON A METHOD WHICH IS A MOD-                  C
C   IFICATION OF THE H.H.F. METHOD, WHICH IS BASED ON               C
C   THE DEBYE-HUCKEL APPROXIMATION FOR THE REPULSION                C
C   BETWEEN TWO PLATES OF CONSTANT POTENTIAL.                       C
C                                                                   C
C   MODIFICATIONS INCLUDE:                                          C
C     -USING AN EFFECTIVE HAMAKER CONSTANT FOR TWO                  C
C     PARTICLES IN A DISPESING MEDIUM.                              C
C    -USING ZETA POTENTIAL DATA INSTEAD OF CALCULAT-                C
C     ING THE SURFACE POTNTIAL FROM POINT-OF-ZERO-                  C
C     CHARGE DATA.                                                  C
C                                                                   C
CCCCCCCCCCCCCCCCCCCCCCCCCCCCCCCCCCCCCCCCCCCCCCCCCCCCCCCCCCCCCCCCCC
```

FILE NAME:FE40ALF\BFE40ALF
FILE DESCRIPTION:
RUN WITH Constant Potential for Fe40Al/Alumina fiber
THIS DATA WAS AQUIRED ON: 06/02/1993
AQUISITION BY THE PROGRAM STARTED AT... 12:07:52:90
AND FINISHED AT... 12:13:58:38
OVERALL PROPORTION OF COMPONENT 1 IN SYSTEM =.500
CONCENTRATION OF 1-1 ELECTROLYTE IN SYSTEM = .00010 N
ATOMIC PARTICLE RADIUS OF COMPONENT 1 = 11860.0 nm
ATOMIC PARTICLE RADIUS OF COMPONENT 2 = 15000.0 nm
TEMPERATURE OF SYSTEM (IN DEG. C.) = 25.0
HAMAKER CONSTANT OF MEDIUM = .45E-19 J
HAMAKER CONSTANT OF COMPONENT 1 = .22E-18 J
HAMAKER CONSTANT OF COMPONENT 2 = .11E-18 J
ZETA POTENTIAL DATA WAS USED FOR CALCULATIONS.
ZETA POTENTIAL DATA FOR PARTICLE 1:

ZETA POTENTIAL VALUES:	CORESPONDING PH VALUES:
8.2	4.0
8.4	4.1
10.8	4.4
10.7	4.5
12.7	4.9
12.8	5.0
14.4	5.5
15.3	5.5
15.1	6.0
16.1	6.1
14.6	6.4
15.6	6.6
16.3	6.8
15.3	7.1
16.1	7.3
16.9	7.5
15.4	7.9
16.3	8.0
15.6	8.5
15.6	8.9
16.4	9.1
16.3	9.5
15.4	9.5
15.8	9.9
15.5	10.0

ZETA POTENTIAL DATA FOR PARTICLE 2:

ZETA POTENTIAL VALUES:	CORESPONDING PH VALUES:
27.2	4.0
27.1	4.1
27.1	4.5
27.2	4.9
27.1	5.0
26.0	5.4
25.5	5.6
23.5	5.9
22.9	6.0
19.9	6.4
18.4	6.6
15.4	6.9
14.5	7.0
9.2	7.5
8.5	7.6
4.5	7.9
3.3	8.1
1.9	8.4
-1.8	8.5
-3.8	8.9
-4.2	9.0
-5.7	9.5
-5.8	9.6
-6.3	9.9
-6.4	10.0

CALCULATED OVERALL STABILITY RATIO DATA:

OVERALL STABILITY RATIO: (W11,W12,W22,WT)				CORESPONDING PH VALUES:
4.00 ,	.3320E+00 ,	.9314+259 ,	.2596+304 ,	.7414E+00
4.50 ,	.2620E-15 ,	.2325+304 ,	.2596+304 ,	.5850E-15
5.00 ,	.1662E+66 ,	.2325+304 ,	.2596+304 ,	.3711E+66
5.50 ,	.3070+181 ,	.2325+304 ,	.2596+304 ,	.6854+181
6.00 ,	.1240+216 ,	.2325+304 ,	.2596+304 ,	.2770+216
6.50 ,	.5857+197 ,	.2325+304 ,	.2596+304 ,	.1308+198
7.00 ,	.1429+234 ,	.2325+304 ,	.2596+304 ,	.3191+234
7.50 ,	.2053+304 ,	.2516+205 ,	.8491+146 ,	.7760+147
8.00 ,	.3545+271 ,	.1130E+00 ,	.6953E+00 ,	.2454E+00
8.50 ,	.6530+231 ,	.5728E+00 ,	.6953E+00 ,	.1075E+01
9.00 ,	.3804+249 ,	.5728E+00 ,	.6953E+00 ,	.1075E+01
9.50 ,	.2602+230 ,	.5728E+00 ,	.6162E+09 ,	.1294E+01
10.00 ,	.2156+226 ,	.5728E+00 ,	.5465E+28 ,	.1294E+01

FILE NAME:FE40ALG\BFE40ALG
FILE DESCRIPTION:
RUN WITH Constant Potential for Fe40Al/Alumina fiber, reduced pwdr size
THIS DATA WAS AQUIRED ON: 06/02/1993
AQUISITION BY THE PROGRAM STARTED AT... 12:16:26:57
AND FINISHED AT... 12:20:46:20
OVERALL PROPORTION OF COMPONENT 1 IN SYSTEM =.500
CONCENTRATION OF 1-1 ELECTROLYTE IN SYSTEM = .00010 N
ATOMIC PARTICLE RADIUS OF COMPONENT 1 = 6000.0 nm
ATOMIC PARTICLE RADIUS OF COMPONENT 2 = 15000.0 nm
TEMPERATURE OF SYSTEM (IN DEG. C.) = 25.0
HAMAKER CONSTANT OF MEDIUM = .45E-19 J
HAMAKER CONSTANT OF COMPONENT 1 = .22E-18 J
HAMAKER CONSTANT OF COMPONENT 2 = .11E-18 J
ZETA POTENTIAL DATA WAS USED FOR CALCULATIONS.
ZETA POTENTIAL DATA FOR PARTICLE 1:

ZETA POTENTIAL VALUES:	CORESPONDING PH VALUES:
8.2	4.0
8.4	4.1
10.8	4.4
10.7	4.5
12.7	4.9
12.8	5.0
14.4	5.5
15.3	5.5
15.1	6.0
16.1	6.1
14.6	6.4
15.6	6.6
16.3	6.8
15.3	7.1
16.1	7.3
16.9	7.5
15.4	7.9
16.3	8.0
15.6	8.5
15.6	8.9
16.4	9.1
16.3	9.5
15.4	9.5
15.8	9.9
15.5	10.0

ZETA POTENTIAL DATA FOR PARTICLE 2:

ZETA POTENTIAL VALUES:	CORESPONDING PH VALUES:
27.2	4.0
27.1	4.1
27.1	4.5
27.2	4.9
27.1	5.0
26.0	5.4
25.5	5.6
23.5	5.9
22.9	6.0
19.9	6.4
18.4	6.6
15.4	6.9
14.5	7.0
9.2	7.5
8.5	7.6
4.5	7.9
3.3	8.1
1.9	8.4
-1.8	8.5
-3.8	8.9
-4.2	9.0
-5.7	9.5
-5.8	9.6
-6.3	9.9
-6.4	10.0

CALCULATED OVERALL STABILITY RATIO DATA:

OVERALL STABILITY RATIO: (W11,W12,W22,WT)				CORESPONDING PH VALUES:
4.00 ,	.3346E+00 ,	.1800+191 ,	.2596+304 ,	.3788E+00
4.50 ,	.9661E-07 ,	.1818+304 ,	.2596+304 ,	.1094E-06
5.00 ,	.8223E+34 ,	.1818+304 ,	.2596+304 ,	.9309E+34
5.50 ,	.1876E+93 ,	.1818+304 ,	.2596+304 ,	.2123E+93
6.00 ,	.6178+110 ,	.1818+304 ,	.2596+304 ,	.6994+110
6.50 ,	.3269+101 ,	.1818+304 ,	.2596+304 ,	.3701+101
7.00 ,	.8571+119 ,	.1818+304 ,	.2596+304 ,	.9704+119
7.50 ,	.3382+165 ,	.1247+162 ,	.8491+146 ,	.2347+149
8.00 ,	.7254+138 ,	.1547E+15 ,	.6953E+00 ,	.1922E+03
8.50 ,	.5605+118 ,	.2007E+01 ,	.6953E+00 ,	.1625E+02
9.00 ,	.5505+127 ,	.2007E+01 ,	.6953E+00 ,	.1625E+02
9.50 ,	.1097+118 ,	.2007E+01 ,	.6162E+09 ,	.1775E+02
10.00 ,	.9420+115 ,	.2007E+01 ,	.5465E+28 ,	.1775E+02

FILE NAME:FE40ALH\BFE40ALH
FILE DESCRIPTION:
RUN WITH Constant Potential for Fe40Al/Alumina fiber, p.s.<10 microns
THIS DATA WAS AQUIRED ON: 06/08/1993
AQUISITION BY THE PROGRAM STARTED AT... 02:35:18:05
AND FINISHED AT... 02:46:51:26
OVERALL PROPORTION OF COMPONENT 1 IN SYSTEM =.500
CONCENTRATION OF 1-1 ELECTROLYTE IN SYSTEM = .00010 N
ATOMIC PARTICLE RADIUS OF COMPONENT 1 = 3000.0 nm
ATOMIC PARTICLE RADIUS OF COMPONENT 2 = 15000.0 nm
TEMPERATURE OF SYSTEM (IN DEG. C.) = 25.0
HAMAKER CONSTANT OF MEDIUM = .45E-19 J
HAMAKER CONSTANT OF COMPONENT 1 = .22E-18 J
HAMAKER CONSTANT OF COMPONENT 2 = .11E-18 J
ZETA POTENTIAL DATA WAS USED FOR CALCULATIONS.
ZETA POTENTIAL DATA FOR PARTICLE 1:

ZETA POTENTIAL VALUES:	CORESPONDING PH VALUES:
8.2	4.0
8.4	4.1
10.8	4.4
10.7	4.5
12.7	4.9
12.8	5.0
14.4	5.5
15.3	5.5
15.1	6.0
16.1	6.1
14.6	6.4
15.6	6.6
16.3	6.8
15.3	7.1
16.1	7.3
16.9	7.5
15.4	7.9
16.3	8.0
15.6	8.5
15.6	8.9
16.4	9.1
16.3	9.5
15.4	9.5
15.8	9.9
15.5	10.0

ZETA POTENTIAL DATA FOR PARTICLE 2:

ZETA POTENTIAL VALUES:	CORESPONDING PH VALUES:
27.2	4.0
27.1	4.1
27.1	4.5
27.2	4.9
27.1	5.0
26.0	5.4
25.5	5.6
23.5	5.9
22.9	6.0
19.9	6.4
18.4	6.6
15.4	6.9
14.5	7.0
9.2	7.5
8.5	7.6
4.5	7.9
3.3	8.1
1.9	8.4
-1.8	8.5
-3.8	8.9
-4.2	9.0
-5.7	9.5
-5.8	9.6
-6.3	9.9
-6.4	10.0

CALCULATED OVERALL STABILITY RATIO DATA:

OVERALL STABILITY RATIO: (W11,W12,W22,WT)				CORESPONDING PH VALUES:
.3365E+00,	.2178+128,	.2596+304,	.3419E+00	4.00
.1504E-02,	.4062+211,	.2596+304,	.1528E-02	4.50
.4991E+18,	.3367+293,	.2596+304,	.5071E+18	5.00
.8402E+47,	.1558+304,	.2596+304,	.8537E+47	5.50
.4943E+56,	.1558+304,	.2596+304,	.5022E+56	6.00
.1123E+52,	.1558+304,	.2596+304,	.1141E+52	6.50
.1863E+61,	.2422+232,	.2596+304,	.1893E+61	7.00
.1233E+84,	.1884+114,	.8491+146,	.1253E+84	7.50
.5547E+70,	.4843E+22,	.6953E+00,	.1104E+05	8.00
.4758E+60,	.6231E+05,	.6953E+00,	.1101E+05	8.50
.1508E+65,	.5734E+05,	.6953E+00,	.1100E+05	9.00
.2103E+60,	.5540E+05,	.6162E+09,	.3518E+07	9.50
.1943E+59,	.5472E+05,	.5465E+28,	.3475E+07	10.00

FILE NAME:FE40ALINBFE40ALI
FILE DESCRIPTION:
RUN WITH Const. Potn. for Fe40Al/Alumina fiber, mod. AlO zp, ps<10 microns
THIS DATA WAS AQUIRED ON: 06/08/1993
AQUISITION BY THE PROGRAM STARTED AT... 02:46:51:76
AND FINISHED AT... 02:54:21:87
OVERALL PROPORTION OF COMPONENT 1 IN SYSTEM =.500
CONCENTRATION OF 1-1 ELECTROLYTE IN SYSTEM = .00010 N
ATOMIC PARTICLE RADIUS OF COMPONENT 1 = 3000.0 nm
ATOMIC PARTICLE RADIUS OF COMPONENT 2 = 15000.0 nm
TEMPERATURE OF SYSTEM (IN DEG. C.) = 25.0
HAMAKER CONSTANT OF MEDIUM = .45E-19 J
HAMAKER CONSTANT OF COMPONENT 1 = .22E-18 J
HAMAKER CONSTANT OF COMPONENT 2 = .11E-18 J
ZETA POTENTIAL DATA WAS USED FOR CALCULATIONS.
ZETA POTENTIAL DATA FOR PARTICLE 1:

ZETA POTENTIAL VALUES:	CORESPONDING PH VALUES:
8.2	4.0
8.4	4.1
10.8	4.4
10.7	4.5
12.7	4.9
12.8	5.0
14.4	5.5
15.3	5.5
15.1	6.0
16.1	6.1
14.6	6.4
15.6	6.6
16.3	6.8
15.3	7.1
16.1	7.3
16.9	7.5
15.4	7.9
16.3	8.0
15.6	8.5
15.6	8.9
16.4	9.1
16.3	9.5
15.4	9.5
15.8	9.9
15.5	10.0

ZETA POTENTIAL DATA FOR PARTICLE 2:

ZETA POTENTIAL VALUES:	CORESPONDING PH VALUES:
45.3	4.0
45.2	4.5
45.0	5.0
42.9	5.5
38.2	6.0
32.1	6.5
24.2	7.0
15.3	7.5
6.8	8.0
-3.0	8.5
-7.0	9.0
-9.5	9.5
-10.0	10.0

CALCULATED OVERALL STABILITY RATIO DATA:

OVERALL STABILITY RATIO: (W11,W12,W22,WT)				CORESPONDING PH VALUES:
.3365E+00,	.3709+144,	.2596+304,	.3419E+00	4.00
.1504E-02,	.3253+242,	.2596+304,	.1528E-02	4.50
.4991E+18,	.1558+304,	.2596+304,	.5071E+18	5.00
.8402E+47,	.1558+304,	.2596+304,	.8537E+47	5.50
.4943E+56,	.1558+304,	.2596+304,	.5022E+56	6.00
.1123E+52,	.1558+304,	.2596+304,	.1141E+52	6.50
.1863E+61,	.1558+304,	.2596+304,	.1893E+61	7.00
.1233E+84,	.2225+264,	.2596+304,	.1253E+84	7.50
.5547E+70,	.1169E+66,	.1688E+43,	.2680E+47	8.00
.4758E+60,	.5921E+05,	.6953E+00,	.1101E+05	8.50
.1508E+65,	.5395E+05,	.5402E+50,	.3426E+07	9.00
.2103E+60,	.5193E+05,	.1762+178,	.3298E+07	9.50
.1943E+59,	.5158E+05,	.1531+211,	.3276E+07	10.00

FILE NAME:FE40ALT\BFE40ALT
FILE DESCRIPTION:
RUN WITH Constant Potential for Fe40Al/Alumina fiber; modified AlO zp
THIS DATA WAS AQUIRED ON: 06/03/1993
AQUISITION BY THE PROGRAM STARTED AT... 8:45:48:87
AND FINISHED AT... 8:57:35:21
OVERALL PROPORTION OF COMPONENT 1 IN SYSTEM =.500
CONCENTRATION OF 1-1 ELECTROLYTE IN SYSTEM = .00010 N
ATOMIC PARTICLE RADIUS OF COMPONENT 1 = 11860.0 nm
ATOMIC PARTICLE RADIUS OF COMPONENT 2 = 15000.0 nm
TEMPERATURE OF SYSTEM (IN DEG. C.) = 25.0
HAMAKER CONSTANT OF MEDIUM = .45E-19 J
HAMAKER CONSTANT OF COMPONENT 1 = .22E-18 J
HAMAKER CONSTANT OF COMPONENT 2 = .11E-18 J
ZETA POTENTIAL DATA WAS USED FOR CALCULATIONS.
ZETA POTENTIAL DATA FOR PARTICLE 1:

ZETA POTENTIAL VALUES:	CORESPONDING PH VALUES:
8.2	4.0
8.4	4.1
10.8	4.4
10.7	4.5
12.7	4.9
12.8	5.0
14.4	5.5
15.3	5.5
15.1	6.0
16.1	6.1
14.6	6.4
15.6	6.6
16.3	6.8
15.3	7.1
16.1	7.3
16.9	7.5
15.4	7.9
16.3	8.0
15.6	8.5
15.6	8.9
16.4	9.1
16.3	9.5
15.4	9.5
15.8	9.9
15.5	10.0

ZETA POTENTIAL DATA FOR PARTICLE 2:

ZETA POTENTIAL VALUES:	CORESPONDING PH VALUES:
45.3	4.0
45.2	4.5
45.0	5.0
42.9	5.5
38.2	6.0
32.1	6.5
24.2	7.0
15.3	7.5
6.8	8.0
-3.0	8.5
-7.0	9.0
-9.5	9.5
-10.0	10.0

CALCULATED OVERALL STABILITY RATIO DATA:

OVERALL STABILITY RATIO: (W11,W12,W22,WT)				CORESPONDING PH VALUES:
.3320E+00,	.2325+304,	.2596+304,	.7414E+00	4.00
.2620E-15,	.2325+304,	.2596+304,	.5850E-15	4.50
.1662E+66,	.2325+304,	.2596+304,	.3711E+66	5.00
.3070+181,	.2325+304,	.2596+304,	.6854+181	5.50
.1240+216,	.2325+304,	.2596+304,	.2770+216	6.00
.5857+197,	.2325+304,	.2596+304,	.1308+198	6.50
.1429+234,	.2325+304,	.2596+304,	.3191+234	7.00
.2053+304,	.2325+304,	.2596+304,	.2219+304	7.50
.3545+271,	.5409E+93,	.1688E+43,	.1543E+44	8.00
.6530+231,	.5728E+00,	.6953E+00,	.1075E+01	8.50
.3804+249,	.5728E+00,	.5402E+50,	.1294E+01	9.00
.2602+230,	.5728E+00,	.1762+178,	.1294E+01	9.50
.2156+226,	.5728E+00,	.1531+211,	.1294E+01	10.00

FILE NAME:FE40ALI\BFE40ALI
FILE DESCRIPTION:
RUN WITH Const. Potn. for Fe40Al/Alumina fiber, mod. AlO zp, ps<10 mic
THIS DATA WAS AQUIRED ON: 06/08/1993
AQUISITION BY THE PROGRAM STARTED AT... 02:46:51:76
AND FINISHED AT... 02:54:21:87
OVERALL PROPORTION OF COMPONENT 1 IN SYSTEM =.500
CONCENTRATION OF 1-1 ELECTROLYTE IN SYSTEM = .00010 N
ATOMIC PARTICLE RADIUS OF COMPONENT 1 = 3000.0 nm
ATOMIC PARTICLE RADIUS OF COMPONENT 2 = 15000.0 nm
TEMPERATURE OF SYSTEM (IN DEG. C.) = 25.0
HAMAKER CONSTANT OF MEDIUM = .45E-19 J
HAMAKER CONSTANT OF COMPONENT 1 = .22E-18 J
HAMAKER CONSTANT OF COMPONENT 2 = .11E-18 J
ZETA POTENTIAL DATA WAS USED FOR CALCULATIONS.
ZETA POTENTIAL DATA FOR PARTICLE 1:

ZETA POTENTIAL VALUES:	CORESPONDING PH VALUES:
8.2	4.0
8.4	4.1
10.8	4.4
10.7	4.5
12.7	4.9
12.8	5.0
14.4	5.5
15.3	5.5
15.1	6.0
16.1	6.1
14.6	6.4
15.6	6.6
16.3	6.8
15.3	7.1
16.1	7.3
16.9	7.5
15.4	7.9
16.3	8.0
15.6	8.5
15.6	8.9
16.4	9.1
16.3	9.5
15.4	9.5
15.8	9.9
15.5	10.0

ZETA POTENTIAL DATA FOR PARTICLE 2:

ZETA POTENTIAL VALUES:	CORESPONDING PH VALUES:
45.3	4.0
45.2	4.5
45.0	5.0
42.9	5.5
38.2	6.0
32.1	6.5
24.2	7.0
15.3	7.5
6.8	8.0
-3.0	8.5
-7.0	9.0
-9.5	9.5
-10.0	10.0

CALCULATED OVERALL STABILITY RATIO DATA:

OVERALL STABILITY RATIO: (W11,W12,W22,WT)				CORESPONDING PH VALUES:
.3365E+00,	.3709+144,	.2596+304,	.3419E+00	4.00
.1504E-02,	.3253+242,	.2596+304,	.1528E-02	4.50
.4991E+18,	.1558+304,	.2596+304,	.5071E+18	5.00
.8402E+47,	.1558+304,	.2596+304,	.8537E+47	5.50
.4943E+56,	.1558+304,	.2596+304,	.5022E+56	6.00
.1123E+52,	.1558+304,	.2596+304,	.1141E+52	6.50
.1863E+61,	.1558+304,	.2596+304,	.1893E+61	7.00
.1233E+84,	.2225+264,	.2596+304,	.1253E+84	7.50
.5547E+70,	.1169E+66,	.1688E+43,	.2680E+47	8.00
.4758E+60,	.5921E+05,	.6953E+00,	.1101E+05	8.50
.1508E+65,	.5395E+05,	.5402E+50,	.3426E+07	9.00
.2103E+60,	.5193E+05,	.1762+178,	.3298E+07	9.50
.1943E+59,	.5158E+05,	.1531+211,	.3276E+07	10.00

FILE NAME:FEAL550\BFEAL550
FILE DESCRIPTION:
RUN WITH Constant Potential for Fe40Al/Alumina fiber file 550
THIS DATA WAS AQUIRED ON: 06/10/1993
AQUISITION BY THE PROGRAM STARTED AT... 19:46:32:83
AND FINISHED AT... 20:14:22:56
OVERALL PROPORTION OF COMPONENT 1 IN SYSTEM =.500
CONCENTRATION OF 1-1 ELECTROLYTE IN SYSTEM = .00010 N
ATOMIC PARTICLE RADIUS OF COMPONENT 1 = 11860.0 nm
ATOMIC PARTICLE RADIUS OF COMPONENT 2 = 15000.0 nm
TEMPERATURE OF SYSTEM (IN DEG. C.) = 25.0
HAMAKER CONSTANT OF MEDIUM = .45E-19 J
HAMAKER CONSTANT OF COMPONENT 1 = .22E-18 J
HAMAKER CONSTANT OF COMPONENT 2 = .11E-18 J
ZETA POTENTIAL DATA WAS USED FOR CALCULATIONS.
ZETA POTENTIAL DATA FOR PARTICLE 1:

ZETA POTENTIAL VALUES:	CORESPONDING PH VALUES:
9.5	4.0
9.7	4.0
10.1	4.5
10.0	4.6
10.2	5.0
10.4	5.0
12.2	5.4
12.7	5.6
13.4	6.0
13.3	6.0
13.0	6.4
13.4	6.5
12.7	7.0
12.6	7.1
12.2	7.4
12.1	7.6
11.5	7.9
11.7	8.1
11.5	8.4
11.2	8.5
10.4	9.0
9.5	9.5
9.4	9.6
9.4	9.9
9.4	10.1

ZETA POTENTIAL DATA FOR PARTICLE 2:

ZETA POTENTIAL VALUES:	CORESPONDING PH VALUES:
27.2	4.0
27.1	4.1
27.1	4.5
27.2	4.9
27.1	5.0
26.0	5.4
25.5	5.6
23.5	5.9
22.9	6.0
19.9	6.4
18.4	6.6
15.4	6.9
14.5	7.0
9.2	7.5
8.5	7.6
4.5	7.9
3.3	8.1
1.9	8.4
-1.8	8.5
-3.8	8.9
-4.2	9.0
-5.7	9.5
-5.8	9.6
-6.3	9.9
-6.4	10.0

CALCULATED OVERALL STABILITY RATIO DATA:

OVERALL STABILITY RATIO: (W11,W12,W22,WT)				CORESPONDING PH VALUES:
.3320E+00,	.2325+304,	.2596+304,	.7414E+00	4.00
.6701E-33,	.2325+304,	.2596+304,	.1496E-32	4.50
.3965E-26,	.2325+304,	.2596+304,	.8853E-26	5.00
.2260E+47,	.2325+304,	.2596+304,	.5047E+47	5.50
.2505E+93,	.2325+304,	.2596+304,	.5594E+93	6.00
.5083E+92,	.2325+304,	.2596+304,	.1135E+93	6.50
.1120E+61,	.2325+304,	.2596+304,	.2501E+61	7.00
.1053E+37,	.1246+122,	.8491+146,	.2352E+37	7.50
.7698E+14,	.8123E-16,	.6953E+00,	.1835E-15	8.00
.1321E+02,	.5728E+00,	.6953E+00,	.1037E+01	8.50
.2489E-24,	.5728E+00,	.6953E+00,	.5557E-24	9.00
.3320E+00,	.5728E+00,	.6162E+09,	.4713E+00	9.50
.3320E+00,	.5728E+00,	.5465E+28,	.4713E+00	10.00

FILE NAME:FEAL32A\BFEA32A
FILE DESCRIPTION:
RUN WITH Constant Potential for Fe40Al 325/Alumina fiber Simulation
THIS DATA WAS AQUIRED ON: 06/16/1993
AQUISITION BY THE PROGRAM STARTED AT... 20:42:12:13
AND FINISHED AT... 21:09:16:28
OVERALL PROPORTION OF COMPONENT 1 IN SYSTEM =.500
CONCENTRATION OF 1-1 ELECTROLYTE IN SYSTEM = .00010 N
ATOMIC PARTICLE RADIUS OF COMPONENT 1 = 11860.0 nm
ATOMIC PARTICLE RADIUS OF COMPONENT 2 = 15000.0 nm
TEMPERATURE OF SYSTEM (IN DEG. C.) = 25.0
HAMAKER CONSTANT OF MEDIUM = .45E-19 J
HAMAKER CONSTANT OF COMPONENT 1 = .22E-18 J
HAMAKER CONSTANT OF COMPONENT 2 = .11E-18 J
ZETA POTENTIAL DATA WAS USED FOR CALCULATIONS.
ZETA POTENTIAL DATA FOR PARTICLE 1:

ZETA POTENTIAL VALUES:	CORESPONDING PH VALUES:
-2.0	4.0
3.0	4.5
10.0	5.0
15.0	5.5
15.1	6.0
15.2	6.5
15.3	7.0
15.4	7.5
15.5	8.0
15.4	8.5
15.3	9.0
15.2	9.5
15.1	10.0

ZETA POTENTIAL DATA FOR PARTICLE 2:

ZETA POTENTIAL VALUES:	CORESPONDING PH VALUES:
27.2	4.0
27.1	4.1
27.1	4.5
27.2	4.9
27.1	5.0
26.0	5.4
25.5	5.6
23.5	5.9
22.9	6.0
19.9	6.4
18.4	6.6
15.4	6.9
14.5	7.0
9.2	7.5
8.5	7.6
4.5	7.9
3.3	8.1
1.9	8.4
-1.8	8.5
-3.8	8.9
-4.2	9.0
-5.7	9.5
-5.8	9.6
-6.3	9.9
-6.4	10.0

CALCULATED OVERALL STABILITY RATIO DATA:

OVERALL STABILITY RATIO: (W11,W12,W22,WT)				CORESPONDING PH VALUES:
.3320E+00,	.5728E+00,	.2596+304,	.4713E+00	4.00
.3320E+00,	.7579E-05,	.2596+304,	.1712E-04	4.50
.1740E-34,	.2325+304,	.2596+304,	.3885E-34	5.00
.1570+191,	.2325+304,	.2596+304,	.3505+191	5.50
.5857+197,	.2325+304,	.2596+304,	.1308+198	6.00
.2622+204,	.2325+304,	.2596+304,	.5855+204	6.50
.1409+211,	.2325+304,	.2596+304,	.3147+211	7.00
.9086+217,	.1736+182,	.8491+146,	.7760+147	7.50
.7032+224,	.1177E-02,	.6953E+00,	.2658E-02	8.00
.9086+217,	.5728E+00,	.6953E+00,	.1075E+01	8.50
.1409+211,	.5728E+00,	.6953E+00,	.1075E+01	9.00
.2622+204,	.5728E+00,	.6162E+09,	.1294E+01	9.50
.5857+197,	.5728E+00,	.5465E+28,	.1294E+01	10.00

REFERENCES

1. Technical Proposal 1990-1991.

2. R.E.F. Technical Proposal.

3. N.S.F. Technical Proposal.

4. D.E. Alman and N.S. Stoloff, "Processing and Properties of Intermetallic Matrix Composites," Mat. Res. Soc. Symp. Proc., 213, 989-1000, 1991.

5. R.M. German and A. Bose, "Fabrication of Intermetallic Matrix Composites," Materials Science and Engineering, A107, 107-116, 1989.

6. R. Bowman and R. Noebe, "Up and Coming IMCs," Advanced Materials and Processes, 8, 35-39, 1989.

7. N.S. Stoloff and D.E. Alman, "Innovative Processing Techniques for Intermetallic Matrix Composites," Mat. Res. Soc. Symp. Proc., 194, 31-43, 1990.

8. K.S. Kumar, M.S. Dipietro, S.A. Brown, J.D. Wittenberger, "Composites of Low-Density Trialuminides: Particulate and Long Fiber Reinforcements," NASA Technical Memorandum, 1992.

9. S. Mourbakhsh, F.L. Liang, H. Margolin, "Pressure Casting of Ni$_3$Al/Al$_2$O$_3$ Composites", Mat. Res. Soc. Symp. Proc., 133, 459-464, 1989.

10. R.M. German, A. Bose, N.S. Stoloff, "Powder Processing of High Temperature Aluminides," MRS Proceedings, 133, 403-414, 1989.

11. D.E. Alman and N.S. Stoloff, "Powder Fabrication of Monolithic and Composite NiAl," The International Journal of Powder Metallurgy, 27, 29-41, 1991.

12. D.J. Shaw, Introduction to Colloid and Surface Chemistry, Butterworths, Boston, 4th Edition, 1992.

13. R.J. Hunter, Foundations of Colloid Science, Volume 1, Clarendon Press, Oxford, 1987.

14. P.C. Heimenz, Principles of Colloid and Surface Chemistry, Marcel Dekker, New York, 2nd Edition, 1986.25. K. Aoki and O. Izumi, J. Jpn. Inst. Met., 43, 1190, 1979.

15. B.A. Wilson, Master of Science Thesis, Michigan State Unversity, 1992.

16. M.J. Crimp, Master of Science Thesis, Case Western Reserve University, 1985.

17. R.W. O'Brien, "Electro-acoustic effects in a Dilute Suspension of Spherical Particles," J. Fluid Mech., 190, 71-86, 1988.

18. R.W. O'Brien, "The Electroacoustic Equations for a Colloidal Suspension," J. Fluid Mech., 212, 81-93, 1990.

19. Tony Oja, Matec Applied Sciences Division, Personal Communications.

20. R. Hogg, T.W. Healy, D.W. Fuerstenau, "Mutual Coagulation of Colloidal Dispersions," Trans. Faraday Soc., 62, 1638-1651, 1966.

21. Deryaguin, B.V. and Landau, L., Acta Phys. Chim. URSS, 14, 633 (1941).

22. D.M. Shah, D.L. Anton, C.W. Musson,"Feasibility Study of Intermetallic Composites," MRS Symp. Proc., 194, 333-340, 1990.

23. S.L. Draper, D.J. Gaydosh, M.V. Nathal, A.K. Misra, "Compatibility of Fe-40Al with Various Fibers," J. Mat. Res., 5(9), 1976-1984, 1990.

24. D.M. Dimiduk and D.B. Miracle, "Directions in High Temperature Intermetallics research," MRS Symp. Proc., 133, 349-359, 1989.

25. K. Aoki and O. Izumi, Nippon Kinzoku Gakkaishi, 43, 1190, (1979).

26. J.A. Moser, M. Aindow, W.A.T. Clark, S. Draper, H.L. Fraser,"Compatibility of Potential Renforcing Ceramics with Ni and Fe Aluminides," MRS Proc., 194, 379-384, 1990.

27. A.B. Strong, Fundamentals of Composite Manufacturing: Materials, Methods, and Applications, 4th Edition, Soc. of Manufacturing Engineers, Dearborn, 1989.

28. F.V. Lenel, Powder Metallurgy: Principles and Applications, Metal Powder Inductries Federation, Princeton, New Jersey, 1980.

29. B.A. Wilson, C.J. Suydam, M.J. Crimp, M.A. Crimp, "Processing of FeAl / Al_2O_3 IMCs Using Advanced Electrodeposition Methods," Mat. Res. Soc. Symp. Proc., 288, 891-896, 1992.

30. B.A. Wilson and M.J. Crimp, "Modelling for Composite Colloidal Suspension Stability Based Upon the HHF Interpretation," Langmuir, submitted for publication, 1993.

31. M.J. Crimp, Personal Communications.

32. D. Maglaya, Senior Thesis, Michigan State University, 1991.

33. Verwey, E.J.W. and Overbeek, J. Th. G., Theory of the Stability of Lyophobic Colloids, Elsevier (1948).

34. D.L. Anton and D.M. Shah,"High Temperature Ordered Compounds for Advanced Aero-Propulsion Applications," MRS Symp. Proc., 133, 361-371, 1989.

35. R.D. Noebe, R.R. Bowman, J.J. Eldridge, "Initial Evaluation of Continuous Fiber Reinforced NiAl Composites," MRS Symp. Proc., 194, 323-331, 1990.

36. D.C. Cranmer, "Fiber Coating and Characterization," Ceramic Bulletin, 68[2], 415-419, 1989.

37. J. Doychak, "Metal- and Intermetallic-Matrix Composites for Aerospace Propulsion and Power Systems," J.O.M., 44[6], 46-51, 1992.

38. B. Schmidt, P. Nagpal, I. Baker, "Annealing Studies of B2 FeAl," MRS Symp. Proc., 133, 755-760, 1989.

39. E. Barouch, E. Matijevic, T.A. Ring, J.M. Finlan, "Heterocoagulation II. Interaction energy of Two Unequal Spheres, J. of Colloid and Interface Science, 67(1), 1978.

40. P.J. Scales and Eileen Jones, "Effect of Particle Size Distribution on the Accuracy of Electroacoustic Mobilities," Langmuir, 8, 385-389, 1992.

41. M. James, R.J. Hunter, R.W. O'Brien, "Effect of Particle Size Distribution and Aggregation on Electroacoustic Measurements of Zeta-Potential," Langmuir, 8, 420-423, 1992.

42. M.J. Crimp and R.F. Preston, "Evaluation of Sedimentation as a Technique for the Separation of Sub-micron Diameter Silicon Carbide Whiskers,"

43. M.J. Crimp and R.C. Piller, "Dispersion of SiC Whiskers in a Si_3N_4 Matrix Using pH Control,"

44. M.J. Crimp, R.E. Johnson, Jr., J.W. Halloran, D.L. Feke, "Colloidal Behavior of Silicon Carbide and Silicon Nitride,"

45. J.T.G. Overbeek, "Recent Developments in the Understanding of Colloid Stability"; pp. 431-45 in Colloid and Interface Science Volume 1, Edited by M. Kerker, K.L. Rowell, A.C. Zettlmoyer, Academic Press, 1976.

46. R.O. James, G.A. Parks, "Characterization of Aqueous Colloids by their electrical Double-Layer and Intrinsic Surface Chemical Properties"; pp. 119-216 in Surface and Colloid Science Volume 12, Edited by E. Matijevic, Plenum Press, New York, 1982.

47. E. Barouch, E. Matijevic, T.A. Ring, J.M. Finlan, "Heterocoagulation II. Interaction Energy of Two Unequal Spheres," J. Col. Int. Sci., 67[1], 1-9, 1978.

48. A. Bierman, "Electrostatic Forces Between Nonidentical Colloidal Particles," J. Col. Int. Sci., 10, 231-245, 1955.

49. A. Bleier and E. Matijevic, "Heterocoagulation I. Interactions of Monodispersed Chromium Hydroxide with Polyvinyl Chloride Latex," J. Col. Int. Sci., 55[3], 510-524, 1976.

50. A. Bleier and E. Matijevic, "Heterocoagulation III. Interactions of Polyvinyl Chloride Latex with Ludox HS Silica," J. Chem. Soc., Faraday Trans. I, 74[6], 1346-1359, 1978.

51. J.T.G. Overbeek, "Double-layer Interaction between Spheres with Unequal Surface Potentials," J. Chem. Soc., Faraday Trans., 84[9], 3079-3091, 1988.

52. E. Barouch, "Double-layer Interaction between Spheres with Unequal Surface Potential," J. Chem. Soc., Faraday Trans. 1, 84[9], 3093-3095, 1988.

53. R.E. Johson, Jr., "A Thermodynamic Description of the Double Layer Surrounding Hydrous Oxides," J. Col. Int. Sci., 100[2], 540-554, 1984.

54. R.O. James, "Surface Ionization and Compexation at the Colloid/Aqueous Electrolyte Interface"; pp. 219-61 in Adsorption of Inorganics at Solid-Liquid Interfaces, Edited by M.A. Anderson, A.J. Rubin, Ann Arbor Science, Ann Arbor, 1981.

55. T.W. Healy and L.R. White, "Ionizable Surface Group Models of Aqueous Interfaces," Advances in Colloid and Interface Science, 9, 303-345, 1978.

56. G. Kar, S.Chander, T.S. Mika, "The Potential Energy of Interaction Between Dissimilar Electrical Double Layers," J. Col. Int. Sci., 44[2], 347-355, 1973.

57. E. Barouch and E. Matijevic, "Double-layer Interactions of Unequal Spheres Part I. The Effect of Electrostatic Attraction with Particles of Like Sign of Potential," J. Chem. Soc., Faraday trans. 1, 81, 1797-1817, 1985.

58. E. Barouch and E. Matijevic, "Double Layer Interactions of Unlike Spheres III. Nonlinear and Two-Dimensional Effects," J. Col. Int. Sci., 105[2], 552-559, 1985.

59. E. Barouch, E. Matijevic, T.H. Wright, "Double-layer Interactions of Unlike Spheres Part II. Numerical Analysis of Electrostatic Interaction Energy," Chem. Soc., Faraday Trans. 1, 81, 1819-1832, 1985.

60. A. Bleier, "Fundamentals of Preparing Suspensions of Silicon and Related Ceramic Powders," J. Am. Cer. Soc., 66, 7981, 1983.

61. J. Gregory, "The Calculation of Hamaker Constants," Advances in Colloid and Interface Science, 2, 397-417, 1968.

62. K. Vendula, R.J. Lauf, C.A. Wells, ECUT Quarterly Report, 1985, July 1 - Sept. 30, Oak Ridge National Lab, p.56.

63. D.R. Gaskell, Introduction to Metallurgical Thermodynamics, 2ND Ed., Hemishpere Publishing Corp., New York, New York, 1981.

64. CRC Handbook of Chemistry and Physics, 73RD Ed. CRC Press, 1993.

65. B. Glime, Undergraduate Senior Thesis, Michigan State University, 1991.